The Study of Hydrogen Adsorbed on Supported Metal Particles by Means of L-edge XANES

(L-edge XANESによる担持金属粒子上の水素吸着状態の研究)

[redacted]

([redacted])

The Study of Hydrogen Adsorbed on Supported Metal Particles by Means of L-edge XANES

by
Takeshi Kubota

A Thesis Submitted to the University of Tokyo
for the Degree of Doctor of Science

January, 1999

Acknowledgment

This work has been performed under Professor Iwasawa's supervision. I deeply appreciate Prof. Iwasawa's continuing guidance and encouragement. I also appreciate Prof. Asakura for his continuing guidance and support on my experiments. I would also like to acknowledge Prof. Onishi, Prof. Sasaki, and Dr. Fukui for their helpful advise, especially for discussion. I would like to acknowledge Prof. Fujikawa and Dr. Ohtani for their collaboration and discussion. I would also like to acknowledge Dr. Onishi and Dr. Watari for their collaboration and discussion.

I would also like to appreciate Dr. Ichikuni, Dr. Tomishige Dr. Inoue, Dr. Okumura, Mr. Yoshikawa, and Dr. Chun for helping me during the experiments and on discussion. Especially, my work could not have been done without Dr. Ichikuni's helpful advice and guidance during my experiments.

I would also like to thank my colleagues, Mr. Nagahiro and Miss. Miyauchi. I also thank all other members of Prof. Iwasawa's laboratory, including alumni and visiting researchers during the period of my research.

I was supported by the staffs of the Photon Factory for all the experiments using the beamlines. I would like to appreciate them, especially Prof. Nomura, Dr. Kitajima, Dr. Koyama and Dr. Usami.

Finally, I deeply appreciate Prof. Okamoto for assistance during acquisition of doctorate.

Part of this work has been supported by CREST (Core Research for Evolutional Science and Technology) of Japan Science and Technology Corporation (JST).

Contents

Chapter1.

General Introduction

1-1. Introduction

In 1836, Berzelius introduced the term "catalysis" (coming from Katalysis in Greek meaning "loosening down"), meaning some mysterious quality. The founders of modern chemistry and physics -Davy, Faraday, Nenst, Kirchifoff and Ostwald- revealed the significance of catalysis in modern science. Nowadays, catalysis is defined as "a substance that increases the rate of attainment of chemical equilibrium by lowering the activation barrier in a reaction without itself undergoing chemical change a kind of reaction" [1, 2]. Many catalysts are used in the industrial process and environmental protection. A typical example is found in a development of ammonia synthesis catalyst started by Haber and Bosch in the early 20th century.

Surface of solid state material provides a field which catalyzed many reactions, such as CO hydrogenation reaction (Fischer Tropsch Reaction), Auto-Exhast reaction, cracking reaction of petroleum, desulfridization reaction and so on. However, development of a new solid state catalyst and catalytic process still seem to be based on a trial and error method and sometimes catalyst preparation is called as a "state of art". It is partly due to the difficulty to characterize the catalyst in a working conditions. Nowadays, many methods have been developed and used to characterize catalysts for research, for example spectroscopies and diffraction. However, many catalysts used as a form of supported metal or metal oxides. Then active metal and metal oxides form microcrystalline structures or amorphous phases without much structural order and therefore X-ray diffraction, which is the most reliable structural analysis technique, can not be directly applied to the catalyst structure. Furthermore, it has been understood that the working catalyst interacts with the ambient reactants and products, constituting "a dynamic equilibrium" (or a steady state). Consequently, without in-situ studies of working catalysts it is impossible to understand "catalysis" and catalytic structure, which also make it difficult to apply physico-chemical techniques such as spectroscopy. The first step of in-situ investigation of catalysis is to characterize the adsorbate and

the adsorbed surface. There are suitable spectroscopic tools to study the state of adsorbate, such as Infrared spectroscopy and NMR. Hydrogen, one of the simplest but one of the most important elements in the catalysis, is, however, difficult to be investigated by these spectroscopic techniques due to the several reasons discussed later. $L_{2,3}$-edge X-ray absorption near edge structure (XANES) of Pt particle has been reported sensitively changed with the adsorption of hydrogen. This spectral feature accompanied with the hydrogen adsorption is expected to be used to characterize the adsorbed hydrogen, however, the origin of the change was unclear. For these 4 years, I have investigated the XANES of Pt particles with adsorbed hydrogen in order to reveal the origin of the spectral change induced by the adsorption of hydrogen and to apply this XANES method to quantitative characterization of adsorbed hydrogen on Pt and Pd.

In this thesis I will describe the change in Pt $L_{2,3}$-edge XANES induced by adsorbed hydrogen. Then I will discuss its origin and application. Before referring how I approached for these matters, I would like to introduce the surface hydrogen, which is concern with many catalytic reaction or surface science in the section 1-2. In the section 1-3, I will introduce fundamentals and applications of XANES and EXAFS ,which have been used for catalysts characterization. I would also like to introduce previous works done by pioneers about changes in Pt $L_{2,3}$-edge XANES spectra in 1-4, which was first recognized by Lytle early 80's. I also summarize the points of disputes. Finally, I will show why I have taken up XANES spectra as characterization of adsorbed hydrogen in 1-5. I will also show how I approached to those proposals, whose results are the main theme of this thesis.

1-2. Surface hydrogen

1-2-1. Adsorbed hydrogen on metal surface and its reactivity

Hydrogen dissociatively adsorbs on metal surface [3, 4]. Heat of adsorption of H_2 on metal surface is not so large (less than 80 kcal / mole). For example, Pt(100) 15-16 kcal / mole, Pt(111) 18

kcal / mole and Ni(110) 23.5 kcal / mole [5]. However, adsorption of hydrogen induces surface reconstructions. For example, streaky 1×2 hydrogen phase on Ni(110) was observed by LEED(Low Energy Electron Diffraction) where reconstruction of Ni surface occurred [6]. Recently, it was confirmed that the missing row type of reconstructure occurs in a 1X2 phase accompanied by - Ni-H-chain growing to [100] direction by STM study [7]. It is known that not only Ni, but VIII elements also adsorbs hydrogen well. Especially, Pd is known as its ability of hydrogen absorption in bulk and using this property, Pd is used as purification of hydrogen gas.

Hydrogen which dissociatively adsorbs on many metal surfaces is involved in important catalytic processes such as hydrogenation, hydrogenolysis, hydrotreating, hydroformylation and so on [4]. The chemisorption and surface reactions of hydrogen and hydrocarbons on metal surface have been investigated intensively from the viewpoint of heterogeneous catalysis. Hydrogenation , dehydrogenation, and skeletal rearrangement reactions are of particular importance for the catalytic reforming of petroleum feedstocks. These reactions are selectively catalyzed by only a small group of transition metals and alloys, most notably platinum and platinum-based alloys.

The hydrogenation of ethene has long been used to monitor the activity of metal catalysts. Yoshitake et al. found that the deuterogenation of ethene was enhanced by Na addition [8]. They concluded that the promotion of the rate was due to the decrease of the amount of adsorbed ethene, creating vacant site on the surface and thus increasing a preexponential factor for the rate constant of D_2 dissociative adsorption which was rate-determing [8, 9]. They also investigated the change of catalytic reactivity by the introduction of substituents to C=C compounds and varying the support (Y_2O_3, ZrO_2, V_2O_3, and TiO_2) [9, 10].

CO hydrogenation on group VII metal catalysts is another important class of catalytic reactions which synthesizes methane, hydrocarbons (Fischer-Tropsch synthesis), and alcohols [11-14]. The hydrogen reaction order in CO hydrogenation on cobalt, iron, and nickel catalysts is typically 0.5 to 1.0. Hence the reaction rate is generally proportional to the concentration of

hydrogen in the gas phase and to the fractional coverage of hydrogen on the surface. In Fischer-Tropsch synthesis, hydrocarbon product selectivities are determinated by the ability of a catalyst to make C-C chain propagation versus C-C chain termination steps. Rates of C-C chain termination are generally more dependent on hydrogen concentration on the surface than are C-C chain propagation rates [15].

As noted above, hydrogen adsorbed on metal surface plays an important role in metal catalysis for many catalytic reactions. Especially, amount of hydrogen determines the selectivity as found in the last examples. Thus it is important to characterize adsorbed hydrogen on surface particularly under in situ conditions.

1-2-2. Methods of characterization for adsorbed hydrogen

As mentioned previously, however, the characterization of adsorbed hydrogen is not easy matter, as most of the surface probing experimental methods are relatively insensitive to adsorbed hydrogen.

The electronic interaction between adsorbed hydrogen and a metal surface also shows up in the Ultra-Violet Photoelectron Spectra (UPS). Fairly broad resonance levels ca. 5-8 eV below the Fermi edge E_f are characteristic of hydrogen adsorption. A UV-photoemmition study of hydrogen on Ni, Pd, and Pt surfaces was reported by Demuth [16]. The broad resonance peak induced by hydrogen is often hindered by a strong peak arising from coadsorption of other species such as CO. Furthermore, UPS works only under ultra high vacuum and is not applicable to the observation of hydrogen under the conditions relevant to catalytic reactions. Because of the same reason, electron spectroscopies such as High Resolution Electron Energy Loss Spectroscopy (HREELS), Electron Stimulated Desorption (ESD) are not able to use for investigation of the metal/gas interface at high gas pressures [4, 17].

Temperature-programed desorption (TPD) studies are used for the characterization of

adsorbed hydrogen. TPD of H_2 from a metal surface gives a characteristic spectrum of the metal-hydrogen interaction as a function of temperature [18]. The chemisorption of H_2 on Pt black in the range 77-670 K was investigated by Tsuchiya et al. using this technique [19]. The appearance of four peaks in the TPD spectrum with their maxima at 170, 250, 350, and 570 K indicates at least four different states (designated as α, β, γ, and δ) of chemisorbed hydrogen on Pt in this range. These states have been tentatively assigned to the each adsorption forms. Miller et al. measured hydrogen TPD of supported platinum catalysts, Pt/K-LTL, Pt/H-LTL, Pt/K-MAZ, Pt/H-MAZ, Pt/Al_2O_3, and Pt/SiO_2 after hydrogen reduction at 300, 450, or 650 degree [20]. They found that reversible desorption of chemisorbed hydrogen occurred at approximately 175 degree for all catalysts. They also observed at least three peaks appearing in higher temperature region in addition to chemisorbed H_2. The high temperature H_2 species desorb irreversibly and are assigned to spillover hydrogen. As noted above, TPD is a typical analysis method for adsorbed hydrogen, but the TPD is also unable to investigate adsorbed hydrogen under the reaction conditions.

Infrared (IR) spectroscopy has been used for a long time to detect surface species at the solid-gas interaction [21, 22]. However, because of the small dynamic dipole polarizability of metal-hydrogn bonds, measurement of the vibrational spectrum for chemisorbed hydrogen by IR or by Raman spectroscopy is difficult. One of the first experiments demonstrating the capability of IR spectroscopy has been shown in the early 1960' s by Pliskin and Eischens [21, 22]. Molecular hydrogen has been adsorbed onto the γ-alumina supported platinum, giving rise to two infrared bands at 2105 and 2055 cm^{-1} at high coverages. The same experiment was repeated using D_2 and again, two bands at 1512 and 1480 cm^{-1} were detected. These observation were attributed to the atop Pt-H or Pt-D stretching normal vibrations. Szilágyi studied IR spectra of weakly bound hydrogen between 300 and 400 K and 1 to 105 Pa [23]. He observed asymmetric IR band shapes and claimed that several kinds of weakly bonded hydrogen coexist on the surface, having essentially the same kind of bonding but differing slightly in bond strength. However, higher energy bands

were assigned to weakly bonded hydrogen because they only appear in the presence of gas phase hydrogen more than 0.1 mbar. The strongly adsorbed hydrogen is believed to appear below 1200 cm^{-1} which is inaccessible in transmission IR analysis of supported metals owing to IR absorption by the support. Thus vibrational modes due to strongly bound hydrogen has been reported by HREELS observation and which are attributed to the hydrogen atoms residing in bridging sites involving two or three metal atoms.

The ^1H NMR spectra of heterogeneous catalyst systems comprising small platinum particles supported on high-surface-area oxides, such as silica or alumina, in the presence of hydrogen gas, have been studied over a period of nearly 20 years. NMR chemical shift changes with hydrogen coverage in a non-linear manner. When the coverage is less than 0.75, the ^1H chemical shift is constant and -53 ppm. When the coverage exceeds that value, it increases with the coverage upto -20 ppm. There are two interpretations of this non-linear behavior in chemical shift. Rouabah et al. explained the interpretation of the variation of chemical shift based on the knight shift of conduction electron and invariant part of the chemical shift at low coverage region is due to inhomogeneous distribution of the hydrogen. Rouabah et al. found that the spectrum of hydrogen chemisorbed on platinum supported on silica depends on the coverage and the size of the metal particles and on the temperature [24]. They concluded that it includes as many components as there are particle-size distributions with well distinguished maxima. They proposed that from the variation of the chemical shift with the number of adsorbed hydrogen atoms, it is possible to determinate the metal dispersion. On the other hand, Chesers et al. proposed another model in which strongly adsorbed and weakly adsorbed hydrogen has different chemical shift and proportion of these hydrogen species changes with coverage. Chesters et al. recorded ^1H NMR spectra resulting from the adsorption of hydrogen by a silica-supported platinum catalyst quantitatively over a wide coverage range to produce an NMR adsorption isotherm [25-27]. They analyzed the coverage dependence metal-hydrogen resonance frequency in terms of a three-state model that includes terms for strongly and weakly

adsorbed hydrogen as well as gas-phase hydrogen. Their analysis of the metal-hydrogen resonance frequency yielded values for the frequency position of the strongly bound hydrogen of ca. -48 $\pm$2 ppm and of +37 $\pm$10 ppm for the weakly bound hydrogen. In addition them, they observed a resonance which is tentatively assigned to hydrogen present at the interface between the platinum particles and the support at about -20 ppm. Thus NMR have been used to investigate adsorbed hydrogen and relevant to the observation of hydrogen under real in situ condition. However, the analysis of NMR spectrum is complicated and is not established yet.

I have introduced some methods to analyze adsorbed hydrogen. In-situ spectroscopic characterization of chemisorbed hydrogen on supported metal particles is difficult to achieve by conventional spectroscopic techniques, so new method to characterize chemisorbed hydrogen is expected.

1-3. X-ray Absorption Near Edge Structure (XANES)

XANES (X-ray Absorption Near Edge Structure) is known as a fine structure which appears in X-ray absorption spectra. XANES reflects local structure or electronic states around X-ray absorbing atom. Especially, XANES exhibits its ability for catalyst characterization under in-situ conditions due to X-ray's large penetration length [28, 29].

In this subsection, I introduce "XAFS" (X-ray absorption Fine Structure) first, which is more general term involving XANES and EXAFS(Extended x-ray absorption fine structure). EXAFS is more popular analysis tool for catalyst because its simplicity in analysis. Then I introduce theory and applications of XANES.

1-3-1. History of XAFS

From the 1920's, a fine structure has been recognized at higher energy region of X-ray absorption edge in X-ray Adsorption Spectra (XAS). In 1923 Kronig observed an oscillatory

structure from absorption edge upto the energy of 1000 eV in X-ray absorption spectra. This structure was called as "Kronig structure" or now generally Extend X-ray Absorption Fine Structure (EXAFS). The origin of this structure was well explained by Stern, Sayers and Lytle in 1971 on the basis of short-range order theory and they proposed analysis method in which Fourier transform of EXAFS oscillation provide radial distribution function. This method can provide information nearest-neighbor intratomic distance around X-ray.absorbing atoms. Thus EXAFS has been rapidly developed as a structural analysis method together with the advent of synchrotron radiation facilities [29, 30].

On the other hand, in the same 1920's Kossel observed fine structure at a near edge region in X-ray absorption spectra. This structure was called "Kossel structure" or now generally X-ray Absorption Near Edge Structure (XANES) or Near Edge X-ray Absorption Fine Structure (NEXAFS). EXAFS and XANES are altogether called as X-ray Absorption Fine Structure (XAFS). Kossel interpreted XANES in terms of transition to exited bound states, but chemical information using the near-edge structure was obtained only sporadically. In spite of its potential, XANES spectra have not been used so widely as EXAFS spectra because XANES is complicated phenomena with multiple scattering of photo electron, transition to quasi-bounded states and multiconfiguration excitation process. For these reasons, analysis method for XANES spectra is not standardized so far. But very recently theories to describe XANES have been rapidly developed and some attempts have been made to use XANES as quantitative analysis.

1-3-2. Quick review of theory of XANES

Fig. 1-1 shows Pt L_3-edge XAFS spectra of Pt foil. The largest and most detailed structures are in the near-edge region. As mentioned above XAFS is conventionally divided into near-edge region and extended fine structure region. A fine structure which extends from adsorption edge about up to 50 eV is assigned to XANES. A fine structure which covers an energy range from about

50 eV to over 1000 eV past the absorption edge is called as EXAFS.

The X-ray absorption intensity is given as the transition probability from the state of initial core electron to the state of final exited electron according to Fermi's golden role. The general X-ray absorption cross section is given by

$$\sigma = 4/3\ \pi^2\ \alpha\ h\nu\ \Sigma\ |<f|r|i>|^2\ \delta(E_i - E_f + h\nu) \qquad (1\text{-}1)$$

where α is the fine structure constant, $h\nu$ is the energy of the absorbed photon, and r is the interaction operator. $|i>$ represents the initial state and in single-particle model, initial state is the core state from which photoelectron emitted. $|f>$ represents the final state of the photoelectron, which is described as continuum state or unoccupied discrete level.

X-ray Absorption-edge spectroscopy deals with electronic transition from a core atomic level to unoccupied conduction states. In this process X-ray photons promote a bound electron from an inner level to the empty energy state, thereby increasing the X-ray absorption coefficient. When the photon energy exceeds the threshold level, photoelectron is ejected whose kinetic energy of the ejected core electron is $E = h\nu - E_B$, where E_B is core-state binding energy. In addition to the energy conservation rule, dipole selection rule is applied in the absorption process which is involved in $|<f|r|i>|^2$. When the wave functions are expressed in spherical coordinates $<f|$ should have an angular momentum $l_f = l_i \pm 1$, where l_i is an angular momentum for initial state $|i>$. For the K-edge where initial state angular momentum is 0 only p state is permitted as final states in a dipole transition approximation. The $L_{2,3}$-edge arises from the transitions between the 2p core state and the d states with a small contribution of transition between the 2p core state and the s states.. The L_1-edge arises from the transitions from the 2s core state to the p states and whose structure is quite different from the $L_{2,3}$ structures.

In order to calculate the equation (1), there are two approaches : molecular orbital theory and multiple scattering theory. In a MO approach, LCAO molecular orbitals are used to describe final states [31, 32], while in a multiscattering approaches final state is expressed by plane or spherical

waves and one-electron Schrödinger equation is solved as scattering problems [33-35]. Because in edge regions final states are located just at threshold and expressed by both continuum wave functions and bound state wave functions. The contribution of former is larger as photon energy becomes smaller. Thus the two approaches are complimentary and necessary to understand XANES correctly. At the same time double sided character of XANES make itself unwieldy.

1-3-3. Measurements of XANES

Similar to EXAFS, XANES measurements are usually done in a transmission mode. Since amplitude of EXAFS oscillation is so small as about a few per cent to absorption edge jump, EXAFS measurements requires high S/N(Signal to noise ratio (S/N > 1000) [36]. A conventional X-ray source such as rotating anode x-ray generator has a strong characteristic peak with a weak white X-ray radiation Bremsstrahlung radiation. Therefore it takes a long time to get reliable EXAFS signals. Synchrotoron radiation is an ideal X-ray sources for EXAFS measurement. First of all , much high intensity and flux (about 1000 times to X-ray tube), which results in improvement of S/N of the data and shorter acquisition times. All spectra presented in this thesis were collected at a synchrotron(KEK-PF, Tsukuba, Japan).

Fig. 1-2 shows set-up transmission experiment at BL-10B at Photon Factory (KEK). The beamline consists of three primary components: (i) an X-ray source, (ii) a monochromator, (iii) a detector. In Fig. 1-2, the incident X-ray beam from synchrotron is monochromatized by a channel monochromator made of Si(311) single crystal, which monochromatizes a X-ray with a specific energy determined by the Bragg diffraction:

$$\lambda = 2d \sin\theta, \qquad (1\text{-}2)$$

where d is the lattice spacing of the crystals, θ is the incident angle. The monochromatized X-ray is monitored by a front ionization chamber(I_0) and transmitted X-ray through the sample is monitored by a rare ionization chamber (I). The absorbance of a sample is calculated by :

$$\mu(E)x = \ln(I_0(E) / 1(E)) \qquad (1\text{-}3)$$

In addition to transmission mode, it is possible to detect X-ray absorption by fluorescence experiments. Fluorescence detection can be used for very diluted systems. In fluorescence mode, fluorescence is detected by Solid State Detector(SSD), proportional counter, and scintillation counter.

1-3-4. Features of XANES spectroscopy

The capabilities of XANES spectroscopy that make XANES suitable for structural studies are the following:

(1) applicability to any form and state of material such as amorphous, powder

(2) element specific;

(3) diagnostic value in monitoring chemical effects (symmetry of the unoccupied electronic states, effective atomic charge, d-band occupancy)

(4) determination of site symmetry around a particular species of atom in both periodic and nonperiodic arrangements;

Although these advantages, as mentioned above, the analysis method to obtain quantitative parameter for XANES is not generalized like EXAFS. So, practical application of XANES is to compare XANES spectrum of an unknown sample with those of reference compounds. However, there are some useful characteristic features in XANES spectra to be used for analysis. I would like to introduce those features and examples below

1-3-4-1. s -> d transition

The K or L_1 absorption edge maximum corresponds to the allowed *ns* -> *np* transitions, which merge into the continuum at higher energy. Sometimes pre-edge peaks or shoulders are observed below the absorption edge maximum, reflecting transitions to empty orbitals, for example,

1s -> 3d. These transitions are assigned to quadrupole transitions ($\Delta l = \pm 2$) usually much weaker than dipole transition. However, when the molecule has no inversion center, 3d state can be hybridized with p type wave function. In consequence, the 1s->3d pre-edge peak intensity is enhanced. Thus octahedral MX_6 gives weaker 3d pre-edge peak though, distorted octahedral and tetrahedral MX_n shows stronger 3d pre-edge peak.

Wong et al. recorded vanadium K-edge XANES spectra for a number of selected vanadium compounds of known chemical structure [37]. They found that the intensity of the 1s -> 3d pre-peak increases with progressive relaxation from perfect octahedral symmetry (as in VO) to distorted octahedral VO_6 groups, as in V_2O_3, V_4O_7, and V_2O_4, and to a lower coordination with a short V-O bond in square-pyramidal symmetry (as in V_2O_5) as shown in Fig. 1-3. The change in intensity can be explained by the symmetry of the VO_x unit mentioned above. Therefore progressively lowering the site symmetry to distorted geometries promotes the dipole allowedness of the pre-edge peak and yields as increasing intensity. They also found the energy shifts, so-called chemical shifts, of the pre-edge peak, which varied linearly with the valence of the absorbing vanadium atom.

Yoshida et al. noticed that the intensity of pre-peak for metal oxides decreases in the order $ZnFe_2O_4 > FeO > CoO > NiO$ (Fig. 1-4) [38]. This is not caused by a difference of the local structure as mentioned above because these oxides have a similar octerhedra structure of a metal ion - first neighbor oxygen ions in a regular. The electron configurations in the valence shell are d^5, d^6, d^7, d^8 for $ZnFe_2O_4$, FeO, CoO and NiO, respectively, and the unoccupancy of d-orbitals correlates to the peak intensity in this case. As seen in the Fig. 1-4, the pre-peak of FeO or $ZnFe_2O_4$ is split into two peaks. This indicates crystal field splitting of the d-orbitals (t^2_g, e_g). In CoO and NiO, such splitting is not observed because the d-orbitals of the t^2_g state(d_{xy}, d_{xz}, d_{yz}) are occupied and transition from the 1s-orbital to these orbitals is impossible. Kosugi et al. proposed that the valence states of Fe atom in hexacyanoferrate ion are determined using this splitting of the pre-peak [39].

In summary, the *ns*->*n*d pre-peak has very small intensity in itself but the peak is enhanced

by the lack of inversion center. The pre-peak is useful to the determination of local symmetry or valence states of X-ray absorbing atom, since the pre-peak is observed just below the absorption edge, where other fine structures are not overlapped.

1-3-4-2. White lines

The sharp peak observed in $L_{2,3}$-edge XANES spectra for the transition metals called "white line" as historically it was detected in an X-ray film as a very strong exposure. Fig.1-5 shows normalized XANES spectra of metallic platinum, platinum oxide, metallic gold, metallic tantalum and tantalum oxide [38]. It is noticed that a sharp and intense edge peak is observed for platinum oxide, metallic tantalum and tantalum oxide. The white line peak is strong because it is a dipole transition from 2p to 5d immediately above the threshold to the continuum level and has a large cross-section. The intensity of the white line correlates to unoccupancy of 5d orbitals so that the peak is weak for metallic platinum and is not observed for metallic gold in which the 5d orbitals are fully occupied. By the same reason, the white line for tantalum oxide (electron configuration; d^0) is more intense than that for metallic tantalum (electron configuration; d^5).

It is intriguing to note the difference between $L_{2,3}$-edge XANES spectra. For both metallic tantalum and tantalum oxide, the $L_{2,3}$-edge XANES spectra resemble each other, while the situation is different for metallic platinum where a white line is observed in the L_3-edge XANES spectrum but not in the L_2-edge XANES. The difference is caused by the splitting of the 5d orbitals of platinum to $5d_{5/2}$ and $5d_{3/2}$ states by spin-orbital coupling, corresponding to L_3 and L_2-edge, respectively and the $5d_{3/2}$ state (L_2-edge) is fully occupied. Thus, the intensity of the white line reflects density of states for X-ray absorbing atom, therefore, L-edge XANES has been used to estimate the density of unoccupied d-state of X-ray absorbing atoms. Lytle et al. measured the L_3-edge XANES spectra of the elements such as iridium, platinum, and gold in the pure metallic state and in a variety of compounds [40]. They found that when normalized spectra obtained on the metals are subtracted

from those obtained on the compounds, the resulting difference spectra are related to differences in the electronic structure of the X-ray absorbing atom in the two types of environment. They concluded that the change in area of a white line obtained from such a difference spectrum can be related to the ionicity of the bonds of the absorbing atom in its compounds. Horsley investigated the relationship between the intensity of the $L_{2,3}$ white line and d orbital occupancy for a series of compounds of platinum and iridium and the pure metals, using Xα-SW molecular orbital calculations to obtain the number of unoccupied d orbital states [41]. He obtained the areas of the white line by a deconvolution of the absorption edge into a Lorenzian component and an underlying "step function" representing the onset of absorption to continuum states (Fig. 1-6). He found a linear relationship between the calculated unoccupied d orbital states and sum of the areas of the $L_{2,3}$ white line.for a series of platinum compounds. Mansour et al. have proposed a technique to extract the number of unoccupied d-state in a material utilizing measurements of the L-XANES spectra [42]. This method follow to theory by Dietz and Mattheiss [43]. They illustrated the applicability and validity of the technique with a platinum catalyst supported on silica. This technique is applied to estimate of the fractional change of the d-band occupancy for Pt catalysts.

1-3-4-3. Others

Broad maxima around the core ionization threshold are observed in the NEXAFS spectra of many molecules. These features usually occur above the ionization potential (I.P.) but sometimes they occur below the edge. The former peak is called s shape resonance, which is assigned to transition from core electron to unoccupied σ* levels and the latter is to π shape resonance occurring in the "discrete" portion of NEXAFS spectra of molecules containing unoccupied π* levels. Stöhr et al. reported angular dependent NEXAFS spectra for the N K-edge of NO adsorbed on Ni(100) at 90 K [44]. The π* peak becomes the most intense when the incident X-ray radiation is perpendicular to the surface, while σ* shape resonance reaches a maximum at glancing angles. The angular

dependence of the intensity of the p resonance is given by the formula for 4 fold symmetry:

$$I = I_0 [1-0.25(3\cos 2\alpha-1)(3\cos^2\theta-1)] \qquad (1\text{-}4)$$

where α and θ refer to the angles of the molecular axis and the radiation electric vector with respect to the surface normal, respectively. Calculating for a in this case indicates that the NO adsorb with its main axis oriented perpendicular to the nickel surface. Similar studies have been carried out for a wide variety of diatomic adsorbed systems. Sette et al. revealed a correlation between the position of a characteristic K shell excitation feature, the σ shape resonance, and the intramolecular bond length as a result of a systematic analysis of K shell excitation spectra of gas phase molecules containing B, C, N, O, and F [45]. They found that when referenced to the 1s ionization threshold the position of the σ shape resonance is found to vary linearly with the internuclear distance between the pair of atoms which gives rise to the scattering resonance [46, 47].

When there are more than two environments around X-ray absorbing atom, sometimes XANES spectra for such systems can be resolved into a set of components [48-50]. Fernández-García et al. interpreted XANES spectra using factor analysis to follow the temperature-programmed reduction (TPR) of Cu-Pd/KL-zeolite catalysts [49]. They identified and quantified the chemical components in which a metal is present during a reduction treatment with this analysis method. When the method applied to the Cu K-edge XANES-TPR spectra of two bimetallic catalysts containing (1% Pd + 0.5% Cu), and (1% Pd +0.25% Cu), it is shown that Cu is initially present in both as two oxidic species, a Cu-Pd mixed oxide and a Cu-exchanged in L-zeolite. Both catalysts show a similar behavior under reduction yielding only one zero valence phase, a Cu-Pd alloy. Yoshida et al. measured XANES spectra of silica-supported vanadium oxide catalysts. They found that the XANES spectrum of 11.6 wt% V_2O_5/SiO_2 consists of two components, V_2O_5 microcrystals and VO_4 species. They concluded that 60% the vanadium atoms are present in V_2O_5 microcrystals and the rest is present in VO_4 tetrahedra on 11 wt% V_2O_5/SiO_2 [50].

1-4. Effects of adsorbed hydrogen on XANES

As noticed previously, interaction of an adsorbed molecules that changes the density of states at the Fermi level is expected to exert a marked influence on the white line [51-53]. These changes may depend upon the electronic state of Pt whether the the sorbed molecules donate electrons to the metal or withdraw electrons from it. We can, therefore, use the sorption-induced changes in the white line to monitor the interaction between the sorbed molecule and the metal particle, on the other hand traces of sorbed molecules might influence the XANES of reduced metals and need to be taken into account.

It has been known that Pt $L_{2,3}$-edge XANES spectra for highly dispersed supported Pt particles is broadened at higher energy side of white line by hydrogen adsorption. Samant et al. reported a decrease of the Pt white line of the L_3 XANES, when sorbed hydrogen hydrogen was removed at low temperatures [54] (Fig. 1-7, 1-8). This was primarily attributed to the creation of an unoccupied antibonding state above the Fermi level due to the Pt-H bond. Lytle et al. reported that when L_3-edge XANES for 1wt% Pt catalyst were measured in H_2, the peak appears in the difference spectra obtained by subtracting the high-temperature measurement (773 K) from each of the other spectra [55]. They found that this peak diminished gradually with temperature and this trend is the same either with increasing or decreasing temperature. They reported that the effect was present for both Pt L_2-and L_3-edges and was present in both H_2 and He. They concluded that this is due to making and breaking Pt-O bonds to the support and assigned this peak to transition to the antibonding orbitals of Pt-O bonds. Boyanov et al. examined the effects of Brønsted acidity on the spatial structure and electronic properties of platinum clusters supported on zeolite Y with EXAFS and XANES and X-ray photoelectron spectroscopy (XPS) [56, 57]. They also reported similar change in XANES difference spectra and claimed that XANES modifications are not caused by charge transfer between the metal cluster. They proposed that this modifications are caused by creation of unoccupied antibonding levels above the Fermi level of the supported metal. Vaarkamp

et al. measured XANES spectra for reduced Pt/K-LTL catalysts [58]. They observed that the white line intensity decreases with increasing reduction temperature. They concluded that this change in white line was ascribed to the removal of hydrogen from metal-support interface by reduction at high temperature [20, 59]. Reifsnyder et al. investigated hydrogen chemisorption on small silica-supported Pt clusters using in -situ EXAFS spectroscopy and XANES spectroscopy [60]. They also observed that a hydrogen-related $L_{2,3}$ XANES feature at 9 eV appears with nearly equal intensity at each other. They assigned this peak to electronic transition from Pt 2p levels to H 1s-Pt 5d antibonding states with mixed $d_{3/2}$-$d_{5/2}$ character. Similar change has also been reported on Pt particles in fuel cell electrodes, induced by electrochemically generated hydrogen [61, 62].

As described above, the origin of the broadening of the peaks in Pt $L_{2,3}$ XANES has been discussed in terms of several mechanisms involving the metal-support interaction, Pt-hydrogen antibonding, and the multiple scattering induced by hydrogen adsorption. Although, the origin of this broadening of the peaks is still not clarified, if the change of the XANES spectra has a direct correlation with the amount of adsorbed hydrogen, it can be expected that we have a new way to characterize adsorbed hydrogen on Pt particles particularly under in situ conditions at least compatible with the catalytic reactions.

1-5. The aim and strategy in this thesis

As mentioned in 1-1, I have investigated the change of XANES spectra by hydrogen adsorption for supported metal particles.

I thought that XANES spectroscopy has a potential to be a new method for characterization to hydrogen adsorbed on surfaces because hydrogen adsorption on small Pt particles causes change in Pt L edge XANES spectra as referred in 1-4. But it should be confirmed to quantitative analysis that what parameter affects to this change ; support, particle size, coverage of hydrogen, coadsorbates.

I tried to overcome them by measuring XANES spectra for dispersion-varied Pt particles supported on several metal oxides with and without adsorbed hydrogen. The results are presented in Chapter 3. Because catalytic reactions occur in the presence of other gas components. Thus the effect of coadsorption on the XANES spectra is an important factor. In the study of CO-H coadsorbed system, I have found that the peak appeared in CO-H adsorbed system was deconvoluted to two components due to adsorbed hydrogen and CO by a linear least-square fitting technique. Further, it was found that the fitting coefficient with respect to adsorbed hydrogen was proportional to the amount of adsorbed hydrogen, and the results appear in Chapter 4.

In Chapter 3, I have investigated XANES spectra in detail, and found general relation between hydrogen-induced feature and amount of adsorbed hydrogen. Further, I have measured L-edge XANES spectra for supported Pd particles to examine whether this change appears in the spectra of other metal particles. These results are presented in Chapter 4.

In conclusion remarks, I would like to consider the future vision in application of XANES to surface characterization, and to summarize my work as well.

References

1. J. M. Thomas and W. J. Thomas, *Principles and practice of Heterogeneous catalysis*. Weinheim: VCH, 1996.

2. G. C. Bond, *Heterogeneous catalysis: principles and applications*. Oxford: Clarendon Press, 1987.

3. K. Christmann, *Surf. Sci. reports*, **9**, 1(1988).

4. Z. Paal and P. G. Menon, *Hydrogen Effects in Catalysis*. New York: Marcel Dekker, 1988.

5. I. Toyoshima and G. A. Somorjai, *Catal.Rev.Sci.Eng*, **19**, 105(1979).

6. G. Kleinle, V. Penka, R. J. Behm, G. Ertl, and W. Moritz, *Phys. Rev. Lett.*, **58**, 148(1987).

7. L. P. Nielsen, F. Besenbacher, E. Laegsgaard, and Stensgaard, *Phys. Rev.*, **B44**, 13156(1991).

8. H. Yoshitake and Y. Iwasawa, *J. Catal.*, **131**, 276(1991).

9. H. Yoshitake and Y. Iwasawa, *J. Phys. Chem.*, **95**, 7368(1991).

10. H. Yoshitake and Y. Iwasawa, *J. Phys Chem.*, **96**, 1329(1992).

11. M. A. Vannice and C. Sudhakar, *J. Phys. Chem.*, **88**, 2429(1984).

12. S. Taniguti, Y. Mori, T. Hattori, and Y. Murakami, *J. Chem. Soc.,Faraday Trans. 1*, **85**, 3135(1989).

13. J. L. Robbins and E. Marucchi-Soos, *J. Phys. Chem.*, **93**, 2885(1989).

14. C. S. Keller and A. T. Bell, *J. Catal.*, **75**, 251(1982).

15. C. H. Bartholomew, "Role of hydrogen in CO hydrogenation," in *Hydrogen Effects in Catalysis*, Z. Paál and P. G. Menon, Eds. New York: Marcel Dekker, 1988.

16. J. E. Demuth, *Surf. Sci.*, **65**, 369(1977).

17. W. Brenig and D. Menzel, *Desorption Induced by Electron Transitions, DIET II*,. Berlin: Spring-Verlag, 1985.

18. P. G. Menon, "Hydrogen as a tool for characterization of catalyst surfaces by chemisorption, gas titration, and Temperature-Programed techniques," in *Hydrogen Effects in Catalysis*, Z. Paál and P. G. Menon, Eds. New York: Marcel Dekker, 1988.

19. S. Tsuchiya, Y. Amenomiya, and R. J. Cvetanovic, *J. Catal.*, **19**, 245(1970).

20. J. T. Miller, B. L. Meyers, F. S. Modica, G. S. Lane, M. Vaarkamp, and D. C. Koningsberger, *J. Catal.*, **143**, 395(1993).

21. L. H. Little, A. V. Kiselev, and V. I. Lygin, *Infrared spectra of adsorbed species*. London: Academic Press, 1966.

22. M. W. Urban, *Vibrational spectroscopy of melecules and macromolecules on surfaces*. New York: A Wiley-Interscience publication, 1993.

23. T. Szilágyi, *J. Catal.*, **121**, 223(1990).

24. D. Rouabah, R. Benslama, and J. Fraissard, *Chem. Phys. Lett.*, **179**, 218(1991).

25. M. A. Chesters, A. Dolan, D. Lennon, D. J. Williamson, and K. J. Packer, *J. Chem. Soc. Faraday Trans.*, **86**, 3491(1990).

26. M. A. Chesters, K. J. Packer, H. E. Viner, M. A. P. Wright, and D. Lennon, *J. Chem. Soc. Faraday Trans.*, **91**, 2203(1995).

27. M. A. Chesters, K. J. Packer, D. Lennon, and H. E. Viner, *J. Chem. Soc. Faraday Trans.*, **91**, 2191(1995).

28. J. C. J. Bart, *Adv. Catal.*, **34**, 203(1986).

29. Y. Iwasawa, *X-Ray Absorption Fine Structure for Catalysis and surface*. Singapore: World Scientific, 1996.

30. J. C. J. Bart and G. Vlaic, *Adv. Catal.*, **35**, 1(1987).

31. N. Watari and S. Ohnisi, *J. Chem. Phys.*, **106**, 7532(1997).

32. H. Nakamatsu, T. Mukoyama, and H. Adachi, *J. Chem. Phys.*, **95**, 3167(1991).

33. T. Fujikawa, T. Matsuura, and H. Kuroda, *J. Phys. Soc. Jpn.*, **52**, 905(1983).

34. D. Bazin, D. Sayers, J. J. Rehr, and C. Mottet, *J. Phys. Chem.*, **B101**, 5332(1997).

35. A. V. Soldatov, S. Della Longa, and A. Bianconi, *Solid State Comm.*, **85**, 863(1993).

36. M. Nomura, "Measurement of XAFS: instrumentation," in *X-Ray Absorption Fine Structure for*

Catalysis and surface, Y. Iwasawa, Ed. Singapore: World Scientific, 1996, pp. 92.

37. J. Wong, F. W. Lytle, R. P. Messmer, and D. H. Maylotte, *Phys. Rev.*, **B30**, 5596(1984).

38. S. Yoshida and T. Tanaka, "Application s of XANES to Catalyst Characterization: Metal Oxide Catalysts," in *X-Ray Absorption Fine Structure for Catalysis and surface*, Y. Iwasawa, Ed. Singapore: World Scientific, 1996, pp. 304.

39. N. Kosugi, T. Yokoyama, and H. Kuroda, *Chem. Phys.*, **104**, 449(1986).

40. F. W. Lytle, P. S. P. Wei, R. B. Greegor, G. H. Via, and J. H. Sinfelt, *J. Chem. Phys.*, **70**, 4849(1979).

41. J. A. Horsley, *J. Chem. Phys.*, **76**, 1451(1982).

42. A. N. Mansour, J. W. Cook, Jr., and D. E. Sayers, *J. Phys. Chem.*, **88**, 2330(1984).

43. L. F. Mattheiss and R. E. Dietz, *Phys. Rev.*, **B22**, 1663(1980).

44. J. Stöhr and R. Jaeger, *Phys. Rev.*, **B26**, 4111(1982).

45. F. Sette, J. Stöhr, and A. P. Hitchcock, *J. Chem. Phys.*, **81**, 4906(1984).

46. A. P. Hitchcock, S. Beaulieu, T. Steel, J. Stöhr, and F. Sette, *J. Chem. Phys.*, **80**, 3927(1984).

47. J. Stöhr, J. L. Gland, W. Eberhardt, D. Outka, R. J. Madix, F. Sette, R. J. Koestner, and U. Doebler, *Phys. Rev. Lett.*, **51**, 2414(1983).

48. T. Yoshida, T. Tanaka, H. Yoshida, T. Funabiki, S. Yoshida, and T. Murata, *J. Phys. Chem.*, **99**, 10890(1995).

49. M. Fernandez-Garcia, C. Marquez Alvarez, and G. L. Haller, *J. Phys. Chem.*, **99**, 12565(1995).

50. S. Yoshida, T. Tanaka, T. Hanada, T. Hirakawa, H. Kanai, and T. Funabiki, *Catal. Lett.*, **12**, 277(1992).

51. A. Jentys, M. Englisch, G. L. Haller, and J. A. Lercher, *Catal. Lett.*, **21**, 303(1993).

52. B. L. Mojet and D. C. Koningsberger, *Catal. Lett.*, **39**, 191(1996).

53. I. T. Bae and A. Scherson, *J. Phys. Chem.*, **100**, 19215(1996).

54. M. G. Samant and M. Boudart, *J. Phys. Chem.*, **95**, 4070(1991).

55. F. W. Lytle, R. B. Greegor, E. C. Marques, D. R. Sandstrom, G. H. Via, and J. H. Sinfelt, *J. Catal*, **95**, 546(1985).

56. B. I. Boyanov and T. I. Morrison, *J. Phys. Chem.*, **100**, 16310(1996).

57. B. I. Boyanov and T. I. Morrison, *J. Phys. Chem.*, **100**, 16318(1996).

58. M. Vaarkamp, J. T. Miller, F. S. Modica, and D. C. Koningsberger, *Jpn. J. Appl. Phys.*, **32**, 454 (1992).

59. M. Vaarkamp, B. L. Mojet, M. J. Kappers, J. T. Miller, and D. C. Koningsberger, *J. Phys. Chem.*, **99**, 16067(1995).

60. S. N. Reifsnyder, M. M. Otten, D. E. Sayers, and H. H. Lamb, *J. Phys. Chem.*, **B101**, 4972(1997).

61. P. G. Allen, S. D. Conradson, M. S. Wilson, S. Gottesfeld, I. D. Raistrick, J. Valerio, and M. Lovato, *Electrochimica Acta*, **39**, 2415(1994).

62. H. Yoshitake, T. Mochizuki, O. Yamazaki, and K. Ota, *J. Electroanalytical Chem.*, **361**, 229(1993).

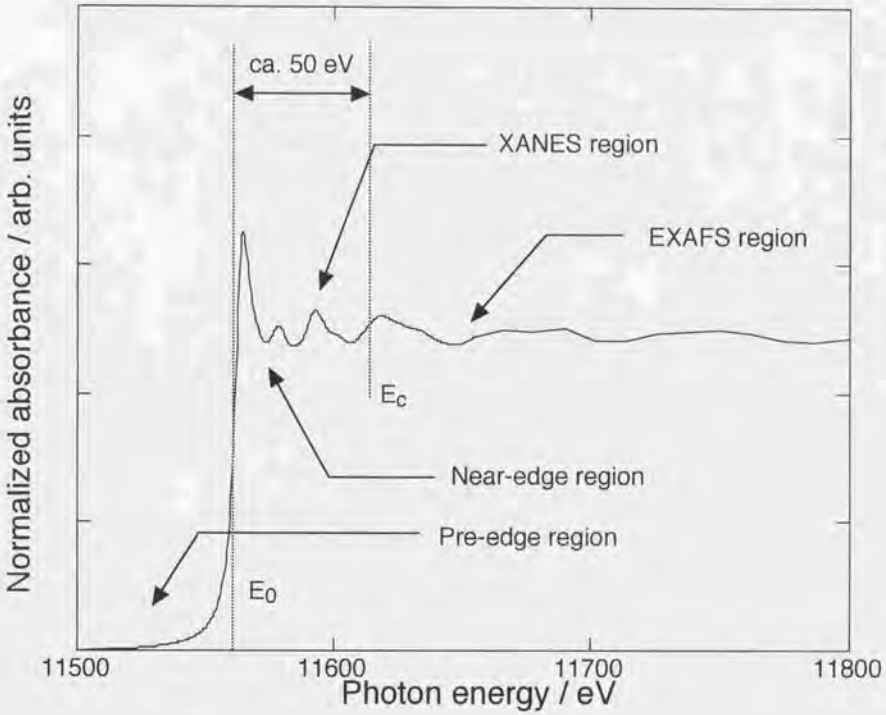

Fig. 1-1. Phenomenological energy ranges in an X-ray absorption spectrum; E_0 is the threshold energy for photoemission, E_c is the energy where the wavelength of the initially excited photoelectron conforms to the interatomic distance (ca. 50 eV).

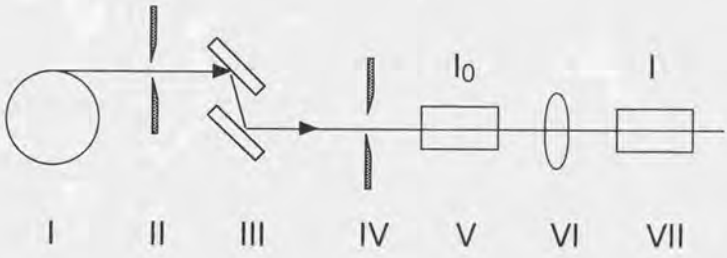

Fig. 1-2. Experimental arrangement for transmisstion measurement at BL-10B at KEK-PF(Japan).
I: synchrotron storage ring; II: entrance slits; III: channel-cut crystal monochromator; IV: exit slits; V: ion-chamber I_0; VI: sample; VII: ion-chamber I.

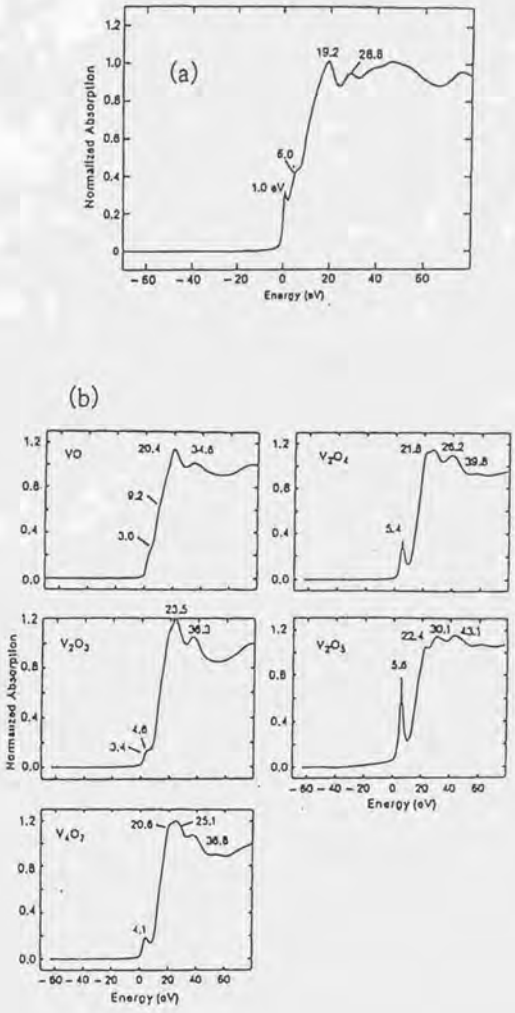

Fig. 1-3. Normalized K-edge XANES spectra of vanadium metal (a) and vanadium oxides (b), the energy taken at 5465 eV (from ref. 37).

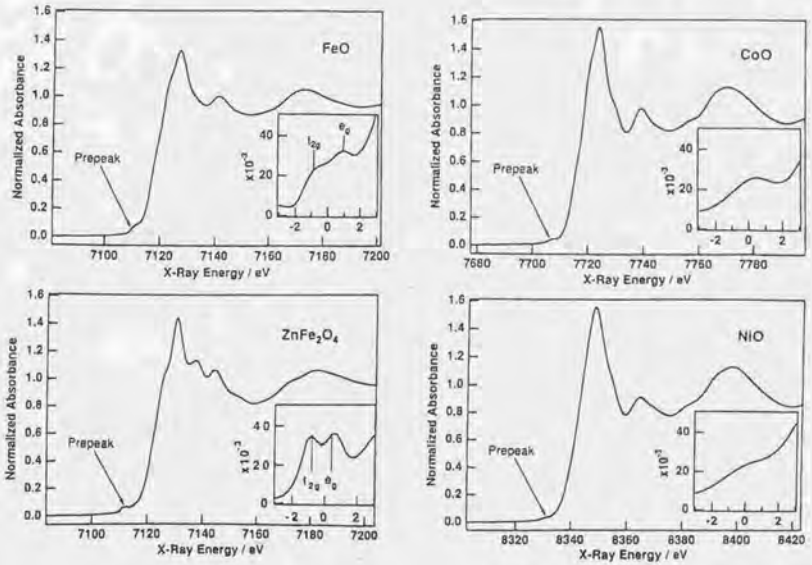

Fig. 1-4. Normalized K-edge XANES spectra of FeO, $ZnFe_2O_4$, CoO and NiO (from ref. 38)

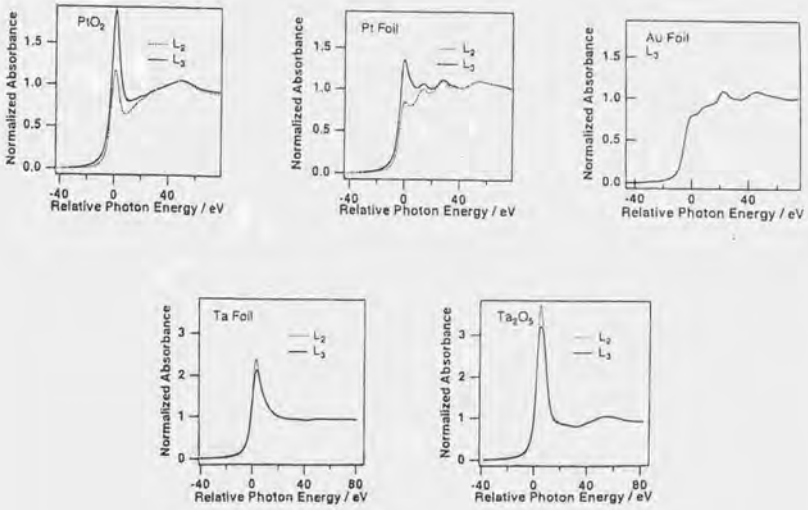

Fig. 1-5. L-edge XANES spectra of platinum oxide, platinum foil, gold foil, tantalum foil and tantalum oxide (from ref. 38)

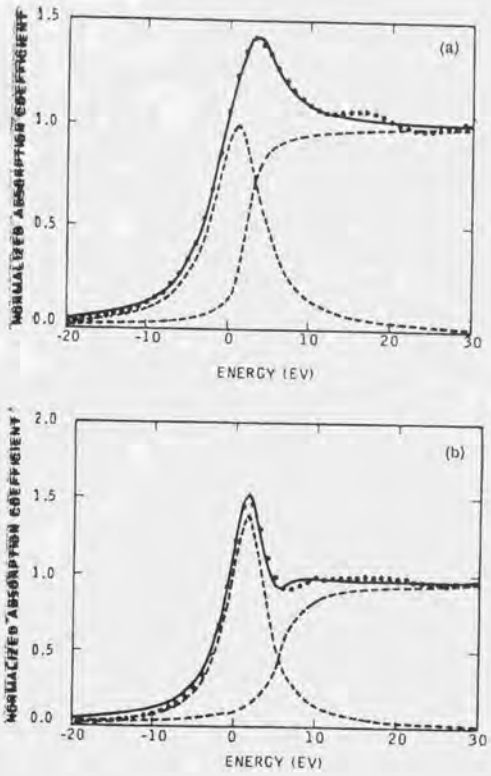

Fig. 1-6. (a) Experimental L_3 threshold resonance for Ir metal (closed circles) together with the fit to the sum of the Lorentzian and step functions. The separate components of this function are also shown. (b) Experimental L_3 threshold resonance for PtI_2 metal (closed circles) together with the fit to the sum of the Lorentzian and step functions (from ref. 41).

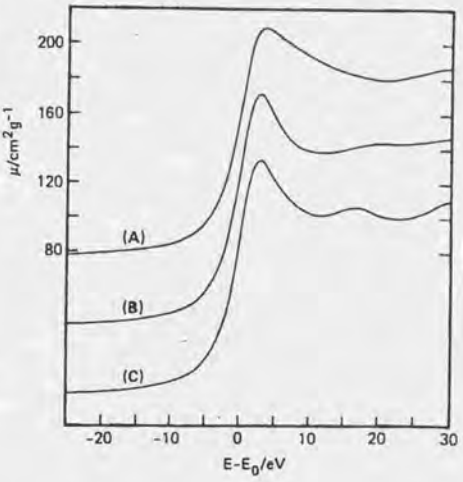

Fig 1-7. XANES around the Pt L_3 absorption edge (E_0 is the position of Pt L_3 absorption edge and m is the mass absorption coefficient): (A) Pt/NaY(H) in dihydrogen, (B) Pt/NaY(H) in helium, (C) Pt foil ; (H) denotes reduction at a conventional temperature of 673 K (from ref. 54).

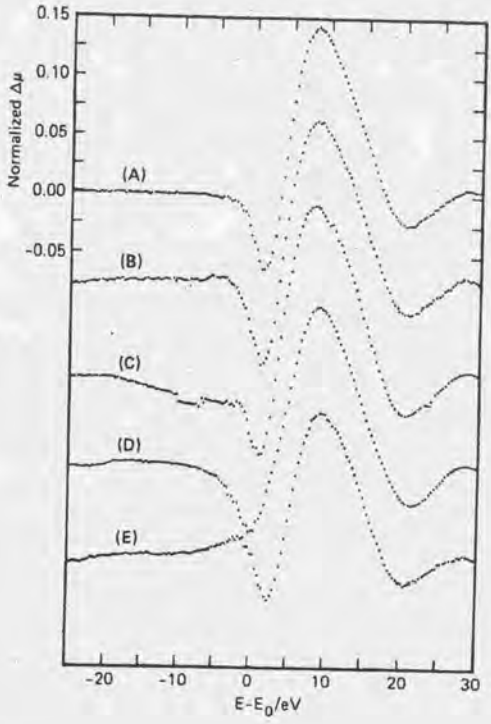

Fig 1-8. Difference spectra for samples in dihydrogen with respect to same sample in helium (E_0 is the position of Pt L_3 absorption edge): (A) Pt/NaY(H), (B) PtCeY(H), (C) Pt/HY(H), (D) Pt/NaY(L), (E) Pt/CeY(L); (H) denotes reduction at a conventional temperature of 673 K and (L) denotes reduction at a lower temperature of 490 K(from ref. 54).

Chapter 2.

Experimental

2-1. Catalyst preparation

2-1-1. Catalyst preparation for Chapter 3-5

SiO_2, Al_2O_3, MgO and TiO_2 were used as supports for Pt particles. Pt/SiO_2 catalysts were prepared by ion-exchange and impregnation methods. In an ion-exchange method $[Pt(NH_3)_4]Cl_2$ was used as precursor to obtain highly dispersed Pt particles on SiO_2. The aqueous solution of SiO_2 (Nippon Aerosil, Aerosil 300; surface area:300 m^2g^{-1}) was regulated to be a pH of 8.6 by adding aqueous solution of NH_3 to exchange proton of hydroxyl group on SiO_2 to ammonium ion. The SiO_2 was impregnated with an aqueous solution of $[Pt(NH_3)_4]Cl_2$ (Soekawa Chemical Co. Ltd.) followed by filtering and water wash until a pH of 7.0. The obtained samples were dried in a oven and calcined at 573 K in a flow of O_2. An impregnation method using aqueous solution of H_2PtCl_6 (Soekawa Chemical Co. Ltd.) was employed to prepare low dispersion Pt/SiO_2 catalysts. The obtained samples were calcined at 673 K in air. For both samples, the Pt loading was regulated to be 1.5 wt%. Pt/Al_2O_3 was prepared by an impregnation method using acetone solution of $Pt(acac)_2$ (Wako Chemical Co. Ltd.) or using triethylamine solution of $Pt(OH)_8$, or using aqueous solution of H_2PtCl_6 followed by calcination at 573-823 K in air, where the calcination temperature was varied to control the size of Pt particles on Al_2O_3 ; the Pt loadings were 0.9-3.1 wt%. Pt/MgO (Pt ; 0.5-1.1 wt%) was also prepared by an impregnation method using acetone solution of $Pt(acac)_2$, followed by calcination at 773 K in air. Pt/TiO_2 was prepared by an impregnation method using aqueous solution of $[Pt(NH_3)_4]Cl_2$ (1.0 wt%).

The samples thus obtained were placed in a U-shaped Pyrex glass tube combined in a closed circulating system, and oxidized with oxygen of 13.3 kPa, followed by reduction with hydrogen of 13.3 kPa and evacuation at given temperatures.

2-1-2. Catalyst preparation for Chapter 6

SiO_2 (Nippon Aerosil, Aerosil 300; surface area:300 m^2g^{-1}) and Al_2O_3 (Nippon Aerosil,

Alon C; surface area: 100 m^2g^{-1}) were used as supports. High dispersion Pd/SiO_2 samples were obtained by an ion-exchange method. In the ion-exchange method, the pH of aqueous suspensions of SiO_2 was regulated to be 9.1 by adding an aqueous solution of NH_3 in order to exchange protons of hydroxyl groups on SiO_2 by ammonium ions. Then the supports were impregnated with an aqueous solution of $[Pd(NH_3)_4]Cl_2$ (Soekawa Chemical Co.) followed by filtering and washing with water until a filtrate pH becomes 7.0. The obtained samples were dried at 393 K and calcined at 573 K in a flow of O_2. The Pd loading was 1.0 wt%. A high dispersion Pd/Al_2O_3 was obtained by using an impregnation of $[Pd(acac)_2]$ (Hacac=acetylaceton) acetone solution with Al_2O_3, which was then dried at 393 K and calcined at 573 K. An impregnation method using an aqueous solution of $Pd(NO_3)_2$ was employed to prepare low dispersion Pd/SiO_2 and Pd/Al_2O_3 samples followed by calcination at 673 K in air.

The samples thus obtained were placed in a U-shaped Pyrex glass tube combined in a closed circulating system, and calcined with oxygen of 13.3 kPa at 573 K, followed by reduction with hydrogen of 13.3 kPa and evacuation at temperatures given in table 1.

2-2. Adsorption measurements

2-2-1. Adsorption measurements for Chapter 3-5

The amount of hydrogen adsorbed on the Pt particles was determined from irreversible adsorption at 293 K using vacuum system shown in Fig. 2-1. The dispersion of the Pt particles is defined as the amount of adsorbed hydrogen atoms divided by the amount of Pt atoms involved in the catalyst (H/Pt). The Pt dispersion was controlled by changing temperature and duration of the treatment. I also estimated total amount of adsorbed hydrogen from irreversible and reversible adsorption.

2-2-2. Adsorption measurements for Chapter 6

The amounts of adsorbed hydrogen and CO relative to Pd atoms in the particles (H_{ad}/Pd and CO/Pd) were determined from irreversible uptakes of hydrogen and CO at 293 K using vacuum system shown in Fig. 2-1, respectively. The method proposed by Boudart et al [1] was adopted for the adsorption measurement of hydrogen on Pd particles. The hydrogen uptake was measured at $P(H_2)$=13.3 kPa. The equilibrium pressure was determined when no change in the H_2 pressure was observed for more than 1 h. After the first hydrogen adsorption measurement, the system was evacuated for 1 h at room temperature. During the evacuation at room temperature, absorbed hydrogen was removed, while the adsorbed hydrogen remained on the surface. Then the second hydrogen uptake was measured and the irreversible hydrogen uptake was regarded as the difference of the two values. Chemisorbed CO was also measured similarly. The ratio of absorbed hydrogen to Pd in the particles was estimated by the second hydrogen uptake measurement at room temperature because the absorbed hydrogen was removed by the evacuation at room temperature [1, 2].

2-3. XAFS measurements and analysis

2-3-1. XANES measurements and analysis for Chapter 3-5

Pt L_3-edge XANES spectra were measured at BL-10B in the Photon Factory in Institute of Materials Structure Science, High Energy Accelerator Research Organization(KEK-IMSS-PF) , operated at 2.5 GeV, 350-250 mA, in a transmission mode. The synchrotron radiation was monochromatized by a Si(311) channel-cut monochromator at BL-10B. The estimated energy resolution near Pt $_{2,3}$-edge was about 1.4 eV. The energy was calibrated by setting the inflection position of L_3-edge of Pt foil to 11563 eV. The incident and transmitted X-ray intensities were detected by ion chambers filled with N_2 gas for I_0 and with N_2/Ar=85/15 mixed gas for I. The voltages applied to electrodes were 500 V.

The sample treated in the closed circulating system shown in Fig. 2-1 was transferred to a cell with two Kapton windows without contacting air. The XANES spectra of the supported Pt particles were measured under vacuum, under 8.0 kPa of hydrogen and then evacuated for 30 min at room temperature. I also measured Pt L-edge XANES of Pt/SiO_2 catalyst in heating condition with hydrogen. Sample was reduced using in-situ cell at 573 K, then sample was cooled at room temperature. After XANES measurement at room temperature, sample was heated stepwise and spectra were measured at each temperature.

In CO-H coadsorbed system, the sample treated in a closed circulating system was exposed to given pressures of CO (0.6-3.1 kPa, volume was 19.0 cm^{-3}) for 1 h to obtain various CO coverages. The sample was transferred to a XANES cell with two Kapton windows without contacting air. The XANES spectra of the supported Pt particles with preadsorbed CO were first measured in vacuum, then the CO-preadsorbed sample was exposed to 8.0 kPa of hydrogen for 30 min. The gas phase analysis showed no desorption of CO by the admission of H_2. After evacuating the sample for 30 min at room temperature the XANES measurement was carried out. The normalized XANES spectra were obtained by subtracting the pre-edge background from the raw data with a modified Victoreen's equation using " Rigaku EXAFS (REX)". Then spectra were normalized by the edge height of estimated by a cubic spline method.

2-3-2. XANES measurements and analysis for Chapter 6

Pd L_3-edge XANES spectra were measured in a fluorescence mode at BL-11B of Photon Factory in Institute of Materials Structure Science, High Energy Accelerator Research Organization(KEK-IMSS-PF). The storage ring was operated at 2.5 GeV and the ring current was 300 mA. The synchrotron radiation was monochromatized by a Ge(111) double-crystal monochromator [3]. The higher harmonics were eliminated using a Ni coated total reflection

mirror. The estimated energy resolution near Pd L_3-edge was about 0.7 eV. The fluorescence detection(I_f) was carried out by using a gas-flow proportional counter [4] filled with Kr/C_2H_6 = 90/10 mixed gas. The 1900 V bias was applied to the electrode of the proportional counter. The incoming X-ray (I_0) was monitored by the photocurrent from a metal mesh placed before the samples. The sample was treated in a closed circulating system and transferred to a cell with two Kapton windows (25 μm) without contacting air, then stored in a N_2 filled reservoir till the measurement. Those cells were placed in a high vacuum chamber ($5\text{-}8\times10^{-6}$ torr) which is installed with the fluorescence detector. The XANES spectra of the supported Pd particles were measured under three different conditions, *i.e.*, under vacuum, in the presence of 13.3 kPa of hydrogen, and after subsequent evacuation at room temperature for 1 h, which are denoted as Pd/SiO_2(VAC), $Pd/SiO_2(H_2)$ and Pd/SiO_2(EVAC), respectively. The X-ray absorbance, μt was obtained from collected data If and I_0 by eq.(2-1),

$$\mu t = I_f / I_0 \qquad (2\text{-}1)$$

The pre-edge background subtraction was carried out by extrapolating the data in the preedge region (3096-3165 eV) to higher energy with a straight line and the data was normalized by the edge height. The inflection point of the absorption edge of Pd powder (3172.8 eV) was used for energy calibration. I discriminated between the effects of adsorbed and absorbed hydrogen, using the behavior of absorbed hydrogen that is easily removed by room-temperature evacuation.

2-3-3. EXAFS measurements and analysis for Chapter 6

Pd K-edge EXAFS spectra of Pd/SiO_2 samples were measured at BL-10B in the Photon Factory in a transmission mode at room temperature. The synchrotron radiation was monochromatized by a Si(311) channel-cut monochromator at BL-10B. The estimated energy resolution near Pd K-edge was about 7 eV. The incident and transmitted X-ray intensities were detected by ion chambers filled with Ar gas for I_0 and with Kr gas for I. The voltages applied to

electrodes were 500 V. The EXAFS data were analyzed using the Rigaku EXAFS (REX). The analysis involves preedge extrapolation, background removal by a spline smoothing method to extract EXAFS oscillation [5]. Then EXAFS data were Fourier transformed from k space (30-140 nm^{-1}) to r space. An inversely Fourier transformation was performed in the range of 0.17-0.30 nm to filter out the Pd-Pd first nearest neighbor contribution. The data were analyzed by a curve fitting procedure to obtain the coordination number N, bond distance r and Debye-Wallor factor σ, E_0 using eq. (2-2) and (2-3).

$$\chi(k_j') = \Sigma N_j F(k_j') \exp(-2k_j'^2 \sigma_j^2) \sin(2k_j' R_j + \phi(k_j')) / k_j' R_j^2 \qquad (2\text{-}2)$$

where k is a wave number of photoelectron and is expressed by eq.(3).

$$k_j' = (k_j^2 - 2m \Delta E_{0j} / h^2)^{1/2} \qquad (2\text{-}3)$$

where m is a mass of electron, and E and E_0 are X-ray photon energy and threshold energy for photoemission, respectively. The backscattering amplitude F(k) and phase shift $\phi(k)$ for Pd-Pd bond were extracted from the EXAFS data of Pd foil with r(Pd-Pd)=0.276 nm and N=12. σ and E_0 are tentatively set to 0.006 nm and 0 eV. Degree of fitting was estimated by R factor (R_f) described below.

$$R_f = \Sigma | k^3\chi^{obs}(k) - k^3\chi^{calc}(k) |^2 / \Sigma | k^3\chi^{obs}(k) |^2 \qquad (2\text{-}4)$$

2-4. IR measurements

FT-IR spectra were measured using JIR-7000 (JEOL) in a transmission mode. An in-situ IR cell was connected to a closed circulating system and gas phase adsorption was subtracted by double beam mode using one more cell. Pt/SiO_2 were pressed to self-supporting disk, and set in IR cell. The IR spectra of the supported Pt particles were measured under the same condition as XANES measurement. The resolution of IR spectra were always 2 cm^{-1}. IR spectra of adsorbed CO were obtained by subtracting spectra of CO-free Pt/SiO_2 from one of CO adsorbed Pt/SiO_2.

2-5. Local Density Functional (LDF) calculation

Using Pt_{13} cluster as model for CO-H coadsorbed Pt particles I calculated electronic state of Pt cluster by Local Density Functional (LDF) method. I used Pt_{13} cuboctahedral cluster (O_h symmetry) as model. I calculated four type of adsorbed cluster; with no adsorbates, with 8 hydrogen atoms on 8 triangle faces (O_h symmetry), with one CO molecules on a Pt atom (C_2 symmetry) and with 8 hydrogen atoms and one CO molecules (C_2 symmetry). Details of the calculation are described in previous paper [6].

References

1. J.E. Benson, H. S.Hwang, and M. Boudart, *J.Catal.*, **30**, 146(1973).

2. A. L. Bonivardi and M. A. Baltans, *J.Catal.*, **138**, 500(1992).

3. T. Ohta, P. M. Stefan, M. Nomura and H. Sekiyama, *Nucl. Instrum. Method*, **A246**, 373(1986).

4. M. Funabashi, T. Ohta, T. Yokoyama, Y. Kitajima and H. Kuroda, *Rev.Sci.Instrum*, **60**, 2505(1989).

5. K. Asakura, in "X-ray Absorption Fine Structure for Catalysts and Surfaces", ed by Y. Iwasawa, World, Scientific,Singapore(1996), Vol. 2, p33.

6. N. Watari and S. Ohnisi, *J. Chem. Phys.* **106**, 7532(1997).

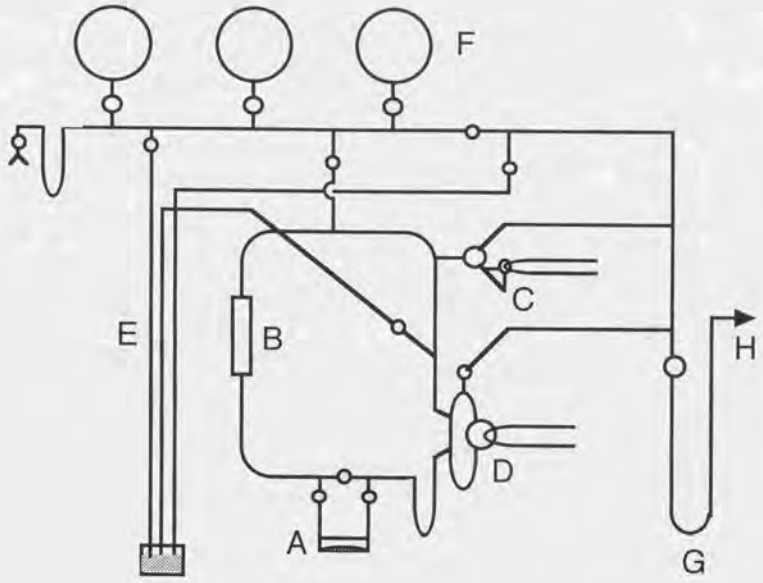

Fig. 2-1. A vacuum system for catalyst treatment and adsorption experiment in Chapter 3-6:
A, catalyst bed; B, circulating pump; C, gas sampler 1; D, gas sampler 2; E, Hg manometer; F, gas reservoirs; G, to diffusion pump; H, main liq. N_2 trap

Chapter 3.

A new method for quantitative characterization of adsorbed hydrogen on Pt particles by means of Pt L-edge XANES

3-1. Introduction

Hydrogen which dissociatively adsorbs on many metal surfaces is involved in important catalytic processes such as hydrogenation, hydrogenolysis, hydrotreating, hydroformylation and so on [1]. However, the quantitative analysis of hydrogen atoms adsorbed on metal surfaces seems to be still difficult because of the small electron density and high mobility on the surfaces [1-3]. Photoelectron spectroscopies like UPS and electron stimulated desorption (ESD) which work under ultra high vacuum are not applicable to the observation of hydrogen in situ under the conditions relevant to catalytic reactions [3,4]. Temperature programmed desorption (TPD) is a typical analysis method for adsorbed hydrogen [5,6], but, the TPD is also unable to investigate adsorbed hydrogen in situ under the conditions.

Pt L_2 and L_3-edge XANES for Pt particles has extensively been studied by Lytle et al., who demonstrated that the area of the first peak (called white line) in the XANES spectra has correlation with the effective charge of Pt atoms [7]. The Pt $L_{2,3}$-edge XANES has also been used to estimate the d-vacancy (d electron density of state) of Pt particles dispersed on inorganic oxide supports [8-10]. Yoshitake et al. showed change in the white line intensities at $L_{2,3}$-edges for Pt particles on SiO_2 by various adsorbates which was related to the catalytic property of the supported Pt particles for hydrogenation reactions of ethene and its derivatives [11,12]. When hydrogen adsorbs on highly dispersed Pt particles, the Pt $L_{2,3}$-edge peaks are shifted and broadened to a higher energy side [13-16]. Similar change has also been reported on Pt particles in fuel cell electrodes, induced by electrochemically generated hydrogen [17,18]. The origin of the broadening of the peaks has been discussed in terms of several mechanisms involving the metal-support interaction [13,14], adsorbed hydrogen-originated antibonding orbital [15,16], and subsurface hydrogen [16]. If the

change of the XANES spectra has a direct correlation with the amount of adsorbed hydrogen, I can get a new way to characterize adsorbed hydrogen on Pt particles particularly in situ under the conditions at least compatible with the catalytic reactions. In this chapter I studied the Pt $L_{2,3}$-edge XANES spectra for supported Pt particles with or without adsorbed hydrogen systematically varying dispersion of the Pt particles and the kind of supports. I found a direct correlation between the amount of adsorbed hydrogen and the peak which appears in the difference spectra before and after H_2 adsorption, irrespective of the kind of supports.

3-2. Results and Discussion

Fig. 3-1 shows Pt L_3-edge XANES spectra for the Pt/SiO_2 catalysts with the dispersion (H/Pt) of 1.2 and 0.18 before and after H_2 adsorption at room temperature. The Pt L_3-edge spectrum of Pt/SiO_2 with H/Pt = 1.2 was broadened by the adsorption of H_2. The edge position also shifted to the higher energy side by about 0.6 eV. For the sample with low dispersion of 0.18, the broadening of the white line and the edge shift were smaller as compared to those for the high dispersion sample in Fig. 3-1. To clarify the influence of hydrogen adsorption on the white line, the difference spectra were obtained by subtracting the spectra measured under vacuum from those measured under hydrogen. The new peak appeared in the difference spectra at about 8 eV above the edge as shown in Fig. 3-1. The position of the new peak was independent of the Pt dispersion, while the intensity of the peak reduced with a decrease in the dispersion.

The L_2-edge XANES spectra for the Pt/SiO_2 catalysts with H/Pt = 1.2 and 0.18 were also measured as shown in Fig. 3-2, where the similar feature in the edge region was observed. The new peak in the difference spectra appeared at about 6 eV above the edge by H_2 adsorption. The peak

intensity increased with an increase in the Pt dispersion similarly to the case of the L_3-edge spectra.

To examine the origin of the new peak in the edge region the intensity (peak area) of the 8 eV peak in the L_3-edge XANES difference spectra was plotted against the dispersion (H/Pt) of Pt particles supported on SiO_2 in Fig. 3-3. The intensity of the peak is defined as area of the linear relationship between the peak intensity and the dispersion means that the new peak is ascribed to adsorbed hydrogen. If the origin of the new peaks arises mainly from Pt-H bond formation, we expect that the correlation between the new peak and the dispersion should also be observed with the Pt particles on the other supports. Thus the peak intensities were plotted as a function of the dispersion for the Pt particles supported on Al_2O_3 and MgO in Fig. 3-3. It was found that the plots for SiO_2, Al_2O_3 and MgO are all on the same line, though there are a little deviations of the data from the line. The results demonstrate that the new peaks are directly related to the hydrogen atoms adsorbed on the Pt particles or equivalently to the Pt-H bonding. The similar linear relationship was obtained for the Pt L_2-edge white line peaks.

To further explore the origin of the new peaks the amount of adsorbed hydrogen on the same Pt/SiO_2 catalyst was varied by evacuating the surface saturated with H_2 at different temperatures. The surface of the Pt/SiO_2 catalyst was saturated with hydrogen atoms (H/Pt = 1.2) by H_2 adsorption (8.0 kPa) at room temperature, followed by evacuation at given temperatures ; the procedure was similar to temperature programmed desorption (TPD). The amount of adsorbed H atoms calculated from the TPD analysis was plotted against the evacuation temperature in Fig. 3-4. I measured the XANES spectra at Pt $L_{2,3}$-edges for the catalysts treated under the identical conditions to the TPD. The normalized intensity of the new peak at the L_3-edge was also plotted as a function of the evacuation temperature in Fig. 3-4. The peak intensity and the amount of

adsorbed hydrogen were normalized to those at room temperature. Both plots showed the same trend against the hydrogen desorption. The results in Fig. 3-3 and Fig. 3-4 reveal that the intensity of the new peak is proportional to the amount of adsorbed hydrogen on the Pt particles. The origin of this peak is not clear, but it may be due to the antibonding orbital of Pt-H bonds [15] or the multiple scattering of adsorbed H atoms with partially negative charge [19,20]. Although we need further investigation for the assignment of the peak, it is to be noted that the L_3-edge peak can be used as a quantitative parameter for the amount of the adsorbed hydrogen on the supported Pt particles in situ under the conditions relevant to catalytic reactions like hydrogen exchange, hydrogenation, hydrogenolysis, etc.

References

1. For example ; Z. Paal and P.G. Menon, Hydrogen Effects in Catalysis, Marcel Dekker, New York, 1988.

2. U.A. Jaysooriya, M.A. Chhesters, M.W. Howard, S.F.A. Kettle, D.B. Powerll and N. Sheppard, *Surface Sci.*, **93**, 526(1980).

3. K. Christmann, *Surf. Sci. reports*, **9**, 1(1988).

4. W. Brenig and D. Menzel, Desorption Induced by Electron Transitions, DIET II, Spring-Verlag, Berlin, 1985.

5. S. Tsuchiya, Y. Amenomiya and R.J. Cvetanovic, *J. Catal.*, **19**, 245(1970).

6. J.T. Miller, B.L. Meyers, F.S. Modica, G.S. Lane, M. Vaarkamp and D. C.Koningsberger, *J. Catal.*, **143**, 395(1993).

7. F.W. Lytle, P.S.P. Wei, R.B. Greegor, G.H. Via and J.H. Sinfelt, *J. Chem. Phys.*, **70**, 4849(1979).

8. D.R. Short, A.N. Mansour, J.W. Cook Jr., D.E. Sayers and J.R. Katzer, *J. Catal.*, **82**, 299(1983).

9. A.N. Mansour, J.W. Cook, and D.E. Sayers, *J. Phys. Chem.*, **88**, 2330(1984).

10. J.A. Horsley, *J. Chem. Phys.*, **76**, 1451(1982).

11. H. Yoshitake and Y. Iwasawa, *J. Phys. Chem.*, **96**, 1329(1991).

12. H. Yoshitake and Y. Iwasawa, *J. Catal.*, **131**, 276(1991).

13. F.W. Lytle, R.B. Greegor, E.C. Marques, D.R. Sandstrom, G.H. Via and J.H. Sinfelt, *J. Catal.*, **95**, 546(1985).

14. M. Vaarkamp, J.T. Miller, F.S. Modica, G.S. Lane and D.C. Koningsberger, *Jpn. J. Appl. Phys.*, **32-2**, 454(1993).

15. M.G. Samant and M. Boudart, *J. Phys. Chem.*, **95**, 4070(1991).

16. N. Ichikuni and Y. Iwasawa, *Catal. Lett.*, **20**, 87(1993).

17. H. Yoshitake, T. Mochizuki, O. Yamazaki and K. Ota, *J. Electroanal. Chem.*, **361**, 229(1993).

18. P.G. Allen, S.D. Conradson, M.S. Wilson, S. Gottesfeld, I.D. Raistrick, J. Valerio and M. Lovato, *Electrochim. Acta*, **39**, 2415(1994).

19. A.V. Soldatov, S. Della Longa and A. Bianconi, *Solid State Commun.*, **85**, 863(1993).

20. T. Matsuura, T. Fujikawa and H. Kuroda, *J. Phys. Soc. Jpn.*, **52**, 3275(1983).

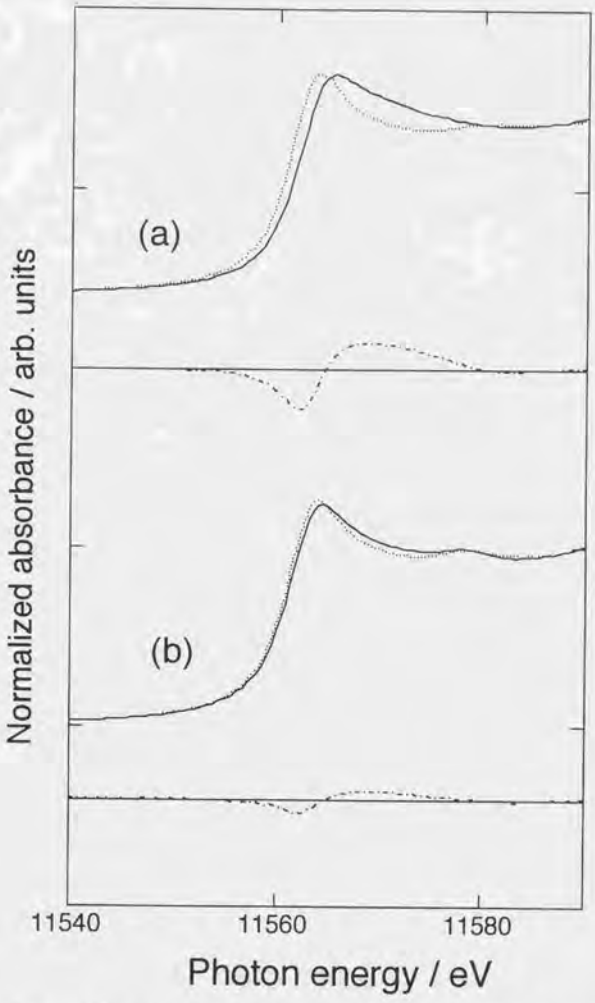

Fig. 3-1. Normalized Pt L_3-edge XANES spectra under vacuum (.....) and 8.0 kPa of H_2 (——) , and the difference spectra (–·–·–) ; (a) dispersion (H/Pt) = 1.2, (b) H/Pt = 0.18.

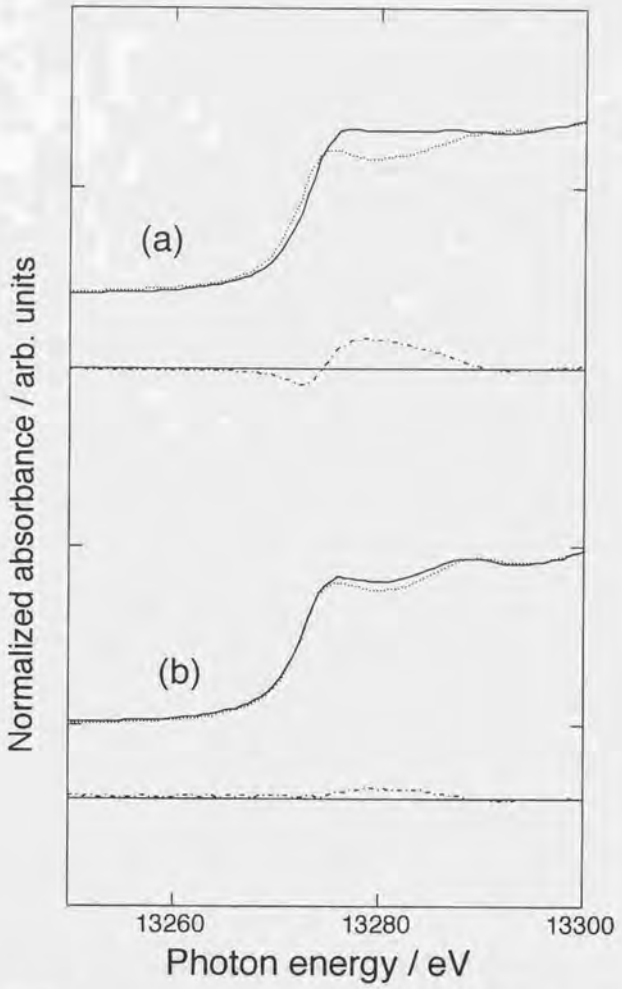

Fig. 3-2. Normalized Pt L_2-edge XANES spectra under vacuum (.....) and 8.0 kPa of H_2 (——) , and the difference spectra (–·–·–) ; (a) dispersion (H/Pt) = 1.2, (b) H/Pt = 0.18.

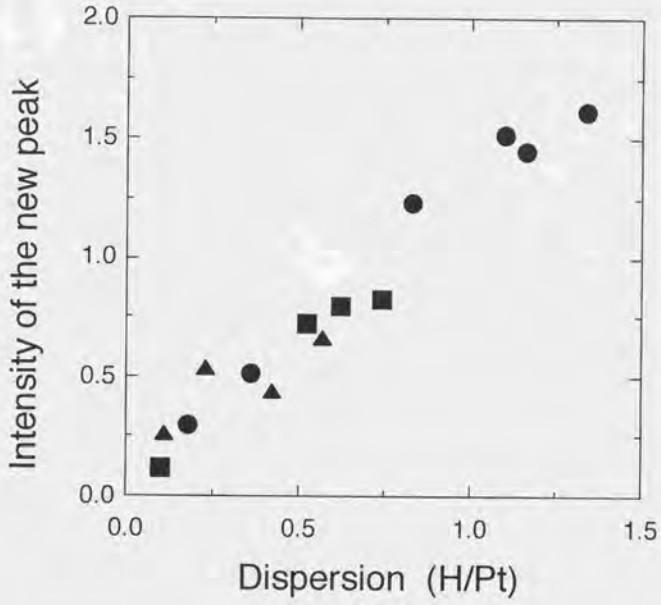

Fig. 3-3. Plots of the intensity of the new peak at the Pt L_3-edge against H/Pt for SiO_2 (●), Al_2O_3 (■), and MgO (▲).

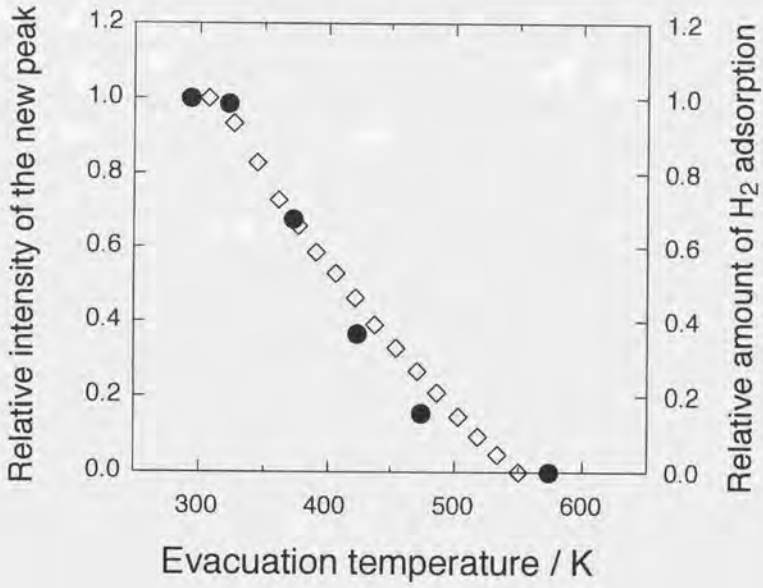

Fig. 3-4. Plots of the relative intensity of the new peak (●) and the relative amount of adsorbed hydrogen (◇) as a function of evacuation temperature for the Pt/SiO_2 catalyst with H/Pt = 1.2.

Chapter 4.

Quantitative analysis of hydrogen adsorbed on Pt particles on SiO_2 in the presence of coadsorbed CO by means of L_3-edge X-ray absorption near-edge structure spectroscopy

4-1. Introduction

Hydrogen plays an important role in metal catalysis for many industrial processes such as hydrogenation, hydrogenolysis, dehydrogenation and isomerization, and hence quantitative analysis of adsorbed hydrogen is a key issue for understanding reaction mechanisms and developing new catalytic systems [1]. Surface hydrogen not only behaves as a reactant itself but also alters reaction paths through the induction of surface reconstruction or the production of different reaction intermediates [1-4]. However, it is rather difficult to characterize the adsorbed hydrogen especially in situ under reaction conditions because hydrogen has a low electron density and high mobility on the surface. In-situ NMR and FT-IR have been only tools to be used for the characterization of adsorbed hydrogen [5-7]. However, the data analysis of solid-state NMR is not easy and the sensitivity of FT-IR is not high enough for surface hydrogen so that they cannot be routinely used.

In previous chapter, I found a new peak in the difference spectra between Pt $L_{2,3}$-edge XANES before and after H_2 adsorption on Pt particles on oxides [8,9]. This new peak appeared at a definite photon energy independent of the amount of adsorbed hydrogen, the size of Pt particles or clusters, and the kind of supports. Moreover, the peak intensity was proportional to the amount of adsorbed hydrogen. These results demonstrate that the L_3-edge peak can be used as a quantitative scale for the amount of adsorbed hydrogen on the supported Pt particles especially under in situ conditions relevant to catalytic reactions. To develop this method as a practical tool for the quantitative analysis of adsorbed hydrogen under reaction conditions, it is necessary to investigate the behavior of Pt $L_{2,3}$ XANES spectra in coadsorbed systems of H_2 and other reactants such as CO. In this chapter I report Pt L_3-edge XANES spectra of Pt particles coadsorbed with H_2 and CO. It was found that there is a direct correlation between the amount of adsorbed hydrogen and the fitting coefficient which appears in the difference spectra before and after $CO+H_2$ coadsorption.

4-2. Results and Discussion

Fig. 4-1(a) shows Pt L_3-edge XANES spectra for Pt/SiO_2 after CO adsorption, where CO coverages (CO/Pt) were varied in the range 0.10 - 0.51. XANES spectrum for Pt/SiO_2 before CO adsorption is also shown in Fig. 4-1(a). The Pt L_3-edge spectrum of the CO-free Pt/SiO_2 was broadened and shifted to the higher energy side by CO adsorption as reported previously [10,11]. As shown in Fig. 4-1(a), the broadening was enhanced by increasing CO coverage on the Pt particles. Interestingly, there is an isosbestic point in the spectra. Fig. 4-1(b) shows the difference spectra derived from Fig. 4-1(a) before and after CO adsorption. A peak appeared at 6 eV above the Pt L_3-edge. The peak position was independent of the CO coverage as shown in Fig. 4-1(b). This value is 2 eV lower than the peak energy induced by adsorbed hydrogen previously reported [8,9]. Fig. 4-2(a) shows the Pt L_3-edge XANES spectra after subsequent exposure of the CO -preadsorbed Pt/SiO_2 to 8.0 kPa of H_2. The CO/Pt values in Fig. 4-2(a) denote the amount of preadsorbed CO per Pt. Comparing Fig. 4-2(a) with Fig. 4-1(a), the edge position shifted to the higher energy side and the white line peak was broadened on the higher energy side upon H_2 adsorption. To clarify this matter I took the difference spectra between the spectra for the $CO+H_2$ coadsorbed Pt/SiO_2 and the spectrum for the fresh Pt/SiO_2 in Fig. 4-2(b). One can find the more broadening of the peak in the difference spectra compared to that in the CO-adsorbed system. The broadening of the difference peak is reasonable because the peak induced by H_2 adsorption appeared at 8 eV above the Pt L_3-edge [8,9]. I first analyzed the difference spectra $\mu d(CO+H)$ between the spectrum for the $CO+H_2$ coadsorbed Pt particles and that for the bare Pt particles by a linear combination of $\mu d(H)$ and $\mu d(CO)$ (eq. 4-1) although there should be broadening of the peak due to interaction of the adsorbed CO and H.

$$\mu d(CO+H) = x \cdot \mu d(CO) + y \cdot \mu d(H) \qquad (4\text{-}1)$$

where μd(CO) and μd(H) denote the difference spectra before and after the mono-adsorptions of H_2 at the coverage of 0.97 and of CO at the coverage of 0.51, respectively (Fig. 4-3(a)). The x and y are the coefficients in the linear combination of two components. Fitting range was chosen in 11566-11595 eV because the difference spectra in the energy region less than 11566 eV are strongly affected by the abrupt change of edge jump. Energy scale of the spectra is not adjusted in the fitting process. The observed difference spectra and the calculated difference spectra according to eq. (1) for the Pt/SiO_2 with different CO coverages are shown in Fig. 4-3(b). Each component in the calculated spectra ($x \cdot \mu d(CO)$ and $y \cdot \mu d(H)$) is also shown in Fig. 4-3(b). The calculated spectra show good agreement with the observed spectra. Thus the peak in the XANES difference spectra at Pt L_3-edge can be deconvoluted to the linear combination of the difference spectra for the CO and H mono-adsorbed systems. It seems that the interaction between adsorbed H and CO affects little on the Pt L_3-edge XANES. Recently, I found the linear relation between the amount of adsorbed hydrogen and the peak height in the difference spectra before and after H_2 adsorption on Pt/oxides (oxides: SiO_2, Al_2O_3, and MgO). Here, to examine whether or not the correlation between the coefficient (y) for μd(H) in the linear combination (eq. (4-1)) and the amount of adsorbed hydrogen exists, the fitting coefficient (y) was plotted as a function of the amount of hydrogen estimated from gas adsorption in Table 1. Fig. 4-4 shows the plots of y vs. H/Pt, where the linear relationship between them is evident. This line has the same slope as that observed in the hydrogen mono-adsorbed system previously reported [8]. These results demonstrate that the fitting coefficient for adsorbed hydrogen (y) in the coadsorbed system is directly related to the number of hydrogen atoms adsorbed on the Pt particles. The fitting coefficient for adsorbed CO (x) also varied nearly linearly

adsorbed on the Pt particles. The fitting coefficient for adsorbed CO (x) also varied nearly linearly with the amount of adsorbed CO in the range of CO coverage 0.10 - 0.51. Although we need further investigation for the whole phenomenon, it is to be noted that the L_3-edge peak can be used as a quantitative measure for the amount of adsorbed hydrogen on the supported Pt particles in coadsorption systems other than CO because the peak in the difference spectra between before and after CO adsorption appears closer to (2 eV) than that for H adsorption case those for several other adsorbates such as NO and C_2H_4 [12]. Thus this technique can be applied to in situ conditions relevant to catalytic reactions involving adsorbed hydrogen. The other point I should mention is the origin for the change of XANES spectra accompanied by adsorption. CO may induce the changes in H adsorption site and in local electronic state of Pt-hydrogen bonding through the delocalization of the Pt-CO charge transfer. The change in spectra due to these CO-induced effects should be too small to be detected by XANES spectroscopy with its finite energy resolution (about 1.5 eV at BL10B in Photon Factory). Consequently the difference spectra in the coadsorbed system reflect the local change of electronic states before and after H_2 adsorption on the Pt atoms with CO preadsorbates. The change in the XANES spectra by adsorption may be caused not only by the Pt-adsorbate electron transfer and the decrease in the electron density of unoccupied d state but also by the change of electronic states due to the formation of Pt-adsorbate bonding.

References

1. For example ; Z. Paal and P.G. Menon, *Hydrogen Effects in Catalysis*, Marcel Dekker, New York, 1988.

2. K. Christmann, *Surf. Sci.* reports, **9**, 1(1988).

3. M.A. Barteau, E.I. Ko and R.J. Madix, *Surf. Sci.*,**102**, 99(1981).

4. G.S. Kellner and A.T. Bell, *J. Catal.*, **75**, 251(1982).

5. M.A. Chesters, K.J. Packer, D. Lennon and H.E. Viner, *J. Chem. Soc. Faraday Trans.*, **91**, 2191(1995).

6. M.A. Chesters, K.J. Packer, H.E. Viner, M.A.P. Wright and D. Lennon, *J. Chem. Soc. Faraday Trans.*, **91**, 2203(1995).

7. T. Szilagyi, *J.Catal.*, **121**, 223(1990).

8. T. Kubota, N. Ichikuni, K. Asakura and Y. Iwasawa, *Chem. Phys. Lett.*, **256**, 445(1996).

9. K. Asakura, T. Kubota, N. Ichikuni and Y. Iwasawa, in "Stud. Surf. Sci.Catal.", ed by J. W. Hightower, W. N. Delgass, E. Iglesia and A. T. Bell, Elsevier Science, Amsterdam(1996), Vol. 101, p911.

10. B.L. Mojet and D.C. Koningsberger, *Catal. Lett.*, **39**, 191(1996).

11. I.T. Bae and A. Scherson, *J. Phys. Chem.*, **100**, 19215(1996).

12. H. Yoshitake and Y. Iwasawa, *J. Phys. Chem.*, **95**, 7368(1991).

Table 4-1. Amounts of adsorbed CO and hydrogen per Pt atom on Pt/SiO_2

CO/Pt	0	0.10	0.24	0.43	0.51
H/Pt	0.97	0.84	0.62	0.43	0.36

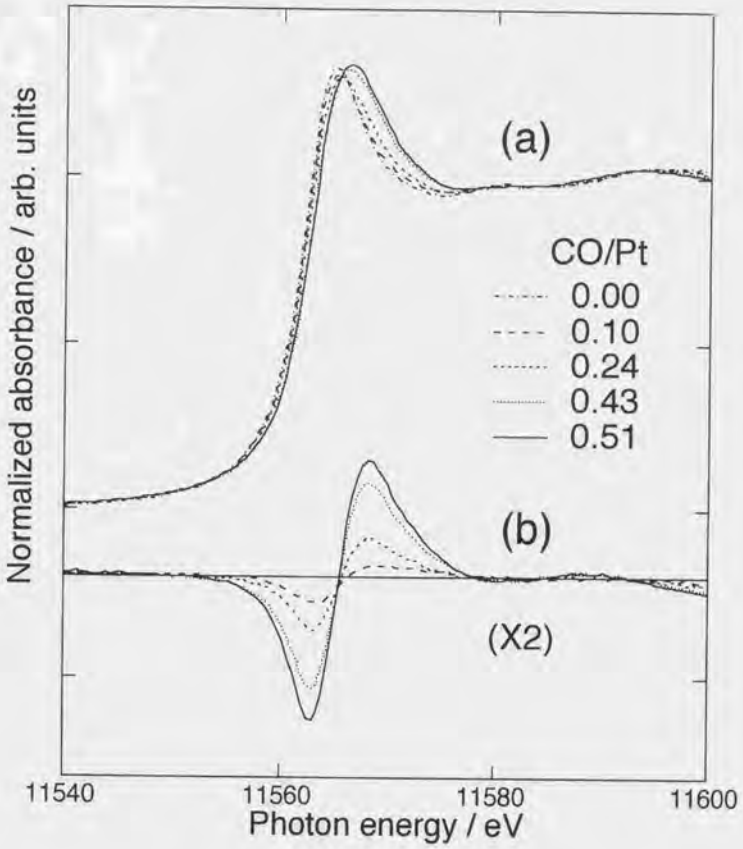

Fig. 4-1. (a) Normalized Pt L_3-edge XANES spectra for CO-preadsorbed and CO-free Pt/SiO_2; (b) difference spectra between them.

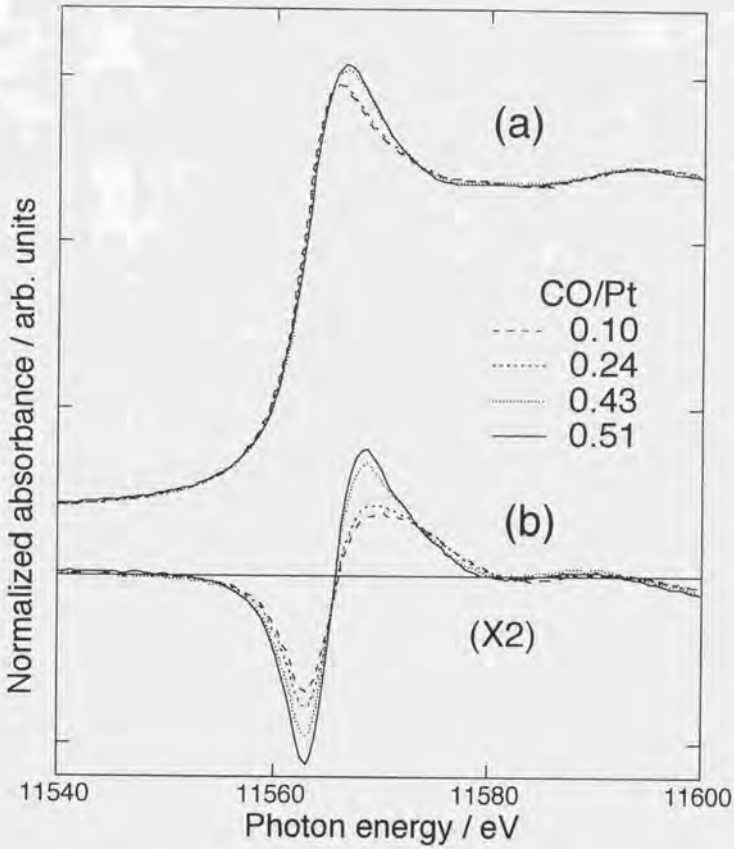

Fig. 4-2. (a) Normalized Pt L_3-edge XANES spectra for $CO+H_2$ coadsorbed Pt/SiO_2; (b) difference spectra obtained by subtracting the CO-free spectra measured in vacuum from spectra (a).

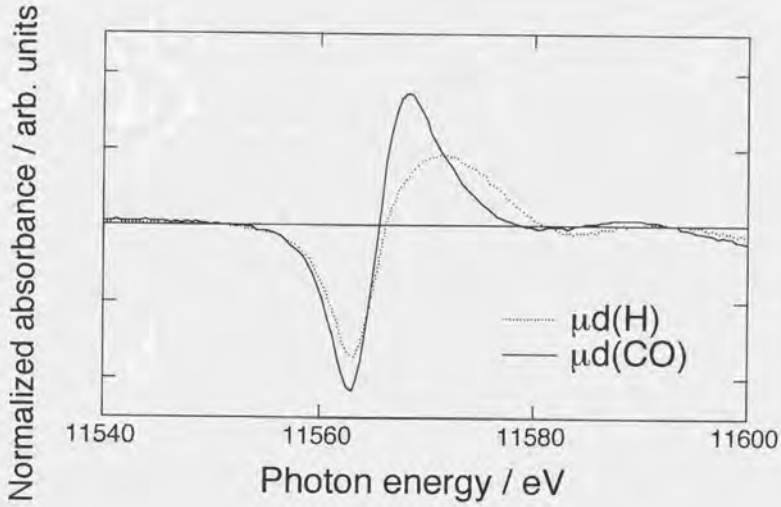

Fig. 4-3(a). Normalized Pt L_3-edge difference spectra before and after the mono-adsorptions of H coverage (0.97) and CO coverage (0.51).

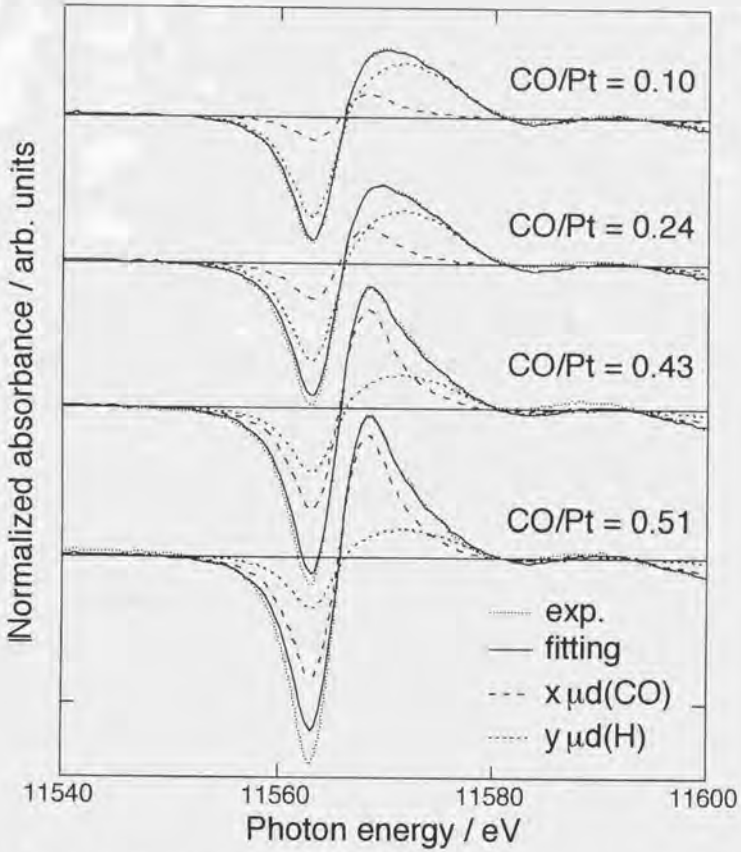

Fig. 4-3(b). Normalized Pt L_3-edge difference spectra measured for $CO+H_2$ coadsorption (solid line) and calculated spectra according to eq.1 (dotted line), and component spectra for the calculation (two kinds of broken line).

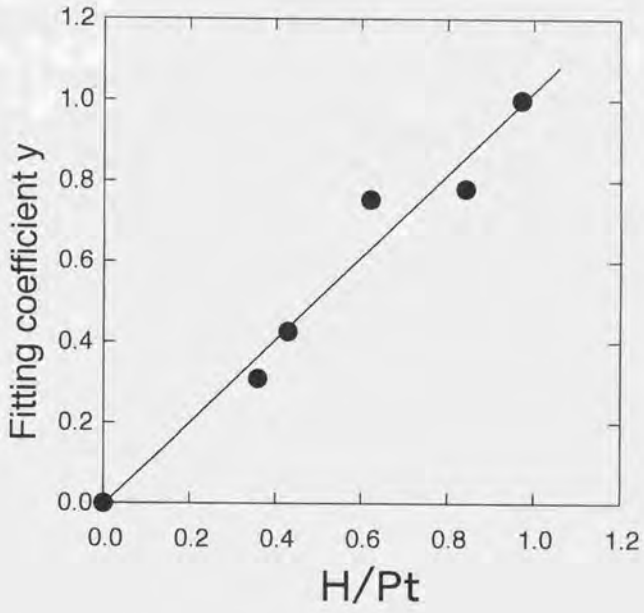

Fig. 4-4. Plots of the fitting coefficients for adsorbed hydrogen as a function of H/Pt.

Chapter 5.

Analysis of $L_{2,3}$-edge XANES spectra for Hydrogen adsorbed Pt Particles on SiO_2 and Quantitative analysis of Adsorbed Hydrogen

5-1. Introduction

Dissociatively adsorbed hydrogen is a important adsorbates in metal catalysis for many industrial processes such as hydrogenation, hydrogenolysis, dehydrogenation and isomerization, and hence quantitative analysis of adsorbed hydrogen is a key issue for understanding reaction mechanisms and developing new catalytic systems [1]. However, it is rather difficult to characterize the adsorbed hydrogen because hydrogen has a low electron density and high mobility on the surface. Usually catalytic reaction is operated under severe condition such as high pressure, and high temperature. So analysis method which can be available in such condition are restricted. In-situ NMR and FT-IR have been only tools to be used for the characterization of adsorbed hydrogen [2, 3, 4, 5]. However, the data analysis of solid-state NMR is not easy because several kind of peaks appear by hydrogen admission [2, 3]. The sensitivity of FT-IR is not so high enough for surface hydrogen [5]. Moreover IR spectra can detect only weakly bounded hydrogen atom, because strongly adsorbed hydrogen occupies three-fold site on Pt surface and its vibrational bands overlap with support absorption for supported Pt particles. So it cannot be routinely used for characterization of adsorbed hydrogen.

X-ray absorption near edge structure (XANES) is explained by the transition from core level to unoccupied valence level or multiple scattering between X-ray absorbing atom and surrounding atoms [6]. It is known that XANES reflects the electronic structure and the local geometrical structure surrounding X-ray absorbing atom, so XANES has been used for the determination of symmetry, bond distance and electronic state around X-ray absorbing atoms using some features appeared, for example, transition to σ^* or π^* state and peak correspond to s->d transition due to quadrupole transition at K-edge XANES [7, 8, 9]. But XANES can not be formulated assuming simple single back scattering like EXAFS oscillation because multiple scattering contribute in

XANES region. So It is still difficult to extract physical parameter from XANES spectra. Quantitative characterization using XANES spectra have been reported for some metal oxides ; for example, in the case of dehydration of $Mg(OH)_2$, TPR of Pd-Cu bimetallic oxide, Ce doping to Nd_2CuO_4 oxide super conductors, and so on [10, 11]. In these cases each measured spectra are represented by summation of some component spectra.

The $L_{2,3}$-edge XANES spectra of transition metal elements with unoccupied d states show a strong adsorption peak just above the absorption edge, called as white line. The white line is assigned to a transition from 2p core level to *n*d unoccupied states, so L-edge XANES has been used to estimate the density of unoccupied d-state of X-ray absorbing atoms. Mansour et al. have suggested the way to estimate vacancy of d-state. This method follow to theory by Ritz and Mattheiss [8, 12, 13]. Thus the XANES spectra have been used to investigate the electronic structure of supported metal catalysts with intensity of white line [14, 15, 16]. Moreover, the large penetration power of X-ray enables us to carry out the XANES measurement in the presence of the reaction gas. Yoshitake et al. found the change of electronic states of Pt particles by the adsorption of various ethylene derivatives systematically by means of the Pt $L_{2,3}$-edge XANES.15]. When hydrogen adsorbs on highly dispersed Pt particles, the Pt $L_{2,3}$-edge peaks are broadened to the higher energy side and the new peak appears at 6-8 eV from the edges in difference spectra obtained by subtracting the spectra in vacuum from the ones with adsorbed hydrogen [16, 17, 18, 19, 20]. Similar change has also been reported on Pt particles in fuel cell electrodes, induced by electrochemically generated hydrogen [21]. The origin of the broadening of the peaks has been discussed in terms of several mechanisms involving the metal-support interaction; for example transition to antibonding orbital between Pt and oxygen of support or interfacial hydrogen between Pt and Oxygen [18, 20], adsorbed hydrogen-originated antibonding orbital [17, 19], and subsurface hydrogen[16].

I reported in previous chapters that peak appears in XANES difference spectra and their intensity is related to amount of adsorbed hydrogen per number of Pt atoms [22, 23, 24]. If the change of the XANES spectra has a direct correlation with the amount of adsorbed hydrogen, we can get a new way to characterize adsorbed hydrogen on Pt particles particularly in situ under the conditions at least compatible with the catalytic reactions. But to apply this method to actual catalytic reaction system, I must investigate more detailed relation between change of XANES induced by hydrogen adsorption and amount of adsorbed hydrogen in several conditions. Further, besides adsorbed hydrogen there are other adsorbates on catalyst surfaces in actual catalytic reactions. So, I must investigate how coadsorbates influence to XANES spectra and peak induced by adsorbed hydrogen.

In this chspter I studied the Pt $L_{2,3}$-edge XANES spectra for supported Pt particles systematically varying coverage of the adsorbed hydrogen and also Pt particles with or without adsorbed hydrogen and varying dispersion and the kind of supports. From these data I discuss origin of this hydrogen-induced feature in Pt L-XANES. Also from experiments of in-situ heating, I demonstrated effectiveness to quantitative analysis of adsorbed hydrogen in the presence of gaseous hydrogen. Furthermore, since it is necessary to investigate the behavior of Pt $L_{2,3}$-XANES spectra in coadsorbed systems of H_2 and other reactants such as CO to develop this method as a practical tool for the quantitative analysis of adsorbed hydrogen under reaction conditions, in this chapter I also report Pt L_3-edge XANES spectra of Pt particles coadsorbed with H_2 and CO. It was found that there is a direct correlation between the amount of adsorbed hydrogen and the fitting coefficient which appears in the difference spectra before and after $CO+H_2$ coadsorption.

5-2. Results

5-2-1. Change in XANES spectra with hydrogen adsorption

Fig. 5-1 shows Pt L_3-edge XANES-TPD spectra for the Pt/SiO_2 catalysts with the dispersion (H/Pt) of 1.2. The surface of the Pt/SiO_2 catalyst was saturated with hydrogen atoms (H/Pt = 1.2) by H_2 adsorption (8.0 kPa) at room temperature, followed by temperature programmed desorption (TPD) from room temperature upto 573 K. The L_2-edge XANES-TPD spectra for the Pt/SiO_2 catalysts with H/Pt = 1.2 were also measured as shown in Fig. 5-2. In L_3- edge hydrogen adsorption change spectra higher side of white line reported previously. Adsorption of higher energy side is broadened compared to spectra of Pt foil. But with increasing evacuation temperature, broadening decreases and the edge position is also shifted to the lower energy side. In L_2-edge, the similar feature around white line region was observed but the edge shift is smaller than L_3-edge. To clarify the influence of hydrogen adsorption on the white line, the difference spectra were obtained by subtracting the spectra measured after after evacuation at 573 K from those measured at each evacuation temperature. The new peak appeared in the difference spectra at about 8 eV above the edge as shown in Fig. 5-1. The position of the new peak was independent of the temperature. While, the intensity of the peak reduced by evacuation at room temperature, then the intensity of the peak reduced with a increase in evacuation temperature. It is considered that the reduced intensity of the peak by evacuation at room temperature is due to desorption of reversible adsorbed hydrogen and following reduction by heating evacuation is due to irreversibly adsorbed hydrogen desorption. So, it is considered that intensity of this new peak is related to amount of adsorbed hydrogen.

To further explore the origin of the new peaks the amount of adsorbed hydrogen, I measured XANES spectra for supported Pt particles using several supports(SiO_2, Al_2O_3, MgO, and TiO_2) in vacuum, in 8.0 kPa of hydrogen and after following evacuation at room temperature respectively.

By varying dispersion of Pt particles, we can obtain spectra with several H/Pt ratio. Fig. 5-3 shows Pt L_3-edge XANES spectra and difference spectra subtracting spectra measured in vacuum for the Pt/SiO_2 catalysts with the dispersion (H/Pt) of 0.97, 0.59 and 0.10 before and after H_2 adsorption at room temperature. The Pt L_3-edge spectrum of Pt/SiO_2 with H/Pt = 0.97 was broadened by the adsorption of H_2. The edge position also shifted to the higher energy side by about 0.6 eV. For the sample with low dispersion of 0.10, the broadening of the white line and the edge shift were smaller as compared to those for the high dispersion sample in Fig. 5-3. It is considered that the reduced intensity of the peak by evacuation at room temperature is also due to desorption of reversible adsorbed hydrogen and following reduction by heating evacuation is due to irreversibly adsorbed hydrogen desorption. The L_2-edge XANES spectra for the Pt/SiO_2 catalysts with H/Pt = 0.97, 0.59 and 0.10 were also measured as shown in Fig. 5-4, where the similar feature in the edge region was observed. The new peak in the difference spectra appeared at about 6 eV above the edge by H_2 adsorption. The peak intensity increased with an increase in the Pt dispersion similarly to the case of the L_3-edge spectra.

To examine the origin of the new peak in the edge region the intensity (peak area) of the 8 eV peak in the L_3 and L_2-edge XANES difference spectra was plotted against the dispersion (H/Pt) of Pt particles supported on SiO_2, in Fig. 5-5(a), (b) respectively. Then in Fig. 5-5(a), (b), the intensity of peak for XANES-TPD was also plotted against the amount of adsorbed H atoms at each evacuation temperature obtained from the TPD analysis. I measured the TPD spectrum for the catalysts treated under the identical conditions to the XANES-TPD spectra at Pt $L_{2,3}$-edges. We can see the linear relationship between the intensity of the peak and the dispersion from Fig. 5-5(a), (b). Furthermore, this linear relation ship hold whether H/Pt ratio is varied by hydrogen coverage or dispersion of Pt particles. These results means that the new peak is ascribed to adsorbed hydrogen. If the origin of

the new peaks arises mainly from Pt-H bond formation, we can expect that the correlation between the new peak and the dispersion should also be observed with the Pt particles on the other supports. Thus the peak intensities were also plotted as a function of the dispersion for the Pt particles supported on Al_2O_3 and MgO and TiO_2 in Fig. 5-5(a), (b). It was found that the plots for SiO_2, Al_2O_3 and MgO and TiO_2 are all on the same line, though there are a little deviations of the data from the line. The results indicate that the new peaks are directly related to the hydrogen atoms adsorbed on the Pt particles or equivalently to the Pt-H bonding. The similar linear relationship was obtained for the Pt L_2-edge white line peaks. These results also indicate that we can estimate amounts of adsorbed hydrogen in the presence of gaseous hydrogen using this linear relation as a calibration curve. So I demonstrated quantitative analysis of adsorbed hydrogen under in-situ condition by XANES spectra. Fig. 5-6 shows Pt L_3-edge XANES spectra measured in 583 kPa of H_2/He = 0.19 gas. Compared with XANES-TPD spectra, spectra are broadened at each temperature In Fig. 5-5 XANES difference spectra are also shown. The peak induced by hydrogen adsorption were appeared and intensity of peak were reduced with temperature increasing. But magnitude of the reduction is small compared to the results of XANES-TPD experiment. This indicates that in hydrogen atmosphere Pt catalysts can adsorb more hydrogen than in vacuum condition. Table 5-1 shows estimated amount of adsorbed hydrogen obtain ed from relation in Fig.4 as a calibration curve. It was demonstrated that XANES can be used as method to quantify amount of hydrogen in the presence of gaseous hydrogen.

5-2-2. XANES spectra for CO and CO+H_2 coadsorbed system

Fig. 5-7(a), 5-8(a) shows Pt $L_{2,3}$-edge XANES spectra for Pt/SiO_2 after CO adsorption, where CO coverages (CO/Pt) were varied in the range 0.10 - 0.51. XANES spectrum for Pt/SiO_2

before CO adsorption is also shown in Fig. 5-7(a), 5-8(a). The Pt $L_{2,3}$-edge spectrum of the CO-free Pt/SiO_2 was broadened and shifted to the higher energy side by CO adsorption. As shown in Fig. 5-7(a), 5-8(a), the broadening was enhanced by increasing CO coverage on the Pt particles. Interestingly, there is an isosbestic point in the spectra. Fig. 5-7(b), 5-8(b) shows the difference spectra derived from Fig. 5-7(a), 5-8(a) before and after CO adsorption. A peak appeared at 6 eV above the Pt L_3-edge. The peak position was independent of the CO coverage as shown in Fig. 5-7(b), 5-8(b). This value is 2 eV lower than the peak energy induced by adsorbed hydrogen previously reported. Fig. 5-9(a), 5-10(a) shows the Pt $L_{2,3}$-edge XANES spectra after introduce of 8.0 kPa of H_2 to CO -preadsorbed Pt/SiO_2 . The CO/Pt values in Fig. 5-7(a), 5-8(a) denote the amount of preadsorbed CO per Pt. Comparing Fig. 5-7(a) with Fig. 5-9(a), the edge position at L_3-edge shifted to the higher energy side and the white line peak was broadened on the higher energy side upon H_2 adsorption. But in L_2-edge, edge shift was not so large compared with L_3-edge. To clarify change due to $CO+H_2$ coadsorption I took the difference spectra between the spectra for the $CO+H_2$ coadsorbed Pt/SiO_2 and the spectrum for the fresh Pt/SiO_2 in Fig. 5-9(b), 5-10(b). One can find the more broadening of the peak in the difference spectra compared to that in the CO-adsorbed system. The more high CO coverage is, the more alike to spectrum of CO mono-adsorption. The more high hydrogen coverage is, the more alike to spectrum of hydrogen mono-adsorption. So, I analyzed the difference spectra $\mu d(CO+H)$ between the spectrum for the $CO+H_2$ coadsorbed Pt particles and that for the bare Pt particles by a linear combination of $\mu d(H)$ and $\mu d(CO)$ (eq. 5-1) although there should be broadening of the peak due to interaction of the adsorbed CO and H.

$$\mu d(CO+H) = x \cdot \mu d(CO) + y \cdot \mu d(H) \qquad (5\text{-}1)\ ,$$

where μd(CO) and μd(H) denote the difference spectra before and after the mono-adsorptions of H_2 at the coverage of 0.97 and of CO at the coverage of 0.51, respectively (Fig. 5-11(a), 5-11(a)). The x and y are the coefficients in the linear combination of two components. Fitting range was chosen in 11566-11595 eV because the difference spectra in the energy region less than 11566 eV are strongly affected by the abrupt change of edge jump. Energy scale of the spectra is not adjusted in the fitting process. The observed difference spectra and the calculated difference spectra according to eq. (5-1) for the Pt/SiO_2 with different CO coverages are shown in Fig. 5-12(a), 5-12(b). Each component in the calculated spectra (x • μd(CO) and y • μd(H)) is also shown in Fig. 5-12(a), 5-12(b) The calculated spectra show good agreement with the observed spectra. R factor using below formula (5-2) were under 5% in all coverages.

$$R_f = \{\Sigma [\mu_{(obs)}-\mu_{(calc)}]^2\}/\{\Sigma[\mu_{(obs)}]^2\} \qquad (5\text{-}2)$$

where $\mu_{(obs)}$ and $\mu_{(calc)}$ denote the difference spectra observed and calculated respectively. Thus the peak in the XANES difference spectra at Pt $L_{2,3}$-edge can be deconvoluted to the linear combination of the difference spectra for the CO and H mono-adsorbed systems. Moreover, the results of deconvoluted and measured difference spectra for CO coverage fixed to CO/Pt=0.20 (and hydrogen coverage were varied) Pt/SiO_2 and hydrogen coverage fixed to H/Pt=0.25 (and CO coverage were varied) Pt/SiO_2 is shown in Fig. 5-13(a), 5-13(b). These results shows that XANES difference spectra for $CO+H_2$ coadsorbed Pt/SiO_2 can be deconvoluted using difference spectra of CO and hydrogen sole adsorbed Pt/SiO_2 irrespective of their coverages. It seems that the interaction between adsorbed H and CO affects little on the Pt $L_{2,3}$-edge XANES because energy scale of the spectra is not adjusted in the fitting process. Hence it can be concluded that these peak induced by hydrogen

and CO are not influenced by each other.. In the previous section, I found the linear relation between the amount of adsorbed hydrogen and the peak intensity in the difference spectra before and after H2 adsorption on Pt/oxides (oxides: SiO_2, Al_2O_3, MgO and TiO_2) . Here, to examine whether or not the correlation between the coefficient (y) for μd(H) in the linear combination (eq. (5-1)) and the amount of adsorbed hydrogen exists, the intensity of peak originated from hydrogen was plotted as a function of the amount of hydrogen estimated from gas adsorption. The intensity of peak was calculated by multiplying the coefficient (y) for μd(H) by intensity of peak for hydrogen. Fig. 5-14(a), 5-14(b) shows the plots of intensity vs. H/Pt, where the linear relationship between them is evident for all hydrogen coverages. And hydrogen coverage was fixed at H/Pt=0.25, then intensity of peak was same for all CO coverages. Moreover, in Fig. 5-14(a), 5-14(b), peak intensity for the hydrogen mono-adsorbed XANES-TPD system previously showed is also plotted. Surprisingly, this line has the same slope as that for CO+H_2 coadsorbed system. These results demonstrate that the deconvoluted hydrogen-induced peak in the coadsorbed system is directly related to the number of hydrogen atoms adsorbed on the Pt particles without influence of coadsorbed CO. On the other hand, the fitting coefficient for adsorbed CO (x) also varied with the amount of adsorbed CO. In Fig. 5-15, the intensity of peak calculated by multiplying the coefficient (x) for μd(CO) by intensity of peak for CO at L_3-edge was plotted. Up to CO/Pt=0.51, intensity of peak shows good linear relationship with amount of CO adsorption, but spectra for saturated CO adsorption has strong intensity and shift to upper side although amount of CO adsorption was not so increased.

5-2-3. IR spectra

To investigate adsorption state of CO on Pt particles, IR spectra for Pt/SiO_2 were measured. Fig. 16 shows FT-IR spectra for Pt particles, after adsorption of CO with indicated

coverages(CO/Pt=0.51, 0.45, 0.30), after evacuation at R. T. and after 100 torr of hydrogen admittion. Peak position of C-O stretching peak (at 2074 cm^{-1}) is little shifted with coverage of CO. After hydrogen admission, C-O stretching peak shifted to lower wave number side. This results indicate absorbing CO is affected by coexistion hydrogen atom contrary to XANES results.

5-2-4. Density functional calculation

Fig. 5-17 shows energy levels of Pt_{13} cluster. s, p, d, f, g and h indicates the partial density of state (DOS) of each molecular orbital projected at the cluster center. DOS plot in Fig. 5-17(a) with no adsorbates shows so-called shell structure as reported before and this indicates Pt_{13} cluster behave as a "giant atom". From Fig. 5-17(b), we can see that this shell structure is preserved by hydrogen adsorption. DOS under 0.40 Hartree are assigned to bonding states between H 1s and Pt 5d and Pt 6s. Above the Fermi level H 1s states only fill the n=3 shell and partially construct the n=4 shell, namely H adsorption gives its 1s states to Pt13 cluster to construct higher order shell. This situation is same in icosahedral Pt_{13} cluster, so shell structure is not sensitive to symmetry of cluster. Fig. 5-17(c) shows partial DOS of CO adsorbed Pt_{13} cluster. Two states assigned to CO 5σ and 4σ appears about 0.5 and 0.6 Hartree respectively. But shell structure is not broken except splits of each states induced by the drop of symmetry from O_h to C_2. Fig. 5-17(d) shows partial DOS of $CO+H_2$ coadsorbed Pt_{13} cluster. Shell structure above -0.5 Hartree is still preserved by $CO+H_2$ coadsorption and CO 5σ and 4σ is little affected by coexistence of adsorbed hydrogen.

5-3. Discussion

I already reported that this hydrogen-induced peak could be related to dispersion of Pt particles. But relation coverage of hydrogen and dispersion of Pt particles was not clear because

these spectra are measured in the presence of H_2 and dispersion was obtained from irreversible adsorbed hydrogen. In this chapter, it was reconfirmed that intensity of peak measured after evacuation was proportional to H/Pt ratio from the comparison between XANES-TPD data and dispersion-varied XANES. This results indicates that with this relation we can estimate amount of hydrogen adsorption in the reaction condition. In practical, from XANES spectra measured in hydrogen heating I estimated amount of hydrogen adsorption using relation in Fig. 5-5. Moreover, results of $CO+H_2$ coadsorption revealed that this relation could be applied by decomvolution even if coadsorbates like CO exist on Pt surface. These results indicates that the L_3-edge peak can be used as a quantitative measure for the amount of adsorbed hydrogen on the supported Pt particles in coadsorption systems other than CO because the peak in the difference spectra between before and after CO adsorption appears closer to (2 eV) than that for H adsorption case those for several other adsorbates such as NO and C_2H_4. Thus this technique can be applied to in situ conditions relevant to catalytic reactions involving adsorbed hydrogen.

The origin of hydrogen induced peak in Pt L-XANES is discussed in some papers using some theoretical method. Watari et al. calculated electronic state of PtI_3 and H_x-Pt_{13} cluster by Local Density Functional (LDF) method [25]. They found hydrogen -induced level appear above Fermi level. They also found electronic state of Pt_{13} cluster form so-called "shell structure" regardless of its structure (octahedron or icosahedron). Hydrogen only provides its 1s states as basis function to Pt_{13} cluster and hydrogen -induced state also form shell structure. They concluded that XANES peak is induced by transition to state which results from high order shell due to hydrogen adsorption which are constructed of H-1s and Pt-6s, 5d states. It is reasonable that this peak is not affected by hydrogen coverage because observed peak in XANES spectra are not affected by size of Pt particles or supports.

Ohtani et al. calculated XANES spectra of Pt_{43} and H_x-Pt_{43} cluster by multiple scattering method [26]. They found that broadening of white line appeared in XANES spectra of hydrogen adsorbed Pt cluster. This hydrogen induced broadening is not sensitive to the hydrogen adsorption site or charge of hydrogen atom. They found that new peak is revealed in calculated XANES difference spectra at 8 eV from the absorption edge. Moreover intensity of this peak is increased with H/Pt ratio. So, these calculation well agree with experimental XANES results here. I have also found that hydrogen adsorbed Pd small particles shows similar change in Pd L-XANES and there are correlation between intensity and dispersion of Pd particles [27]. Ohtani also calculated XANES spectra of Pd and hydrogen adsorbed/absorbed cluster using same method [28]. They found white line broadening appear in Pd L_3-XANES of hydrogen -adsorbed Pd cluster. These results shows that this change caused by adsorbed hydrogen in XANES is a general phenomena in the $L_{2,3}$-edge XANES of metals which adsorb hydrogen on its surfaces.

On the other hand, Koningsberger et al calculated the backscattering amplitude with FEFF7 for Pt-H scattering pairs. They found for hydrogen one maximum is observed in the backscattering amplitude at low k. They concluded that the feature appeases in L_3 edge XANES difference spectra is due to EXAFS for Pt-H scattering pairs and atomic XAFS, while the feature appeases in L_2-edge XANES difference spectra is due to only EXAFS for Pt-H scattering pairs. But if this peak results from EXAFS similar change should be found in L_1-edge XANES. Fig. 18 shows Pt L_1-edge XANES spectra before and after hydrogen admission. L_1-edge XANES spectrum does not shows the change of adsorption edge like $L_{2,3}$-edges. So this peak near the absorption edge should be interpreted by multi scattering process or molecular orbital scheme.

XANES is explained by the dipole (and weak quadipole) transition from core level to unoccupied valence level or multiple scattering between X-ray absorbing atom and surrounding

atoms. Multiple scattering approach is mainly used to assignment for feature of XANES in the hard x-ray region because of a united interpretation between EXAFS, while molecular orbital approach is used rather in the soft x-ray region. But these two approach are essentially same because XANES results from change of transition probability between initial state(core electron) and final state(exited electron). Difference of these two method is that which one select as a basis function to describe final state of exited electron from core level, discrete atomic orbital basis set or free electron continuous wave. In fact, as a method which calculate electronic state of molecules using plane wave basis set for wave function and Xa-potential, SW-Xa method have been developed. On the other hand, there are some attempt to describe electronic state above Fermi level using a lot of atomic basis function [29]. But only either of them not form complete basis function set. In this case about hydrogen adsorption on Pt, either of MS theory and LDF theory could represent the hydrogen-induced peak in the range of 7 eV from Fermi level. If we could assign this hydrogen-induced peak as multiple scattering, it is very reasonable peak intensity is proportional to coordination number of hydrogen, namely amount of hydrogen adsorption. But in MS approach, strongly localized state like white line coud not be represented. If we seek more exact calculation of XANES, we should proceed to use these two function to describe final state.

On the contrary results of XANES of $CO+H_2$ coadsorption system, IR spectra showed shift of C-O stretching peak about 15 cm^{-1} to low wave number side by hydrogen admittion. This shifts indicate increasing of electron donation from Pt atom to CO antibonding orbital. This shift is observed in the some papers IR reflection-absorption spectroscopy. This results in IR spectra suggests modification of electronic state of Pt particles with hydrogen adsorption and this conclusion conflict with results of XANES spectra. LDF calculation for Pt_{13} cluster in this chapter revealed that shell structure of Pt_{13} cluster were either not broken by adsorbed hydrogen nor adsorbed CO. Then

$CO+H_2$ coadsorption does not changed electronic structure of whole Pt_{13} cluster besides without interaction between bonding or anti-bonding orbital of CO and hydrogen. Moreover, energy shifts appear in IR spectra is under energy resolution for XANES measurements (about 1.5 eV at BL-10B) because 1.5 eV corresponds to $1.2X10^4$ cm^{-1}. So, influence between adsorbed hydrogen and adsorbed CO is not found in XANES spectra because of its low energy resolution compared with IR spectra. Consequently the difference spectra in the coadsorbed system reflect only the local change of electronic states before and after H2 adsorption on the Pt atoms with CO preadsorbates.

5-4. Conclusion

1. A new peak in the Pt L-edge XANES spectra for hydrogen adsorbed Pt particles was observed. The peak intensity was proportional to hydrogen coverage or dispersion of Pt particles. This results indicates that one can estimates amount of adsorbed hydrogen even under presence of gaseous hydrogen.

2. A peak in the XANES spectra for $CO+H_2$ coadsorbed Pt particles was deconvoluted by two components ; a peak originated from hydrogen adsorption and a peak originated from CO adsorption. Intensity of this hydrogen-induced peak was proportional to amount of adsorbed hydrogen. This results indicates that one can estimates amount of adsorbed hydrogen even under the reaction conditions.

3. The origine of this hydrogen-induced peak is considered to multiple scattering between hydrogen atom and Pt atom or transition to anti-bonding states between Pt-H bonding. Insensitivity of XANES to hydrogen coverages or coadsorbates is explained by LDF calculation. Namely, electronic states of Pt particles forms shell structure, and this shell structure over Fermi level is not affected by hydrogen coverages or states of coadsorbates.

References

1. Z. Paal and P. G. Menon, "Hydrogen Effects in Catalysis" Marcel Dekker, New York. 1988.

2. M.A. Chesters, K. J. Packer, H. E. Viner, M. A. P. Wright and D. Lennon, *J. Chem. Soc. Faraday Trans.* **91,** 2203 (1995).

3. M. A. Chesters, K. J. Packer, D. Lennon and H. E. Viner, *J. Chem. Soc. Faraday Trans.* **91,** 2191 (1995).

4. D. Hoge, M. Tüshaus and A. M. Bradshaw, *Surf. Sci.* **207,** L935 (1988).

5. T. Szilagyi, *J. Catal.* **121,** 223 (1990).

6. Y. Iwasawa, "X-Ray Absorption Fine Structure for Catalysis and surface" World Scientific, Singapore. 1996.

7. A. P. Hitchcock, S. Beaulieu, T. Steel, J. Stöhr and F. Sette, *J. Chem. Phys.* **80,** 3927 (1984).

8. A. N. Mansour, J. W. Cook, Jr.and D. E.Sayers, *J. Phys. Chem.* **88,** 2330 (1984).

9. J. Wong, F. W. Lytle, R. P. Messmer and D. H. Maylotte, *Phys. Rev. B* **30,** 5596 (1984).

10. M. Fernandez-Garcia, C. Marquez Alvarez and G. L. Haller, *J. Phys. Chem.* **99,** 12565 (1995).

11. T. Yoshida, T. Tanaka, H. Yoshida, T. Funabiki, S. Yoshida and T. Murata, *J. Phys. Chem.* **99,** 10890 (1995).

12. J. A. Horsley, *J. Chem. Phys.* **76,** 1451 (1982).

13. B. Moraweck, A. J. Renouprez, E. K. Hlil and R. Baudoing-Savois, *J. Phys. Chem.* **97,** 4288 (1993).

14. F. W. Lytle, P. S. P. Wei, R. B. Greegor, G. H. Via and J. H. Sinfelt, *J. Chem. Phys.* **70,** 4849 (1979).

15. H. Yoshitake and Y. Iwasawa, *J. Phys. Chem.* **95,** 7368 (1991).

16. N. Ichikuni and Y. Iwasawa, *Catal. Lett.* **20,** 87 (1993).

17. S. N. Reifsnyder, M. M. Otten, D. E. Sayers, and H. H. Lamb, *J. Phys. Chem. B* **101,** 4972 (1997).

18. M. Vaarkamp, J. T. Miller, F. S. Modica and D. C. Koningsberger, *Jpn. J. Appl. Phys.* **32,** 454 (1992).

19. M. G. Samant and M. Boudart, *J. Phys. Chem.* **95,** 4070 (1991).

20. F. W. Lytle, R. B. Greegor, E. C. Marques, D. R. Sandstrom, G. H. Via and J. H. Sinfelt, *J. Catal* **95,** 546 (1985).

21. P. G. Allen, S. D. Conradson, M. S. Wilson, S. Gottesfeld, I. D. Raistrick, J. Valerio and M. Lovato, *Electrochimica Acta,* **39,** 2415 (1994).

22. K. Asakura, T. Kubota, N. Ichikuni and Y. Iwasawa, *in* "Proceedings, 11th Int. Cong. Catal., Baltimore, 1996" Eds.), Vol. 101, p. 911. .

23. T. Kubota, N. Ichikuni, K. Asakura and Y. Iwasawa, *Chem. Phys. Lett.* **256,** 445 (1996).

24. T. Kubota, K. Asakura and Y. Iwasawa, *Catal. Lett.* **46,** 141 (1997).

25. N. Watari and S. Ohnisi, *J. Chem. Phys.* **106,** 7532 (1997).

26. K. Ohtani, T. Fujikawa, T. Kubota, K. Asakura and Y. Iwasawa, *J. Jpn. Appl. Phys.* **36,** 6504 (1997).

27. T. Kubota, Y. Kitajima, K. Asakura and Y. Iwasawa, *Bull. Chem. Soc. Jpn.* **in press,** (1998).

28. K. Ohtani, T. Fujikawa, T. Kubota, K. Asakura and Y. Iwasawa, *J. Jpn. Appl. Phys.* to be published (1998).

29. H. Nakamatsu, T. Mukoyama and H. Adachi, *J. Chem. Phys.* **95,** 3167 (1991).

Table 5-1. Estimated amount of adsorbed hydrogen obtain ed from relation in Fig. 5-5. as a calibration curve.

Temp. / K	R. T.	373	423	473	523
H/Pt	0.92	0.76	0.62	0.48	0.33

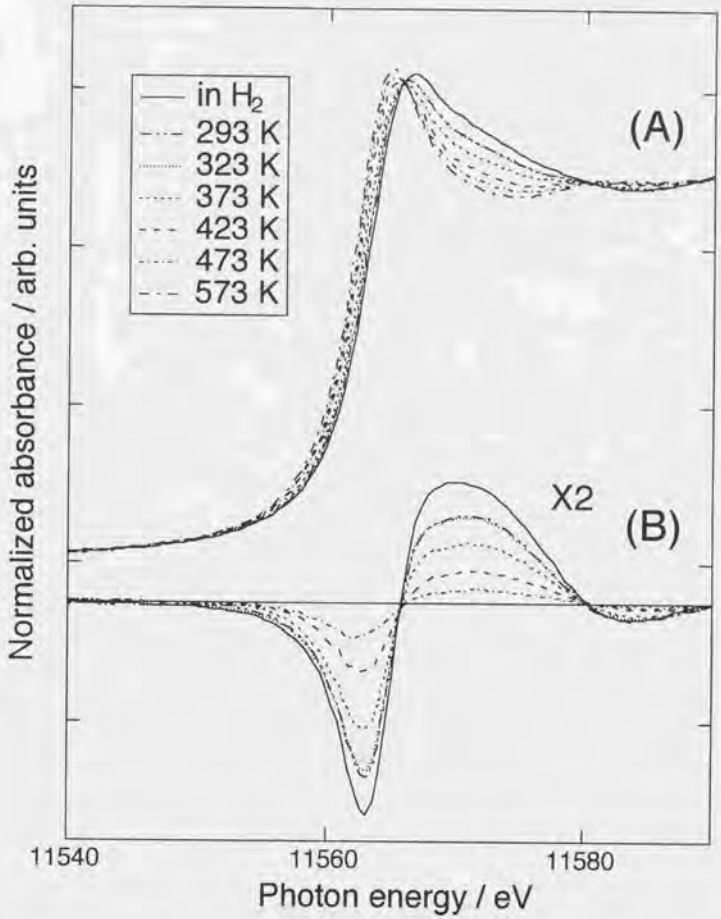

Fig. 5-1. (A) Normalized Pt L_3-edge XANES-TPD spectra for Pt/SiO_2 (H/Pt=1.2) ; (B) XANES difference spectra obtained by subtracting spectra measured after evacuation at 573 K in (A) from spectra measured after evacuation at each temperature.

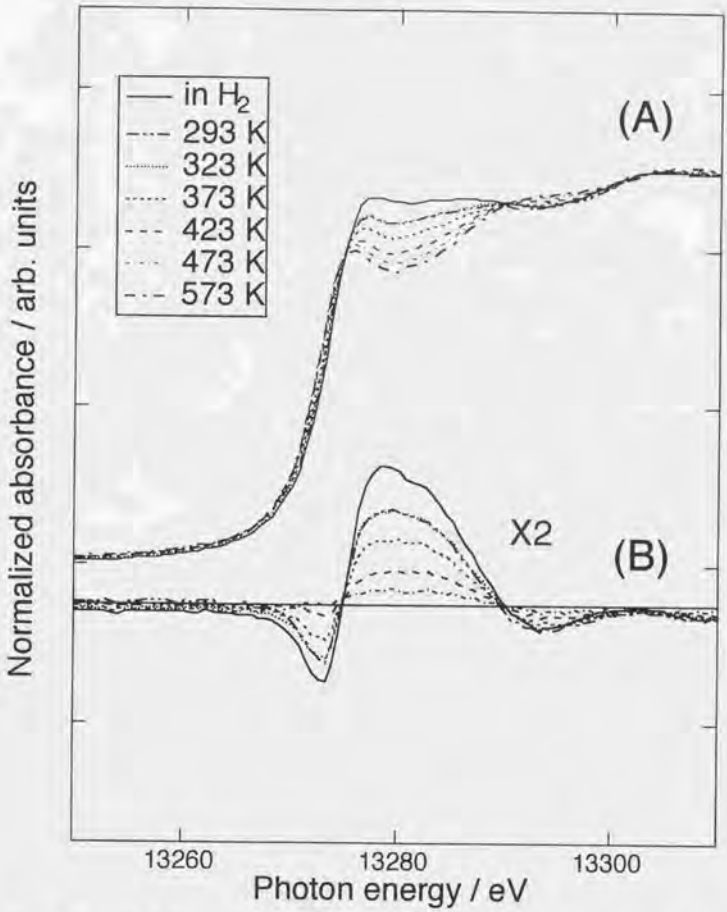

Fig. 5-2. (A) Normalized Pt L_2-edge XANES-TPD spectra for Pt/SiO_2 (H/Pt=1.2) ; (B) XANES difference spectra obtained by subtracting spectra measured after evacuation at 573 K in (A) from spectra measured after evacuation at each temperature.

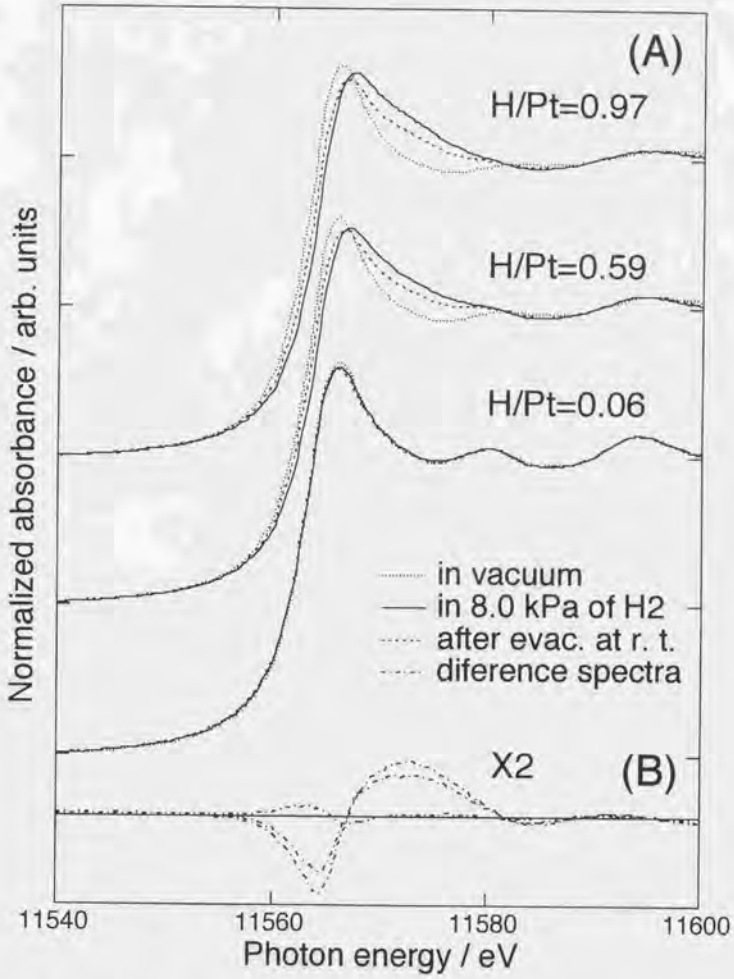

Fig. 5-3. (A) Normalized Pt L_3-edge XANES spectra for hydrogen-free Pt/SiO_2, in 8.0 kPa of H_2, after evacuation at room temperature; (B) difference spectra by subtracting spectra for hydrogen-free Pt/SiO_2.

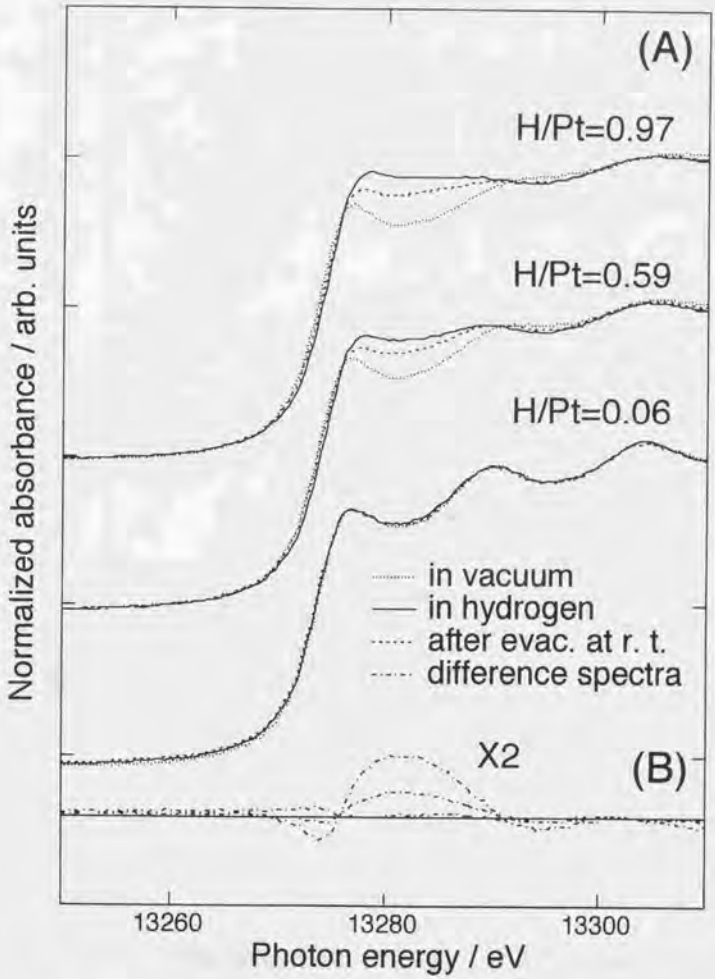

Fig. 5-4. (A) Normalized Pt L_2-edge XANES spectra for hydrogen-free Pt/SiO_2, in 8.0 kPa of H_2, after evacuation at room temperature; (B) difference spectra by subtracting spectra for hydrogen-free Pt/SiO_2.

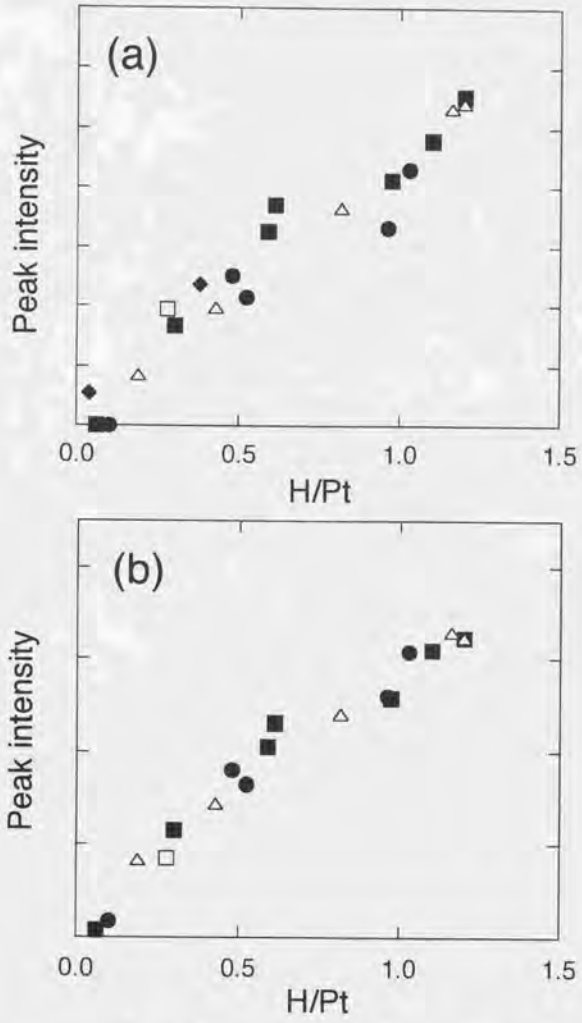

Fig. 5-5. Plots of the intensity of peak for adsorbed hydrogen after evacuation at room temperature as a function of H/Pt at Pt L_3-edge; SiO_2(closed circle), Al_2O_3(open triangle), TiO_2, (open square), MgO(open circle) and XANES-TPD(closed square); (a) at L_3-edge, .(b) same as (a) at L_2-edge.

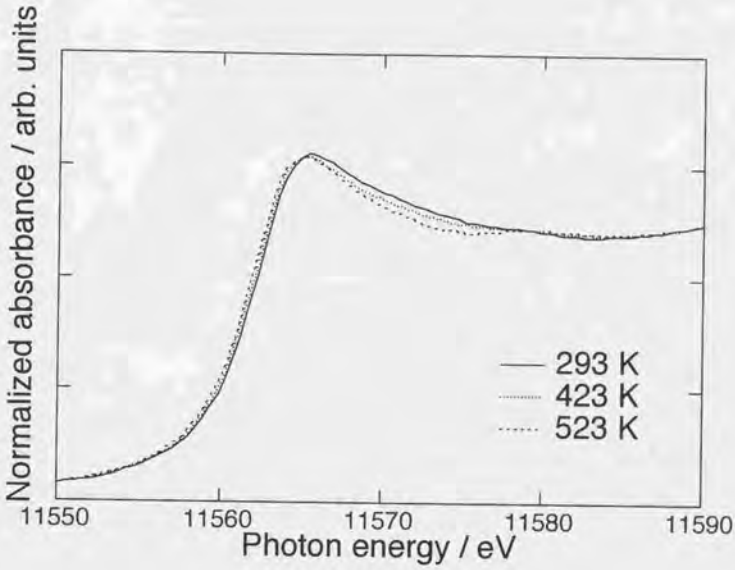

Fig. 5-6. Normalized Pt L_3-edge XANES spectra for Pt/SiO_2 in the presence of 1 atom of $H_2/He = 0.19$ mixing gas measured at indicated temperature.

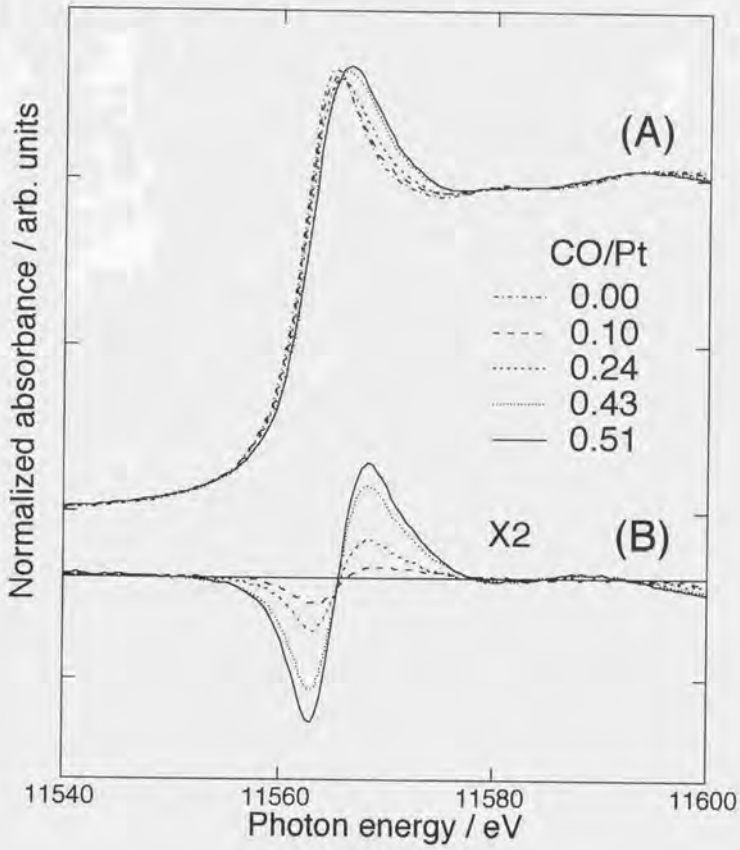

Fig. 5-7. (A) Normalized Pt L_3-edge XANES spectra for CO-preadsorbed and CO-free Pt/SiO_2; (B) difference spectra between them.

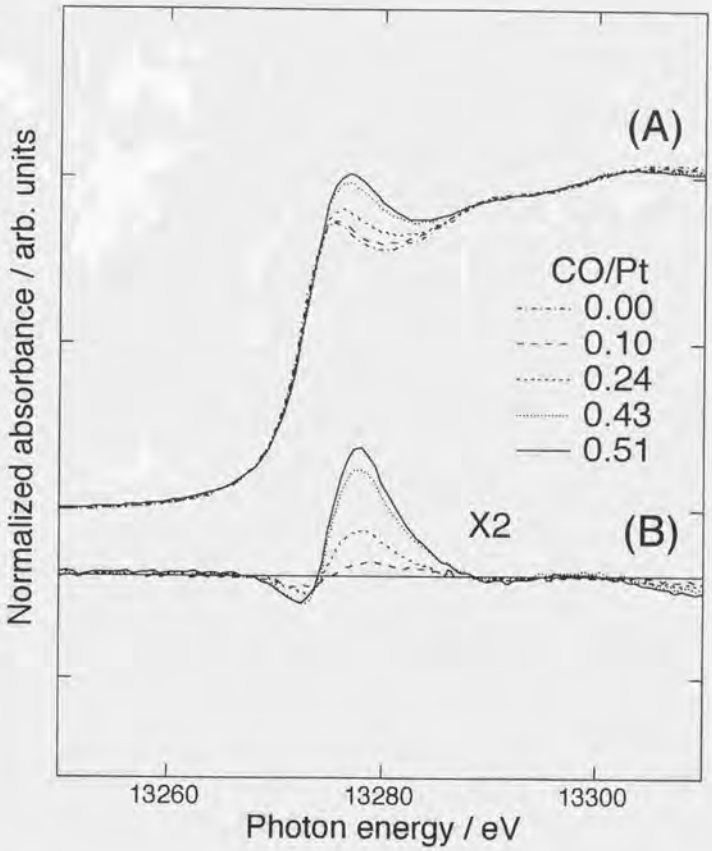

Fig. 5-8. (A) Normalized Pt L_2-edge XANES spectra for CO-preadsorbed and CO-free Pt/SiO_2; (B) difference spectra between them.

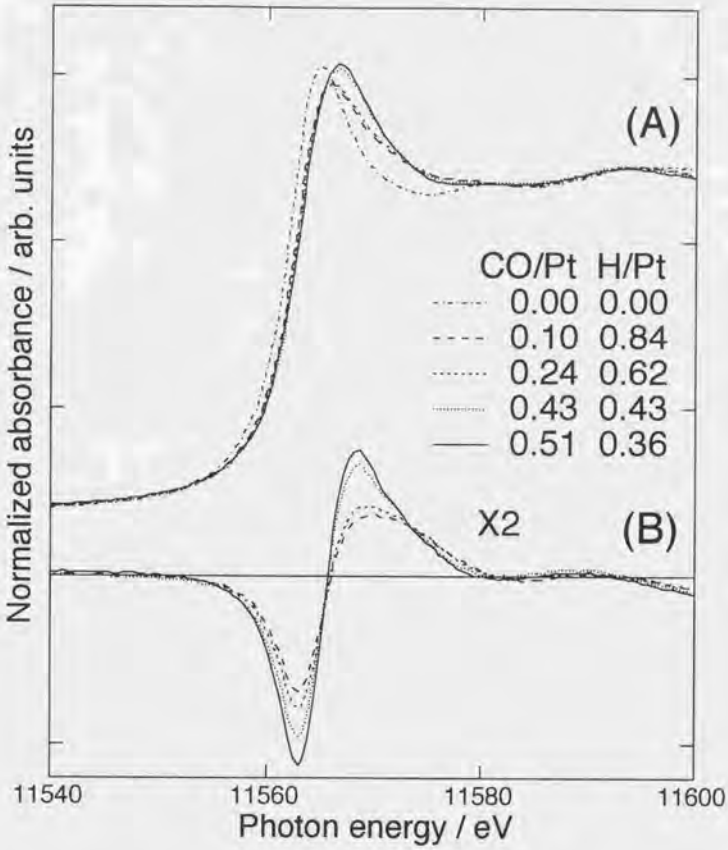

Fig. 5-9. (A) Normalized Pt L_3-edge XANES spectra for $CO+H_2$ coadsorbed Pt/SiO_2; (B) difference spectra obtained by subtracting the CO-free spectra measured in vacuum from spectra (A).

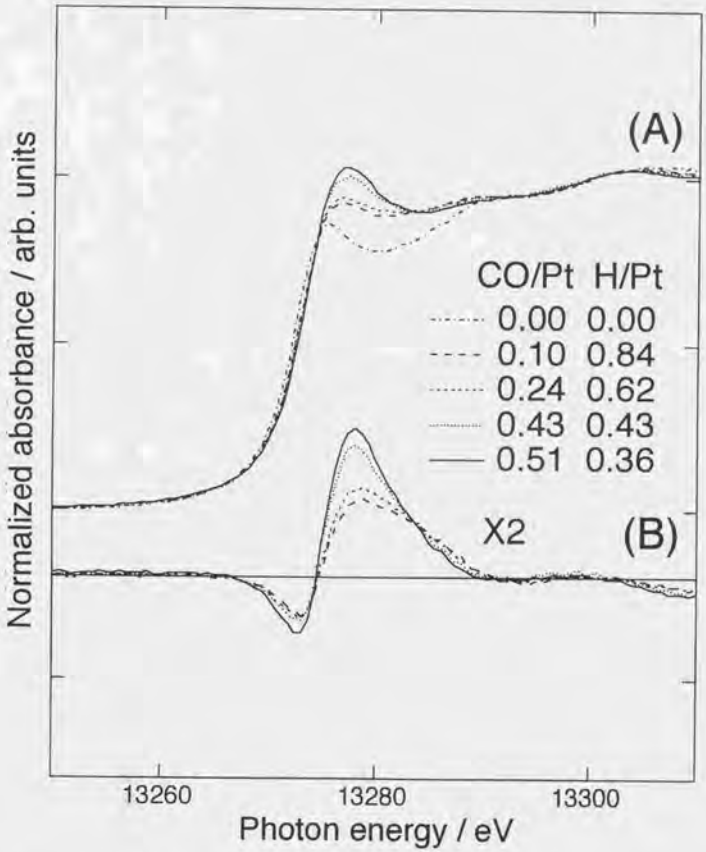

Fig. 5-10. (A) Normalized Pt L_2-edge XANES spectra for $CO+H_2$ coadsorbed Pt/SiO_2; (B) difference spectra obtained by subtracting the CO-free spectra measured in vacuum from spectra (A).

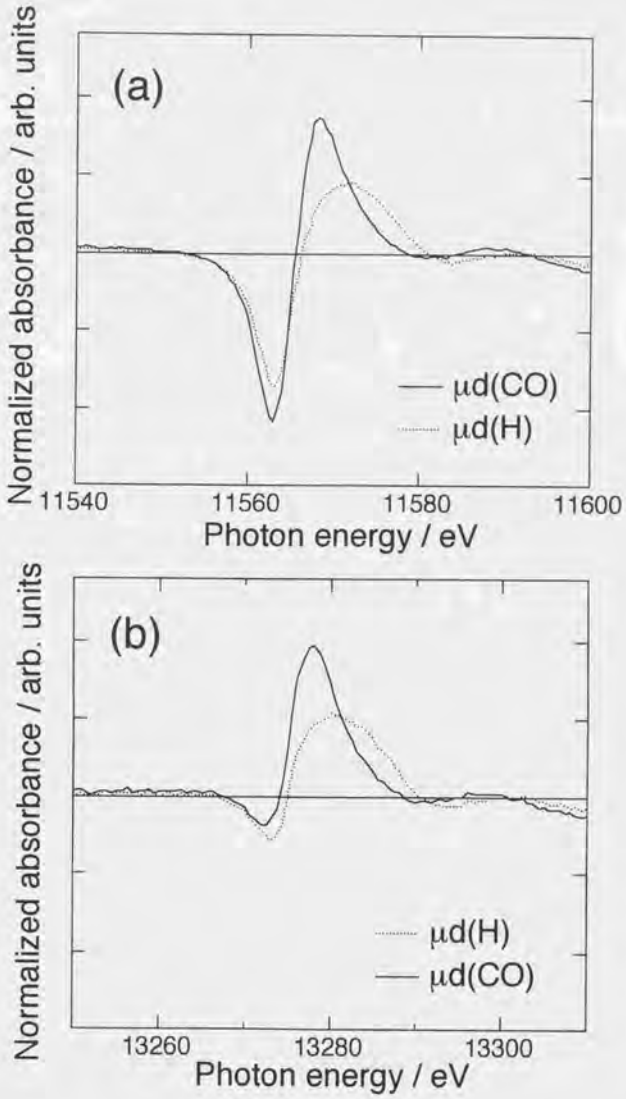

Fig. 5-11. Normalized Pt L-edge difference spectra before and after the mono-adsorptions of H coverage (0.97) and CO coverage (0.51) ; (a) L_3-edge, (b) L_2-edge.

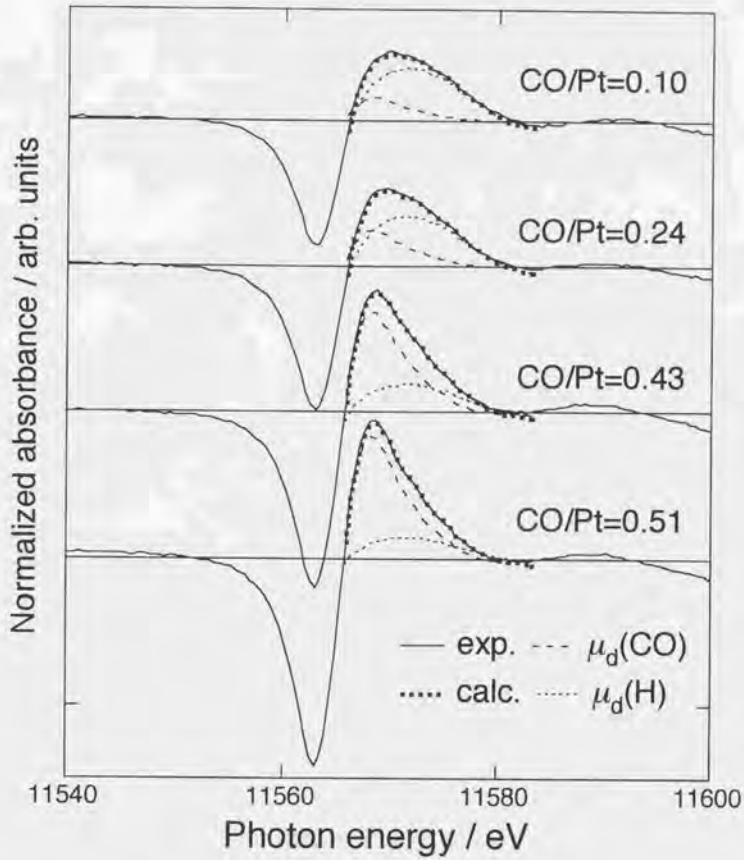

Fig. 5-12. (a) Normalized Pt L_3-edge XANES difference spectra measured for CO+H coadsorption (solid line) and calculated spectra according to eq. 5-1 (dotted line), and component spectra for the calculation (two kinds of broken line).

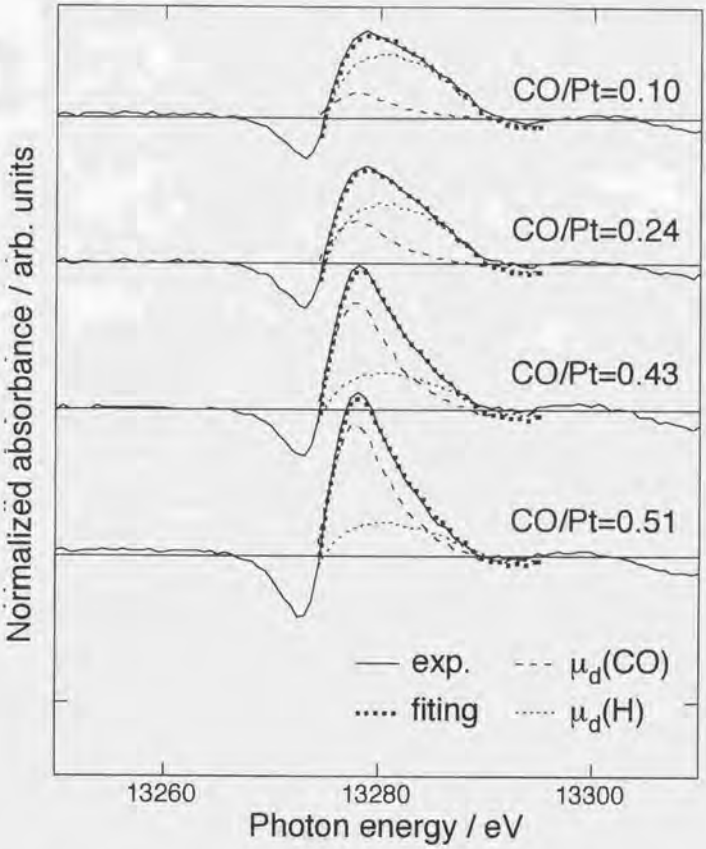

Fig. 5-12. (b) Normalized Pt L_2-edge XANES difference spectra measured for CO+H coadsorption (solid line) and calculated spectra according to eq. 5-1 (dotted line), and component spectra for the calculation (two kinds of broken line).

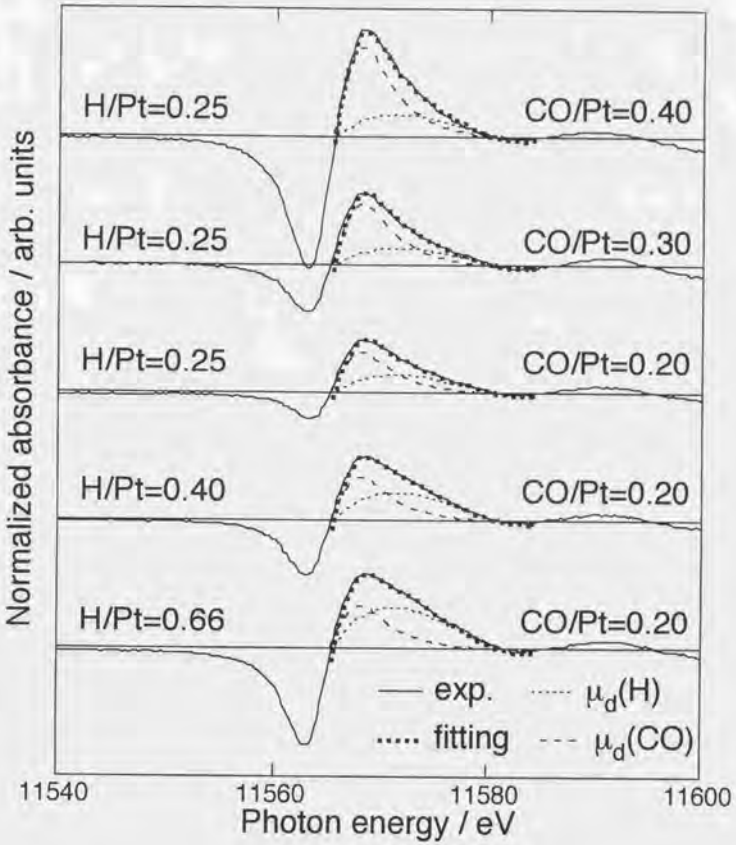

Fig. 5-13. (a) Normalized Pt L_3-edge XANES difference spectra same as Fig. 5-12; coverage were fixed to be CO/Pt=0.2 or H/Pt=0.25.

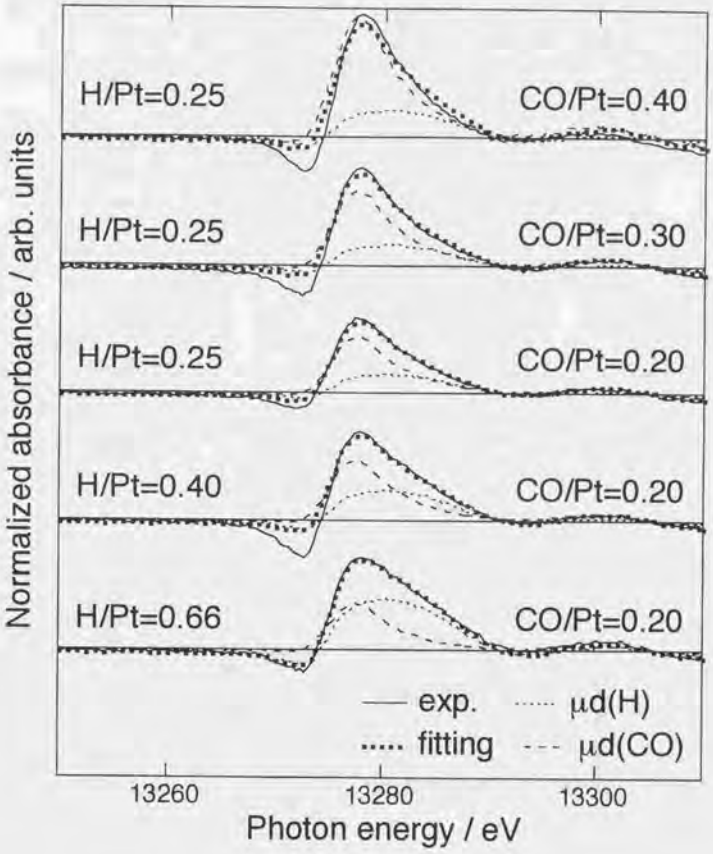

Fig. 5-13. (b) Normalized Pt L_2-edge XANES difference spectra same as Fig. 5-12; coverage were fixed to be CO/Pt=0.2 or H/Pt=0.25.

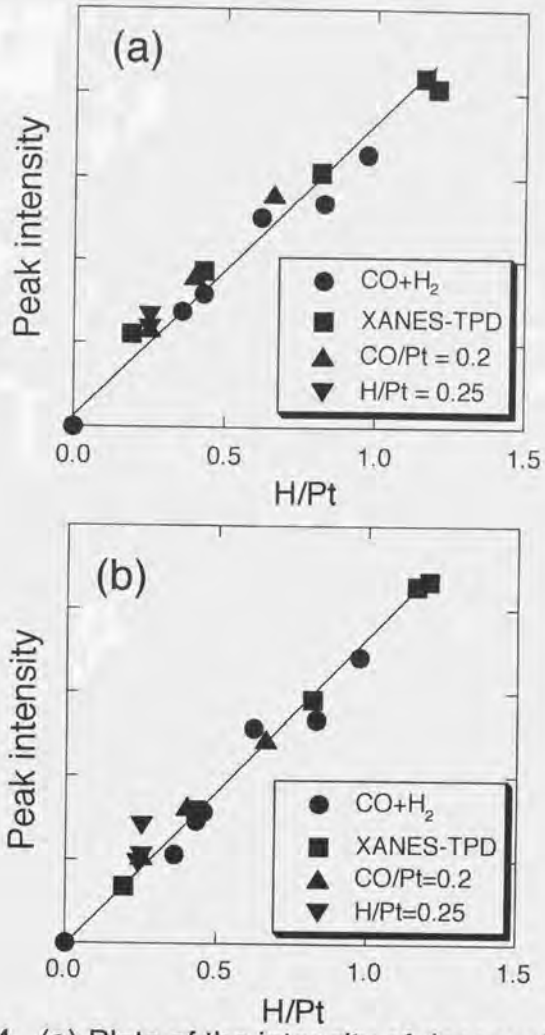

Fig. 5-14. (a) Plots of the intensity of deconvoluted peak for adsorbed hydrogen as a function of H/Pt at Pt L_3-edge; full cuveraged hydrogen (closed circle), CO coverage fixed at CO/Pt=0.2 (open triangle), hydrogen coverage fixed at H/Pt=0.25 (open square), open circle is the intensity of peak for adsorbed hydrogen obtained from XANES-TPD; (b) same as (a) at Pt L_2-edge.

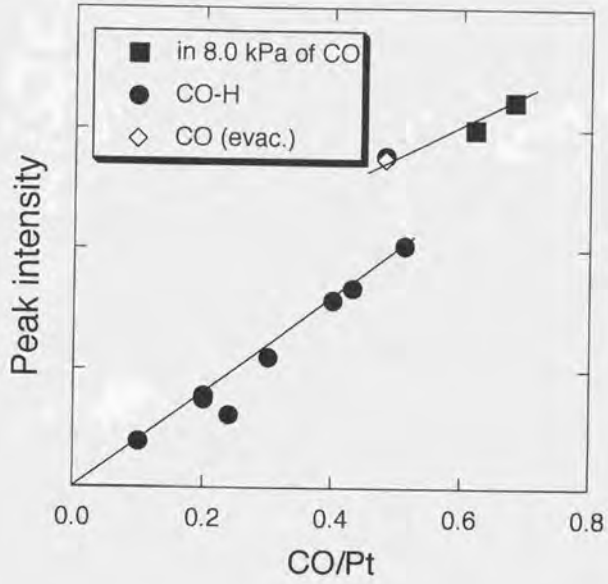

Fig. 5-15. Plots of the intensity of deconvoluted peak for adsorbed CO as a function of CO/Pt at Pt L_3-edge.

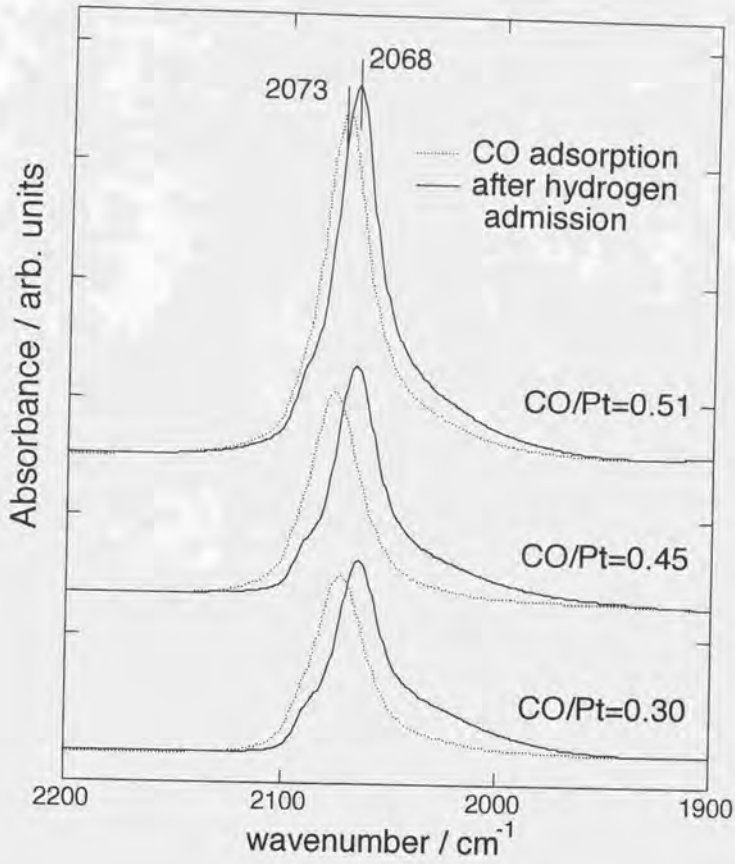

Fig. 5-16. FT-IR spectra for CO adsorbed on Pt/SiO_2 for CO coverages ; (a) CO/Pt=0.30, (b) CO/Pt=0.45, (c)CO/Pt=0.51 (full cuveraged CO).

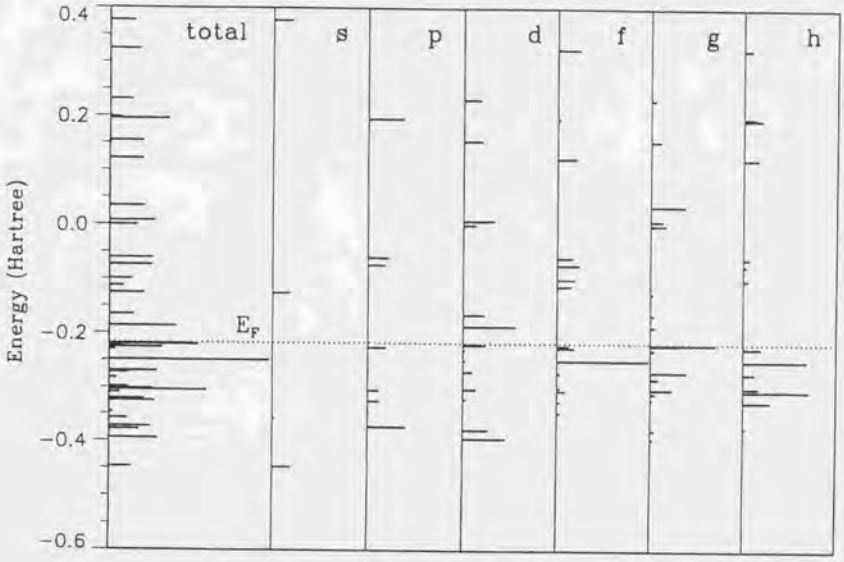

Fig. 5-17(a). Energy levels and density of states (DOS) of Pt_{13} cluster with no adsorbates. s, p, d, f, g and h indicates the partial DOS of each molecular orbital projected at the cluster center. R_{max} for expansion is 1.5 nm.

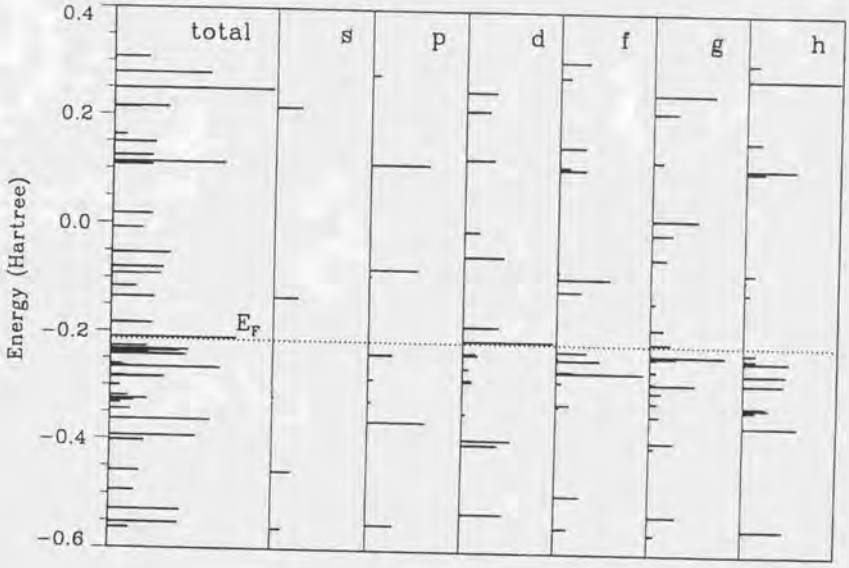

Fig. 5-17(b). Energy levels and density of states (DOS) of Pt_{13} cluster with 8 hydrogen atoms on 8 triangle faces. s, p, d, f, g and h indicates the partial DOS of each molecular orbital projected at the cluster center. R_{max} for expansion is 1.5 nm.

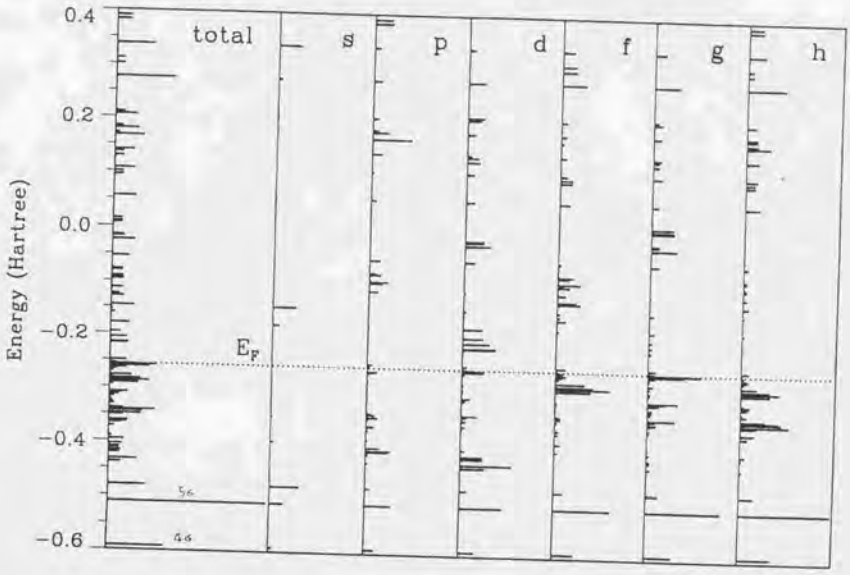

Fig. 5-17(c). Energy levels and density of states (DOS) of Pt_{13} cluster with one CO molecule. s, p, d, f, g and h indicates the partial DOS of each molecular orbital projected at the cluster center. R_{max} for expansion is 1.5 nm.

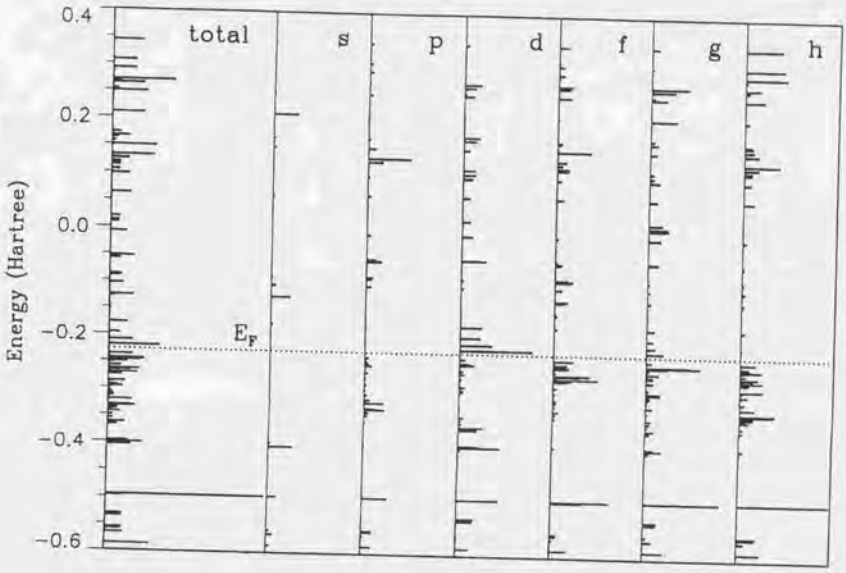

Fig. 5-17(d). Energy levels and density of states (DOS) of Pt_{13} cluster with 8 hydrogen atoms and one CO molecules. s, p, d, f, g and h indicates the partial DOS of each molecular orbital projected at the cluster center. R_{max} for expansion is 1.5 nm.

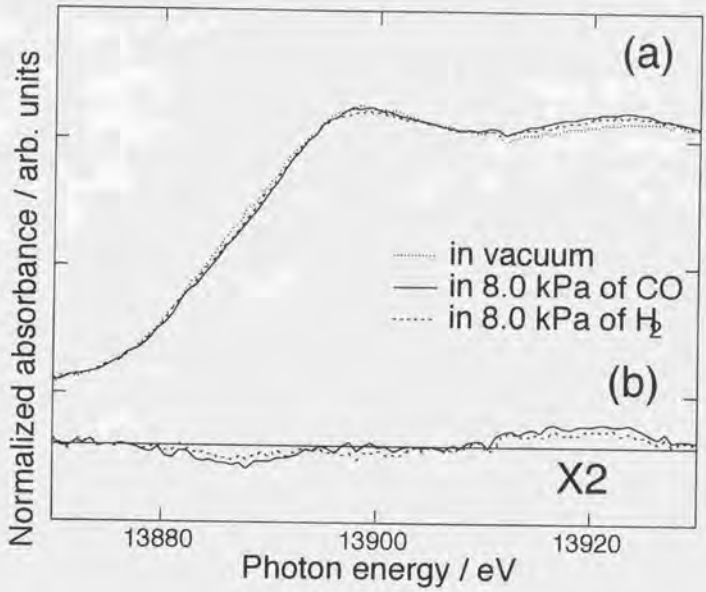

Fig. 5-18. (a) Normalized Pt L_1-edge XANES spectra for hydrogen-free Pt/SiO_2, in 8.0 kPa of H_2 and in 8.0 kPa of CO, (b) difference spectra by subtracting spectra for hydrogen-free Pt/SiO_2.

Chapter 6.

Pd L_3-edge XANES Spectra of Supported Pd Particles Induced by the Adsorption and the Absorption of Hydrogen

6-1. Introduction

X-ray absorption near-edge structure (XANES) is explained by the transition from a core level to unoccupied valence levels or by multiple scattering between an X-ray absorbing atom and surrounding atoms [1, 2]. Since XANES reflects the electronic and local geometrical structures of an X-ray absorbing atom, it has been used to determine symmetry, bond distance and electronic state around the absorbing atom.

The $L_{2,3}$-edge XANES spectra of transition metal elements with unoccupied d states show a strong peak just above the absorption edge, called as white line. As the white line is assigned to a transition from 2p core level to unoccupied nd states, $L_{2,3}$-edge XANES has been used to estimate the density of the unoccupied d-state of X-ray absorbing atoms, [3-5] to investigate the electronic structure of supported Pt small particles [4, 6].

Moreover, the large penetration power of X-ray enables us to carry out *in-situ* XANES measurements in the presence of reaction gas [4, 7, 8]. Yoshitake et al. studied the change of electronic states in Pt particles by the adsorption of various kinds of gas systematically by means of the Pt $L_{2,3}$-edge XANES [7]. When hydrogen adsorbs on highly dispersed Pt particles on oxide surfaces, the Pt $L_{2,3}$-edge peaks are broadened to the higher energy side and the new peak appears at about 8 eV from the edge in difference spectra obtained by subtracting the spectra for clean samples from those for samples adsorbed with hydrogen [8-13]. The origin of H-induced change of XANES has been discussed in terms of several mechanisms involving metal-support interaction [9, 11], Pt-hydrogen antibonding [10, 13, 14], and change of multiple scattering effects induced by hydrogen adsorption [15]. In previouschapter on supported Pt particles, I found that the photon energy of the peak in the Pt L_3-XANES difference spectra before and after H_2 adsorption was independent of the amount of adsorbed hydrogen, the size of Pt particles, and the kind of supports [16-18]. Moreover the peak intensity was proportional only to the amount of adsorbed hydrogen. Thus I have proposed that the intensity of the peak in the difference spectra can be used as a new way to analyze the

amount of adsorbed hydrogen on supported Pt particles *in vacuo* and under the conditions relevant to catalytic reactions [16-18].

It is of interest if this method can be extended to adsorbed hydrogen on other noble metals. In this chapter I will report the change of XANES spectra for small Pd particles on SiO_2 induced by hydrogen. In contrast to Pt, Pd absorbs hydrogen into the bulk to form Pd hydride and thereby acts as a medium for hydrogen storage. The Pd hydride systems have also been studied in relation to catalytic hydrogenation reactions [19-26]. Hydrided Pd catalysts may be resistant to coke formation [26, 27]. Davoli et al. measured Pd L_3-edge XANES spectra of Pd films with absorbed hydrogen [28]. Change in the spectral feature induced by absorbed hydrogen was observed at 5.6 eV above the white line peak (about 8 eV above the absorption edge). Soldatov et al. compared the measured spectra with the spectra calculated by multiple scattering, and concluded that the spectral change induced by hydrogen could be explained by a multiple scattering theory between an X-ray absorbing Pd atom and hydrogen atoms though hydrogen itself is a weak scatterer [29]. But there is little study for Pd L-edge XANES of supported Pd particles and their interaction with H_2.

The purpose of this work is to investigate the change of XANES spectra for small Pd particles on inorganic oxides upon H_2 adsorption and absorption and to develop a new characterization method to determine the amount of adsorbed / absorbed hydrogen on/in Pd particles using XANES spectra.

6-2. Results

6-2-1. H_2 adsorption and absorption and CO adsorption

H_{ad}/Pd(number of adsorbed hydrogen per Pd atom), CO/Pd(number of adsorbed CO per Pd atom) and H_{ab}/Pd(number of absorbed hydrogen per Pd atom) are given in Table 1. Although there is a correlation between the H_{ad}/Pd and CO/Pd, H_{ad}/Pd is always larger than CO/Pd, because the amounts of adsorbed CO and H_2 at saturation are different from each other and CO adsorbed on Pd

surface involves both linear and bridge types as previously reported. H_{ad}/Pd has been used as a measure of metal dispersion or fraction of surface-exposed metal atoms, assuming a stoichiometry of $H_{ad}/Pd_s=1$(Pd_s: surface Pd atoms) [30, 31, 34]. Since I found that Pd particles similarly prepared took a spherical shape on SiO_2 by TEM in a previous work and the averaged particle size derived from TEM agreed with that obtained from H_{ad}/Pd, [36] I estimated the size of Pd particles from the H_{ad}/Pd values assuming a spherical shape of the particles (Table 2). The amounts of absorbed hydrogen (H_{ab}/Pd) decreased with an increase of particle size as shown in Table 1. The relation between H_{ab}/Pd and H_{ad}/Pd in this work well corresponds to the literature data [30].

6-2-2. Results of EXAFS

The EXAFS oscillations and their Fourier transforms for Pd/SiO_2(VAC), Pd/SiO_2(H2)and Pd/SiO_2(EVAC) are shown in Figs. 6-1(A), 6-1(B) and 6-2, respectively. The curve fitting results are tabulated in Table 3. In Pd/SiO_2(VAC) with H_{ad}/Pd=0.74, 0.56, 0.29 and 0.12, the Pd-Pd distances (0.275±0.002 nm) were similar to that for Pd bulk(0.276 nm). The structural parameters such as coordination number, distance and Debye-Wallor factor for Pd/SiO_2(EVAC) are the same within the limit of error as those of the Pd/SiO_2(VAC).

I estimated the average size of Pd particles from the coordination number using a Greegor and Lytle method assuming the spherical shape [37]. In the present study the coordination numbers of Pd/SiO_2(EVAC) were used for the estimation. The results are given in Table 2. The particle sizes derived from the EXAFS coordination numbers a little smaller than those estimated from the adsorption of hydrogen (H_{ad}/Pd) but both values are compatible if the error bars are taken into account.

In Pd/SiO_2(H2)samples, the Pd-Pd distances increased compared with those for Pd/SiO_2(VAC); it increased from 0.275 nm for Pd/SiO_2(VAC) up to 0.284 nm for Pd/SiO_2(H2)with H_{ad}/Pd=0.12. The increase of Pd-Pd distance in Pd/SiO_2(H2)is due to the Pd lattice expansion

induced by the hydrogen absorption. The Pd-Pd distance in bulk PdH_x (x=0.6) is known to be 0.2855 nm which is similar to the values for Pd-Pd in Pd/SiO_2(H2)with H_{ad}/Pd=0.12. The Pd-Pd distances in the Pd/SiO_2 samples with H_{ad}/Pd =0.75 and 0.56 increased after hydrogen absorption, indicating small Pd particles can absorb hydrogen. Interestingly the increase in the Pd-Pd distance becomes smaller with the smaller Pd particle size. When the samples were evacuated at room temperature for 1 h (Pd/SiO_2(EVAC)), the Pd-Pd bond distances decreased to 0.275 -0.277 nm shown in Table 3, indicating that the absorbed hydrogen in all the samples was removed by evacuation at room temperature.

6-2-3. XANES spectra of Pd/SiO_2 under interaction of hydrogen

Figs. from 6-3 to 6-6 show Pd L_3-edge XANES spectra for the Pd/SiO_2 samples with the dispersion (H_{ad}/Pd) of 0.74, 0.56, 0.29 and 0.12, respectively. Each figure contains three sets of the XANES spectra for Pd/SiO_2(VAC), Pd/SiO_2(H2)and Pd/SiO_2(EVAC). The white line peak for Pd/SiO_2(VAC) before exposing to H_2 increased with the decrease in particle size. The white line is caused by the transition from 2p to unoccupied 4d states of Pd. If the transition dipole moment is the same, the intensity of the white line peak indicates the amount of unoccupied d state of the Pd atoms [4-6]. The results in Figs. from 6-3 to 6-6 indicate that the electron density of d-states for Pd particles decreases with the decrease of the particle size, which agrees with the literature [38]. After exposing Pd/SiO_2(VAC) to hydrogen, the white line peak decreased and the absorption coefficient around 3181 eV increased instead. Especially in low dispersion samples, a new definite peak appeared at about 3181 eV in the presence of gas phase H_2 (Figs. 6-5 and 6-6). The new peak decreased in height and is broadened with the increase of dispersion (Figs. 6-3 and 6-4). The peak diminished by evacuation at room temperature as shown in Figs. from 6-3 to 6-6 for Pd/SiO_2(EVAC). On the other hand the white line peak intensity increased by the evacuation at room temperature. For the samples with low dispersions(H_{ad}/Pd=0.12 and 0.29), the intensity of the

white line reverted to that for the corresponding Pd/SiO_2(VAC) samples. On the other hand, the white line peaks for the higher dispersion samples were smaller than those for the corresponding Pd/SiO_2(VAC) samples - due to the influence of chemisorbed hydrogen. Similar changes in XANES spectra were found for two Pd/Al_2O_3 samples with three different treatments. Namely, exposure of Pd/Al_2O_3(H_{ad}/Pd=0.20) to H_2 gas created a sharp peak at 3181 eV which decreased by the evacuation at room temperature. On the other hand the Pd/Al_2O_3 with H_{ad}/Pd=0.81 (higher dispersion) showed a broad peak after the introduction of H_2 which was present even after the evacuation at room temperature.

To clarify these changes in XANES spectra, I took difference spectra. Fig. 6-7 shows the difference spectra obtained by subtracting the spectra measured before hydrogen introduction (Pd/SiO_2(VAC)) from those for Pd/SiO_2(EVAC). The difference spectra between Pd/Al_2O_3(VAC) and Pd/Al_2O_3(EVAC) were also included in the figure. The new peak at about 3181 eV(about 8 eV above the inflection point of the edge) appeared in the difference spectra. The peak energy was independent of a particle size and a kind of support. Because the room temperature evacuation removes the absorbed hydrogen in the Pd bulk, the changes in these difference spectra are considered as the ones induced by the adsorbed hydrogen. The peak is denoted as ads-peak. The ads-peaks well correspond to the peaks in the Pt L-edge difference spectra between before and after H_2 adsorption on Pt particles [16, 17]. The photon energy of the ads-peaks relative to the edge energy in Pd difference spectra is almost the same as that of the peaks observed in Pt L_3-edge difference spectra for the supported Pt samples [16, 17]. Therefore, the ads-peaks in the Pd particles may have the same origin as the peaks found in hydrogen-adsorbed Pt particle samples. In the case of Pt particles, the peak intensity was proportional to the H/Pt value [16, 17]. We plotted the intensity of the ads-peak against H_{ad}/Pd in Fig.6- 8.

Fig. 6-9 shows the difference spectra obtained by subtracting the spectra of Pd/SiO_2(EVAC) from those of Pd/SiO_2(H2)together with corresponding spectra for Pd/Al_2O_3. The difference spectra

are considered to indicate the change in the XANES spectra caused by hydrogen absorbed in the Pd bulk. The peak in the difference spectra appears at about 3181 eV(about 8 eV above the inflection point of the edge). This peak is denoted as abs-peak. The position of the abs-peaks referred to the edge position does not depend on the particle sizes and the kind of supports. The abs-peak appears at almost the same position as that of the ads-peaks. But, the abs-peaks are sharper than the ads-peaks. The abs-peak shows a relatively high intensity for the lower dispersion samples (H_{ad}/Pd=0.12 and 0.29 for SiO_2 and H_{ad}/Pd =0.2 for Al_2O_3) and the abs-peak for the higher dispersion becomes weaker and broader than that for lower dispersion.

6-3. Discussion

Pd is known as a metal which absorbs many hydrogen atoms in the bulk to form hydride PdH_x. A disordered solution, called α-phase is formed under low H_2 pressure at room temperature [39]. Pd-Pd distance little increases in the α-phase. At higher H_2 pressures, α-phase, is transformed to β-phase hydride and Pd-Pd distance is expanded to 0.2855 nm. The ratio of absorbed hydrogen to Pd at saturation is nearly 0.6 at room temperature. In the case of dispersed Pd particles where the fraction of surface Pd atoms is large, the amount of absorbed hydrogen atom per Pd atom (H_{ab}/Pd) is found to decrease [30, 31,35]. Boudart and Hwang measured hydrogen absorption isotherms for Pd/SiO_2 with different particle sizes [35] and concluded that the H_{ab}/Pd decreased as the dispersion of Pd particles increased. They claimed H_{ab}/Pd was converged to zero at dispersion=100 %. Bonivardi et al. found that hydrogen solubility was suppressed with the larger dispersion of Pd particles [30]. But they reported that the H_{ab}/Pd became constant (H_{ab}/Pd=0.3) at a dispersion larger than 0.6.

A characteristic peak appeared at about 8 eV above the edge in the Pd L_3-edge XANES spectra of a hydrogen-absorbing Pd thick film [28]. I found the peak at the same photon energy in the L_3 edge XANES spectrum for the Pd particles on SiO_2 with H_{ad}/Pd = 0.12 when they absorbed

hydrogen. The peak position did not depend on the particle size or kind of supports, indicating that the abs-peak is originating from the transition to a localized state such as Pd-H antibonding similar to the XANES peak in the chemisorbed hydrogen on Pt particles [14-17]. The peak height was a little smaller than that for the Pd films. The intensity of the abs-peak in the difference spectra between the spectra for Pd/SiO_2(H2)and Pd/SiO_2(EVAC) decreased with the decrease of particle size and the abs-peak almost disappeared in the case of Pd/SiO_2 with H_{ad}/Pd=0.74. Furthermore, the intensities of the abs-peaks between H_{ad}/Pd=0.29 and 0.12 were quite different. To explain the change of spectra, I assume that only bulk Pd atoms fewer layers deeper from surface give the abs-peak in the difference spectra. Hydrogen atoms located intermediate layer between surface and bulk, called subsurface hydrogen atoms, does not modify the XANES spectra. I calculated the number of the bulk Pd atoms in the particle using a model shown in Fig. 6-10 where the Pd atoms at the location three layers deeper from the surface are regarded as the bulk Pd atoms, i.e., one-subsurface-layer model. The number of the bulk Pd atoms(Pd_b), the number of total Pd atoms(Pd_t), the number of surface Pd atoms (Pd_s), and the number of subsurface Pd atoms(Pd_{ss}) are related to each other.

$$Pd_t = Pd_b + Pd_s + Pd_{ss}$$

$$Pd_s/Pd_t = H_{ad}/Pd \,, \qquad (6\text{-}1)$$

Fig. 6-11 shows correlation between the intensity of abs-peaks and the fraction of the bulk Pd atoms (Pd_b/Pd_t) calculated based on the model of Fig. 6-10. The peak intensity for H-absorbed Pd film which can be regarded as Pdb/Pd_t= 1 is also plotted using the literature data [28]. I also plotted the peak intensity for H-absorbed Pd/Al_2O_3 samples. I can find the linear relation between the abs-peak intensity and Pd_b/Pd_t in Fig. 6-11 irrespective of the kind of supports. I also calculated other models with the different numbers of near surface layers. Fig.6-11 included the plots for no subsurface and two-subsurface-layer model where Pd atoms deeper than two layers and four layers were regarded as bulk atoms, respectively. In the no subsurface-layer model, I did not obtain linear relation between

the intensity of abs-peak and Pd_b/Pd_t as shown in Fig.6-11. Although two-subsurface-layer model could give a linear correlation between them, the line did not go through the bulk value(Pd_b/Pd_t=1) These results indicate that surface (top layer) and subsurface (second layer) Pd atoms interact with hydrogen atoms in a different manner from the bulk part of Pd atoms.

The presence of "subsurface" hydrogen with different nature from the bulk hydrogen has been demonstrated by kinetics, TDS, LEED, He scattering, ARUPS and theoretical work and the subsurface hydrogen is considered to be in a distinct intermediate state for the transformation of chemisorbed hydrogen (surface) to absorbed one(bulk) [40-55]. The TPD spectra revealed that subsurface hydrogen on Pd(110) surface a different desorption energy from those for chemisorbed and absorbed hydrogen [48]. The Pd-H bond in the subsurface region may be different in bond length and electronic structure from that in the bulk region. In fact the present EXAFS data for the Pd particles with smaller sizes which had surface and subsurface hydrogen atoms showed the smaller Pd-Pd bond expansion. The multiple scattering calculation for absorbed H-Pd particle suggested that the abs-peak appears only when the Pd-Pd distance was expanded and hydrogen had a positive charge [56]. Thus it is concluded that the abs-peak is originated from the hydrides dissolved in the bulk part of Pd particles(from the third layer) and that the interaction of subsurface and surface hydrogen with Pd is different from that of the bulk hydrides and subsurface hydrogen atoms do not change the Pd L_3-edge XANES spectra.

On the other hand, the difference spectra between Pd/SiO_2(VAC) and Pd/SiO_2(EVAC) show the change originating from the hydrogen atoms adsorbed on the Pd surface. It was found that the ads-peak by the surface hydrogen atoms at 8 eV above the edge (Fig. 6-7). The energy of the ads-peaks was independent of the particle size and kind of support. The peak position of the ads-peaks was similar to that of the abs-peaks but the shape of the ads-peaks was relatively broadened. A similar peak has been observed in the Pt $L_{2,3}$-edge XANES spectra for hydrogen-adsorbed Pt particles [16, 17]. The ads-peaks at 8 eV above the edges in the white lines at Pt and Pd L_3-edges

can be explained by the multiple scattering scheme. Ohtani et al. calculated the XANES of hydrogen-adsorbed Pt particles using the multiple scattering theory and found that the peak appears when the charge transfer occurs from Pt 6s to H 1s [15]. They also calculated Pd particles with adsorbed hydrogen [56] and found that the adsorption of hydrogen changes the XANES spectra but the spectra are not so sensitive to the electron structures of the Pd and adsorbed H atoms in contrast to the Pt case. It was found that there is a positive correlation between the ads-peak intensity and the Pd dispersion as shown in Fig.6-8.

6-4. Conclusions

1. A new peak (abs-peak) in the XANES spectra for hydrogen absorbed Pd particles was observed. The peak intensity increased with the size of Pd particles, which indicates that absorbed hydrogen atoms in the Pd bulk can be quantified by the abs-peak in XANES.

2. The Pd-H bonding in the subsurface region did not contribute to the abs-peak.

3. A new peak(ads-peak) at 8 eV higher than the edge in difference spectra was also observed for hydrogen-adsorbed Pd/SiO_2 and Pd/Al_2O_3. The abs-peak corresponds to that found in small Pt particles.

4. The ads-peak intensity had a positive correlation with the Pd dispersion(H_{ad}/Pd) and the amount of adsorbed hydrogen at the Pd surface.

5. A model of Pd particles composed of surface, subsurface and bulk for the adsorption and absorption of hydrogen was presented by the analysis of the Pd L_3-edge XANES spectra for Pd/SiO_2(VAC), Pd/SiO_2(H2)and Pd/SiO_2(EVAC).

References

1. N. Kosugi, in "X-Ray Absorption Fine Structure for Catalysis and surface", ed by Y. Iwasawa, World Scientific, Singapore(1996), Vol. 2, p60.

2. T. Fujikawa, in "X-Ray Absorption Fine Structure for Catalysis and surface", ed by Y. Iwasawa, World Scientific, Singapore(1996), Vol. 2, p76.

3. M. Brown, R. E. Peierls and E. A. Stern, *Phys.Rev.B*, **15**, 738(1977).

4. F. W. Lytle, P. S. P. Wei, R. B. Greegor, G. H. Via and J. H. Sinfelt, *J.Chem.Phys.*, **70**, 4849(1979).

5. J. A. Horsley, *J.Chem.Phys.*, **76**, 1451(1982).

6. A. N. Mansour, J.W.Cook and D. E. Sayers, *J.Phys.Chem.*, **88**, 2330(1984).

7. H. Yoshitake and Y. Iwasawa, *J.Phys.Chem.*, **95**, 7368(1991).

8. N. Ichikuni and Y. Iwasawa, *Catal. Lett.*, **20**, 87-95(1993).

9. F. W. Lytle, R. B. Greegor, E. C. Marques, D. R. Sandstrom, G. H. Via and J. H. Sinfelt, *J. Catal.* **95**, 546(1985).

10. M. G. Samant and M. Boudart, *J.Phys.Chem.*, **95**, 4070(1991).

11. M. Vaarkamp, J. T. Miller, F. S. Modica and D. C.Koningsberger, *Jpn.J.Appl.Phys.*, 32-2, 454(1993).

12. P. G. Allen, S. D. Conradson, M. S. Wilson, S. Gottesfeld, I. D. Raistrick, J. Valerio and M. Lovato, *Electrochimica Acta*, **39**, 2415(1994).

13. S. N. Reifsnyder, M. M. Otten, D. E. Sayers and H. H. Lamb,*J.Phys.Chem.B*, **101**, 4972(1997).

14. N. Watari and S. Ohnishi, *J.Chem.Phys.*, **106**, 7531(1997).

15. K. Ohtani, T. Fujikawa, T. Kubota, K. Asakura and Y. Iwasawa, *Jpn.J.Appl.Phys.*, **36**, 6504-6509(1997).

16. K. Asakura, T. Kubota, N. Ichikuni and Y. Iwasawa, in "Stud. Surf. Sci.Catal.", ed by J. W. Hightower, W. N. Delgass, E. Iglesia and A. T. Bell, Elsevier Science, Amsterdam(1996), Vol. 101,

p911.

17. T. Kubota, K. Asakura, N. Ichikuni and Y. Iwasawa, *Chem. Phys. Lett.*, **256**, 445(1996).

18. T. Kubota, K. Asakura and Y. Iwasawa, *Catal. Lett.*, **46**, 141(1997).

19. W. Palczewska, *Adv.Catal.*, **24**, 245(1975).

20. R. K. Nandi, R. Pitchai, S. S. Wong, J. B. Cohen, R. L. Burwell, Jr. and J. B. Butt, *J. Catal.*, **70**, 298(1981).

21. R. K. Nandi, P. Georgopoulos, J. B. Cohen, J. B. Butt, J. R. L. Burwell and D. H. Bilderback, *J.Catal.*, **77**, 421(1982).

22. G. Carturan, Facchin G, G. Cocco, S. Enzo and G. Navazio, *J.Catal.*, **76**, 405(1982).

23. E. Rorris, J. B. Butt, J. Burwell, R.L., and J. B. Cohen, Proc. 8th Inter.Congre.Catal., Berlin(1984), IV-321.

24. R. Dus, *Surf.Sci.*, **50**, 241(1975).

25. J. M. Moses, A. H. Weiss, K. Matusek and L. Guczi, *J.Catal.*, **76**, 405(1984).

26. W. Palczewska, in "Hydrogen effects in catlaysis", ed by Z. Paal and P. G. Menon, Marcel Dekker, New York(1988), Vol. 31, p373.

27. J. M. Orozco and G. Webb, *Appl.Catal.*, **6**, 67(1983).

28. I. Davoli, A. Marcelli, G. Fortunato, A. D'amico, C. Coluzza and A. Bianconi, *Solid State Comm.*, **71**, 383(1989).

29. A. V. Soldatov, S. D. Longa and A. Bianconi, *Solid State Commun.*, **85**, 863(1993).

30. A. L. Bonivardi and M. A. Baltans, *J.Catal.*, **138**, 500(1992).

31. J.E. Benson, H. S.Hwang, and M. Boudart, *J.Catal.*, **30**, 146(1973).

32. T. Ohta, P. M. Stefan, M. Nomura and H. Sekiyama, *Nucl. Instrum. Method*, **A246**, 373(1986).

33. M. Funabashi, T. Ohta, T. Yokoyama, Y. Kitajima and H. Kuroda, *Rev.Sci.Instrum*, **60**, 2505(1989).

34. K. Asakura, in "X-ray Absorption Fine Structure for Catalysts and Surfaces", ed by Y. Iwasawa,

World, Scientific,Singapore(1996), Vol. 2, p33.

35. M. Boudart and H. S. Hwang, *J. Catal.*, **39**, 44(1975).

36. K. Inukai, K. Asakura, and Y. Iwasawa, *J.Catal* **143,** 22 (1993).

37. R. B. Greegor and F. W. Lytle, *J.Catal.*, **63**, 476(1980).

38. M. G. Mason, *Phys.Rev.B*, **27**, 748(1983).

39. Z. Paal and P. G. Menon, "Hydrogen effects in catalysis", Marcel Dekker, New York, 1988.

40. A. W. Aldag and L. D. Schmidt, *J.Catal.*, **22**, 260(1971).

41. J. F. Lynch and T. B. Flanagan, *J.Phys.Chem.*, **77**, 2628(1973).

42. W. Auer and H. J. Grabke, *Ber.Bunsenges.Phys.Chem.*, **78**, 58(1974).

43. J. A. Konvalinka and J. J. Scholten, *J.Catal.*, **48**, 374(1977).

44. S. G. Louie, *Phys.Rev.Lett.*, **42**, 476(1979).

45. W. Eberhardt, F. Greuter and E. W. Plummer, *Phys.Rev.Lett.*, **46**, 1085(1981).

46. M. G. Cattania, V. Penka, R. J. Behm, K. Christmann and G. Ertl,*Surf.Sci.*, **126**, 382(1983).

47. W. Eberhardt, S. G. Louie and E. W. Plummer, *Phys.Rev.B*, **28**, 465(1983).

48. R. J. Behm, V. Penka, M.-G. Cattania, K. Christamnn and G. Ertl, *J.Chem.Phys.*, **78**, 7486(1983)

49. K. H. Rieder, M. Baumberger and W. Stocker, *Phys.Rev.Lett.*, **51**, 1799(1983).

50. C. T. Chan and S. G. Louie, *Phys.Rev.B*, **30**, 4153(1984).

51. M. Baumberger, W. Stock and K. H. Rieder, *Appl.Phys.*, **A41**, 151(1986).

52. T. E. Felter, S. M. Foiles, M. S. Daw and R. H. Stulen, *Surf.Sci.*, **171**, L379(1986).

53. M. S. Daw and S. M. Foiles, *Phys.Rev.B*, **35**, 2128(1987).

54. R. A. Olsen, P. H. T. Philipsen and E. J. Baerends, *J.Chem.Phys.*, **106**, 9286(1997).

55. R. A. Olsen, G. J. Kroes, O. M. Løvvik and E. J. Baerends, *J.Chem.Phys.*, **107**, 10652(1997).

56. K. Ohtani, T. Fujikawa, T. Kubota, K. Asakura and Y. Iwasawa, *Jpn.J.Appl.Phys.*, **37**, 4134-4139(1998).

Table 6-1. Amounts of adsorbed/absorbed hydrogen and adsorbed CO per Pd atom on Pd/SiO_2 and Pt/Al_2O_3

support	precursor	loading / wt%	Redc. Temp. / K	H_{ad}/Pd	CO/Pd	H_{ab}/Pd
SiO_2						
Aerosil 300	$[Pd(NH_3)_4]Cl_2$	1.0	573	0.74	0.44	0.33
Aerosil 300	$[Pd(NH_3)_4]Cl_2$	1.0	773	0.56	0.32	0.45
Aerosil 300	$Pd(acac)_2$	0.9	673	0.29	0.12	0.48
Aerosil 200	$Pd(NO_3)_2$	2.3	773	0.12	0.07	0.54
Al_2O_3						
Allon C	$Pd(acac)_2$	1.0	573	0.80	0.84	0.40
Allon C	$Pd(NO_3)_2$	1.0	573	0.20	0.13	0.54

Table 6-2. Particle size estimated from adsorption of $H_2(H_{ad}/Pd)$ and EXAFS coordination number

H_{ad}/Pd	d^*	d^{**}
0.74	1.6	1.0±0.8
0.56	2.2	1.2±1.4
0.29	4.0	1.6±2.0
0.12	9.5	n. d.

d^* : from H adsorption,

d^{**} : from EXAFS,

n. d. : The size could not be determined by EXAFS.

Table 6-3. Best-fit results for the EXAFS data of Pd/SiO_2(VAC), $Pd/SiO_2(H_2)$, and Pd/SiO_2(EVAC)

H/Pd		N	R / nm	σ / nm	ΔE_0 / eV	Rf / %
0.74	VAC	7±1	0.275±0.02	0.009±0.001	1±4	2.3
	H_2	6±1	0.281±0.02	0.009±0.001	1±3	0.9
	EVAC	5±1	0.277±0.02	0.007±0.001	0±4	2.3
0.56	VAC	9±1	0.275±0.02	0.007±0.001	0±3	1.1
	H_2	9±1	0.283±0.02	0.008±0.001	0±2	0.8
	EVAC	10±1	0.276±0.02	0.007±0.001	0±3	1.1
0.29	VAC	11±1	0.275±0.01	0.007±0.001	0±2	0.2
	H_2	11±1	0.283±0.01	0.008±0.001	3±2	0.3
	EVAC	11±1	0.276±0.01	0.007±0.001	1±3	0.8
0.12	VAC	12±2	0.275±0.02	0.007±0.001	-1±4	1.4
	H_2	12±2	0.284±0.02	0.008±0.001	0±3	1.0
	EVAC	12±2	0.275±0.02	0.007±0.001	-2±4	1.5

VAC : Pd/SiO_2 in vacuo (without exposure to H_2),

H_2 : Pd/SiO_2 under 13.3 kPa of H_2,

EVAC : Pd/SiO_2 exposed to 13.3 kPa of H_2 and subsequently evacuated at room temperature for 1 h.

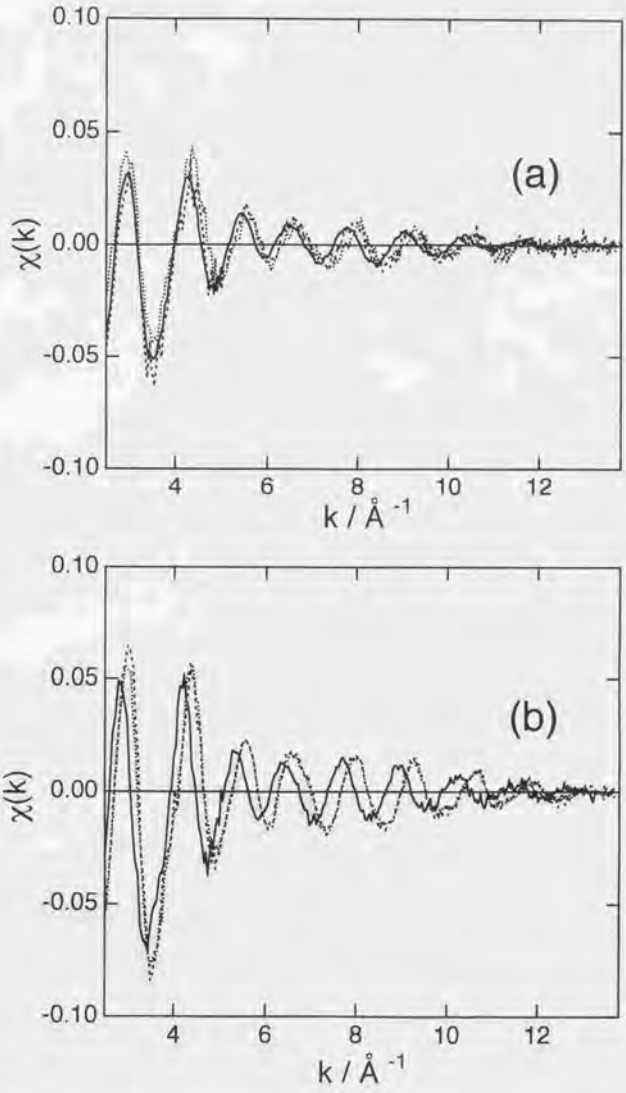

Fig. 6-1(A). Pd K-edge EXAFS oscillations (χ(k)) for Pd/SiO_2 with the dispersion(H_{ad}/Pd) of 0.74 (a), 0.56 (b); dotted line: Pd/SiO_2(VAC), solid line:$Pd/SiO_2(H_2)$; broken line: Pd/SiO_2(EVAC).

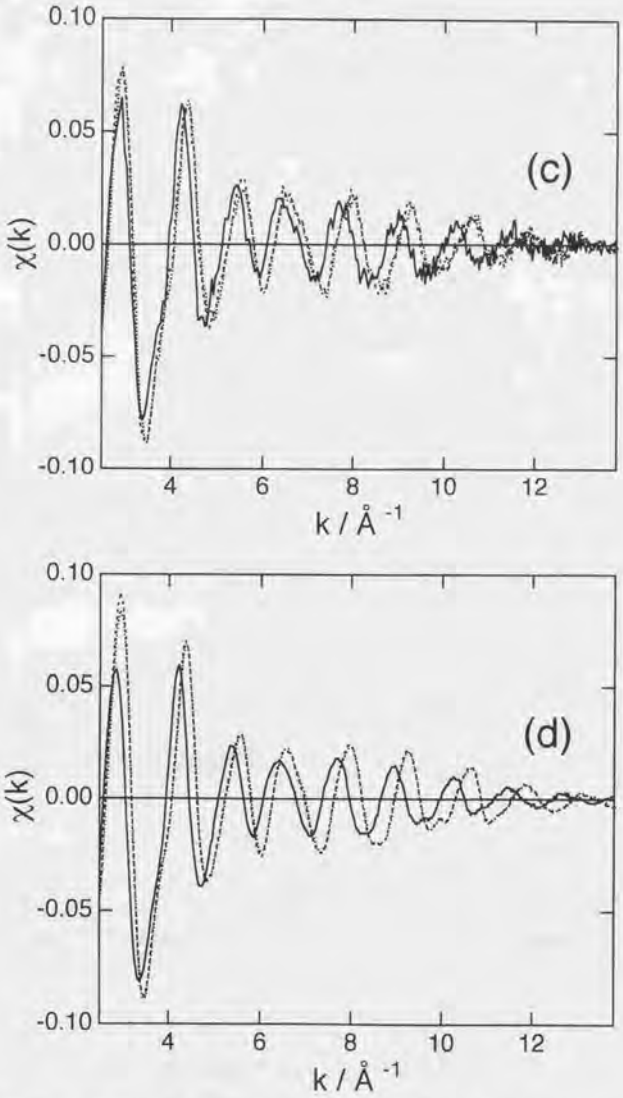

Fig. 6-1(B). Pd K-edge EXAFS oscillations ($\chi(k)$) for Pd/SiO_2 with the dispersion(H_{ad}/Pd) of 0.29 (c), 0.12 (d); dotted line: Pd/SiO_2(VAC), solid line:$Pd/SiO_2(H_2)$; broken line: Pd/SiO_2(EVAC).

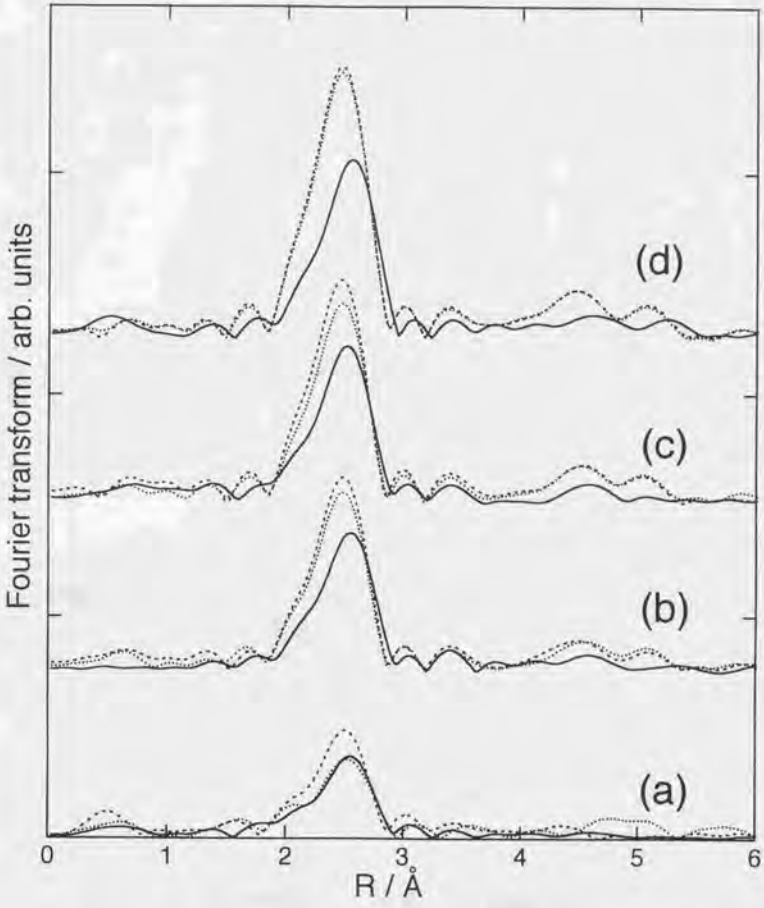

Fig. 6-2. Fourier transforms of k^3- weighted EXAFS for Pd/SiO_2 with the dispersion of 0.74 (a), 0.56 (b), 0.29 (c) and 0.12 (d); dotted line: Pd/SiO_2(VAC), solid line:$Pd/SiO_2(H_2)$; broken line: Pd/SiO_2(EVAC).

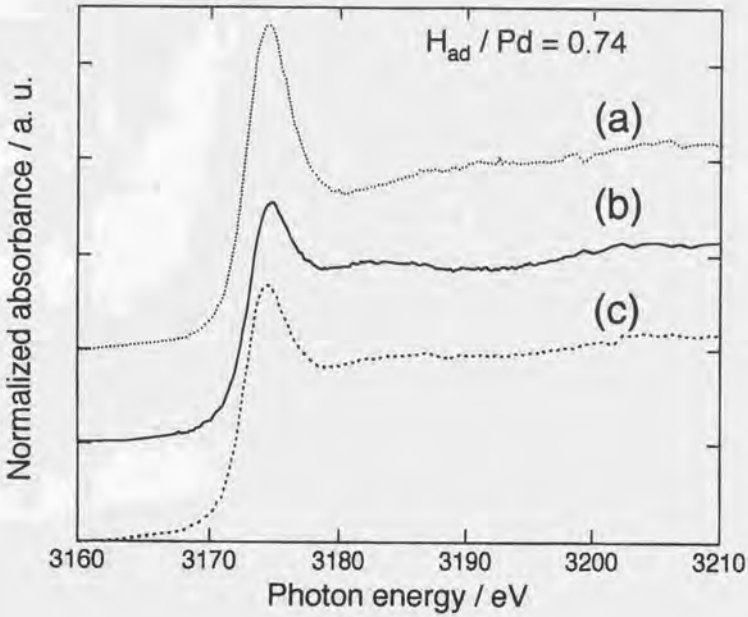

Fig. 6-3. Normalized Pd L_3-edge XANES spectra for Pd/SiO_2 (H_{ad}/Pd=0.74); (a) Pd/SiO_2(VAC), (b)Pd/SiO_2(H2), (c) Pd/SiO_2(EVAC).

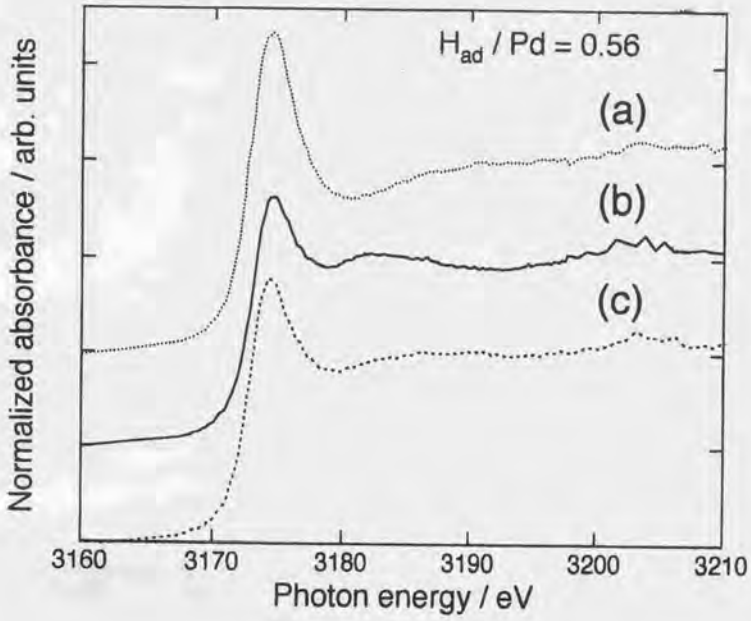

Fig. 6-4. Normalized Pd L_3-edge XANES spectra for Pd/SiO_2 (H_{ad}/Pd=0.56); (a) Pd/SiO_2(VAC), (b)Pd/SiO_2(H2), (c) Pd/SiO_2(EVAC).

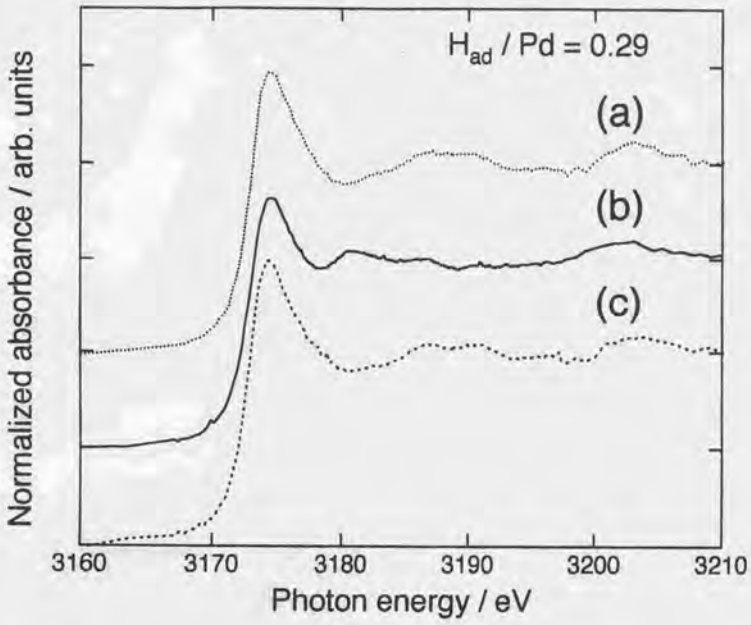

Fig. 6-5. Normalized Pd L_3-edge XANES spectra for Pd/SiO_2 (H_{ad}/Pd=0.29); (a) Pd/SiO_2(VAC), (b)Pd/SiO_2(H2), (c) Pd/SiO_2(EVAC).

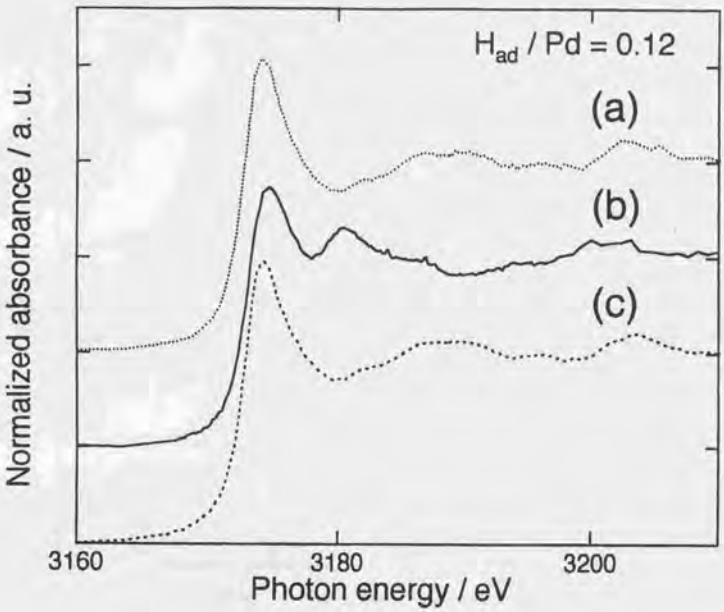

Fig. 6-6. Normalized Pd L_3-edge XANES spectra for Pd/SiO_2 (H_{ad}/Pd=0.12); (a) Pd/SiO_2(VAC), (b)Pd/SiO_2(H2), (c) Pd/SiO_2(EVAC).

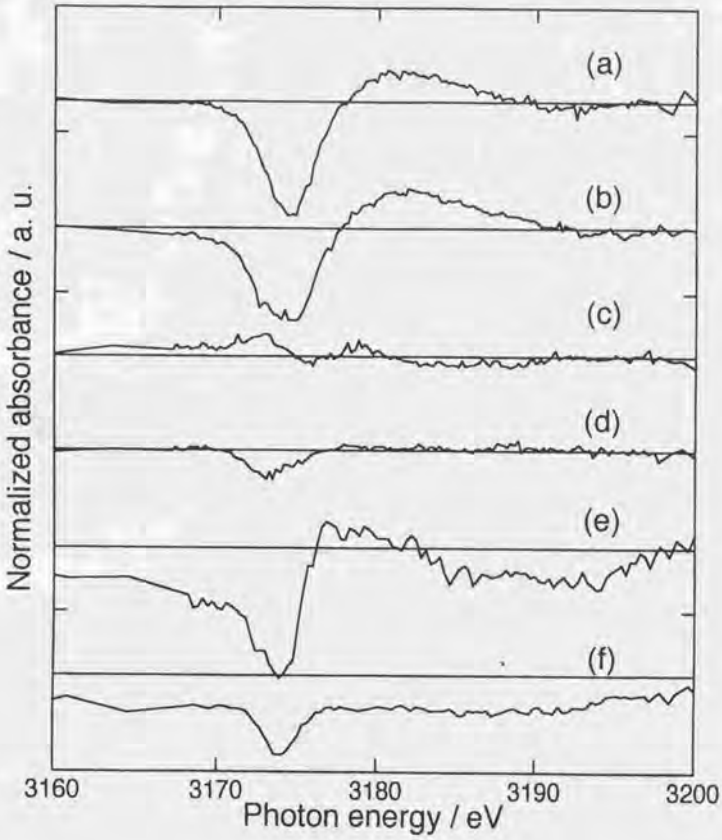

Fig. 6-7. Pd L_3-edge difference spectra for Pd/SiO_2 obtained by subtracting the spectra for Pd/SiO_2(VAC) from those for Pd/SiO_2 (EVAC); (a) $H_{ad}/Pd = 0.74$, (b) $H_{ad}/Pd = 0.56$, (c) $H_{ad}/Pd = 0.29$, (d) $H_{ad}/Pd = 0.12$ and corresponding spectra for Pd/Al_2O_3 with (e) $H_{ad}/Pd = 0.81$, (f) $H_{ad}/Pd = 0.20$.

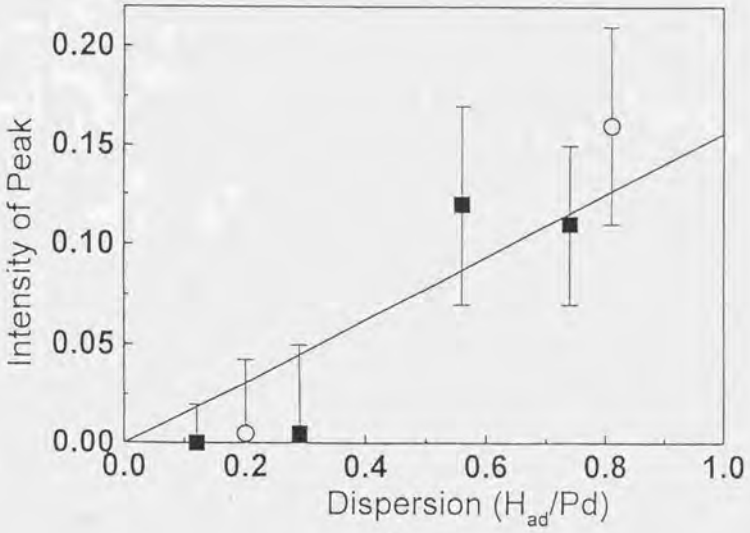

Fig. 6-8. Plots of the intensity of the ads-peak induced by adsorbed hydrogen against the dispersion(H_{ad}/Pd).

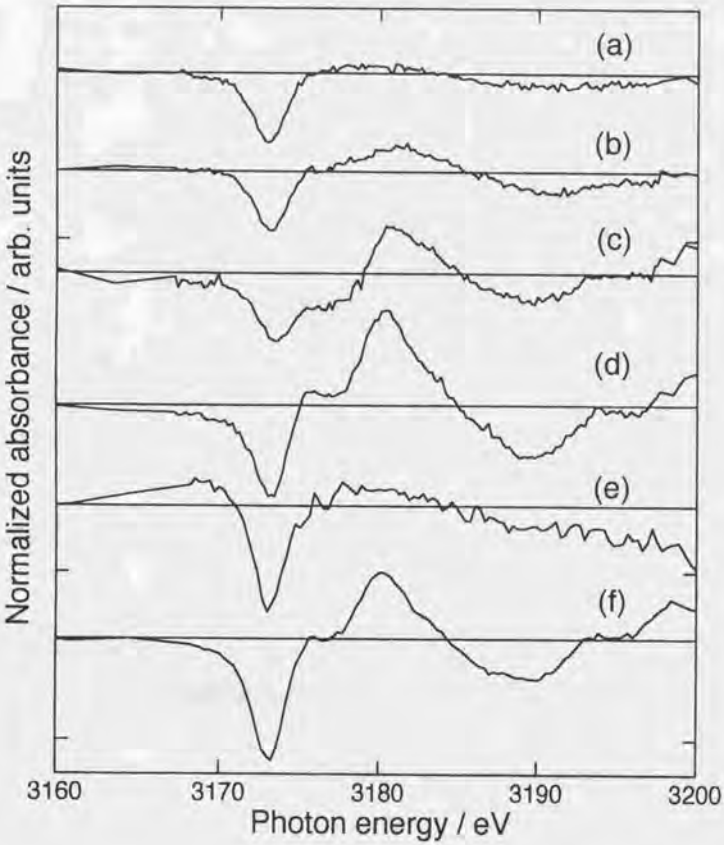

Fig. 6-9. Pd L_3-edge difference spectra for Pd/SiO_2 obtained by subtracting the spectra for Pd/SiO_2(EVAC) from those for Pd/SiO_2 (H2); (a) $H_{ad}/Pd = 0.74$, (b) $H_{ad}/Pd = 0.56$, (c) $H_{ad}/Pd = 0.29$, (d) $H_{ad}/Pd = 0.12$ and corresponding spectra for Pd/Al_2O_3 with (e) $H_{ad}/Pd = 0.81$, (f) $H_{ad}/Pd = 0.20$.

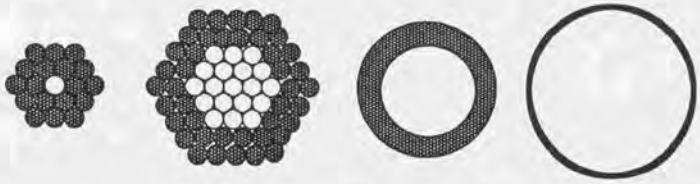

shells*	N=2	N=4	N=8	N=24
$\frac{N_{surf}}{N_{total}}$	0.76	0.52	0.31	0.12
$\frac{N_{bulk}}{N_{total}}$	0.02	0.18	0.45	0.77

*except the central atoms

Fig. 6-10. Models for Pd particles describing three regions (surface, subsurface and bulk), and the fractions of surface Pd atoms(Pd_s/Pd_t) and bulk Pd atoms(Pd_b/Pd_t).

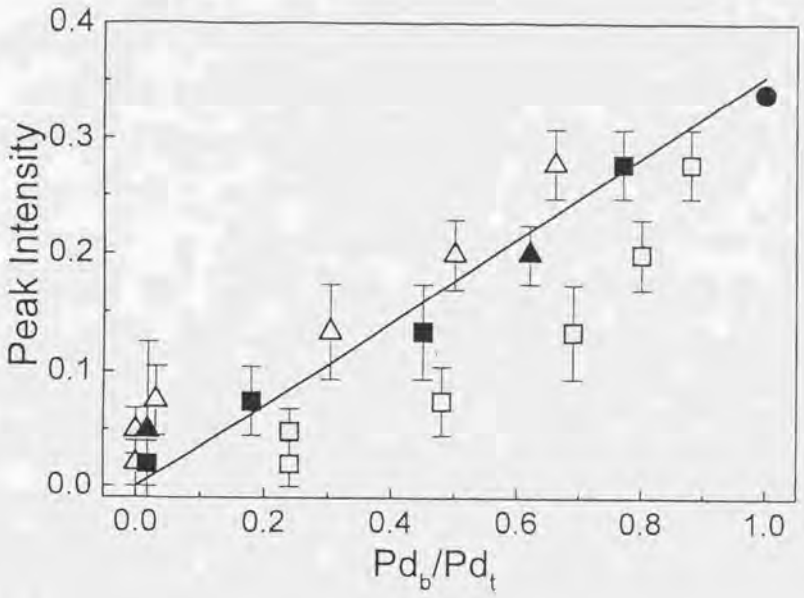

Fig. 6-11. Plots(filled square) of the intensity of abs-peak of Pd/SiO_2 against Pdb/Pdt calculated from the one-subsurface-layer model of Fig. 6-10 The Pd_b/Pd_t values calculated from no subsurface-layer(open circle) and two-subsurface-layer (open triangle) models are also plotted. Filled circle indicates peak intensity estimated from the spectra in Ref. 28). Filled triangles indicated the correponding intensity of abs-peak for Pd/Al_2O_3 against Pdb/Pdt based on one-subsurface-layer model.

Chapter 7.

Concluding Remarks

7. Concluding remarks

In this thesis, I have investigated changes in Pt L edge XANES spectra induced by hydrogen adsorption. To investigate this change in detail, I have studied three factors on Pt particles - hydrogen system, (1) effects of support, particle size, (2) influence of coadsorbates, (3) changes in other metal particles(Pd).

In Chapter 3, I have found a direct correlation between the amount of adsorbed hydrogen and the peak which appears in the difference spectra before and after H_2 adsorption, irrespective of the kind of supports. This results indicate that the L_3-edge peak can be used as a quantitative parameter for the amount of the adsorbed hydrogen on the supported Pt particles in situ under the conditions relevant to catalytic reactions.

In Chapter 4, I have found that the peak in the XANES difference spectra at Pt L_3-edge for $CO+H_2$ coadsorbed system can be deconvoluted to the linear combination of the difference spectra for the CO and H mono-adsorbed systems. It was also found that the fitting coefficient for adsorbed hydrogen (y) in the coadsorbed system is directly related to the number of hydrogen atoms adsorbed on the Pt particles. These results indicate that this technique can be applied to in situ conditions relevant to catalytic reactions involving adsorbed hydrogen.

In Chapter 5, I investigated XANES spectra for supported Pt particles in detail. I found that the linear relationship between the amount of adsorbed hydrogen and the peak intensity in XANES difference spectra hold whether H/Pt ratio is varied by hydrogen coverage or dispersion of Pt particles. Further, this line has the same slope as that for $CO+H_2$ coadsorbed system. These results demonstrate that the hydrogen-induced peak is directly related to the number of hydrogen atoms adsorbed on the Pt particles without influence of coadsorbed CO, kind of supports, particle size. The origin of this hydrogen-induced peak is considered to multiple scattering between hydrogen atom and Pt atom or transition to anti-bonding states between Pt-H bonding.

In Chapter 6, I have found that a new peak appeared at about 8 eV above the inflection point

of the absorption edge when the Pd L_3-edge XANES spectra were measured for the Pd sample with adsorbed hydrogen at the Pd surface. This peak corresponds to that found in small Pt particles and the peak intensity had a positive correlation with the Pd dispersion(H_{ad}/Pd) and the amount of adsorbed hydrogen at the Pd surface. Therefore this peak in the Pd particles may have the same origin as the peaks found in hydrogen-adsorbed Pt particle samples.

In conclusion, I have found a direct correlation between the amount of adsorbed hydrogen and the peak which appears in the difference spectra before and after H_2 adsorption. By the measurement under the conditions relevant to catalytic reactions, it will be expected that we can use this method as a characterization of hydrogen under the reaction conditions.

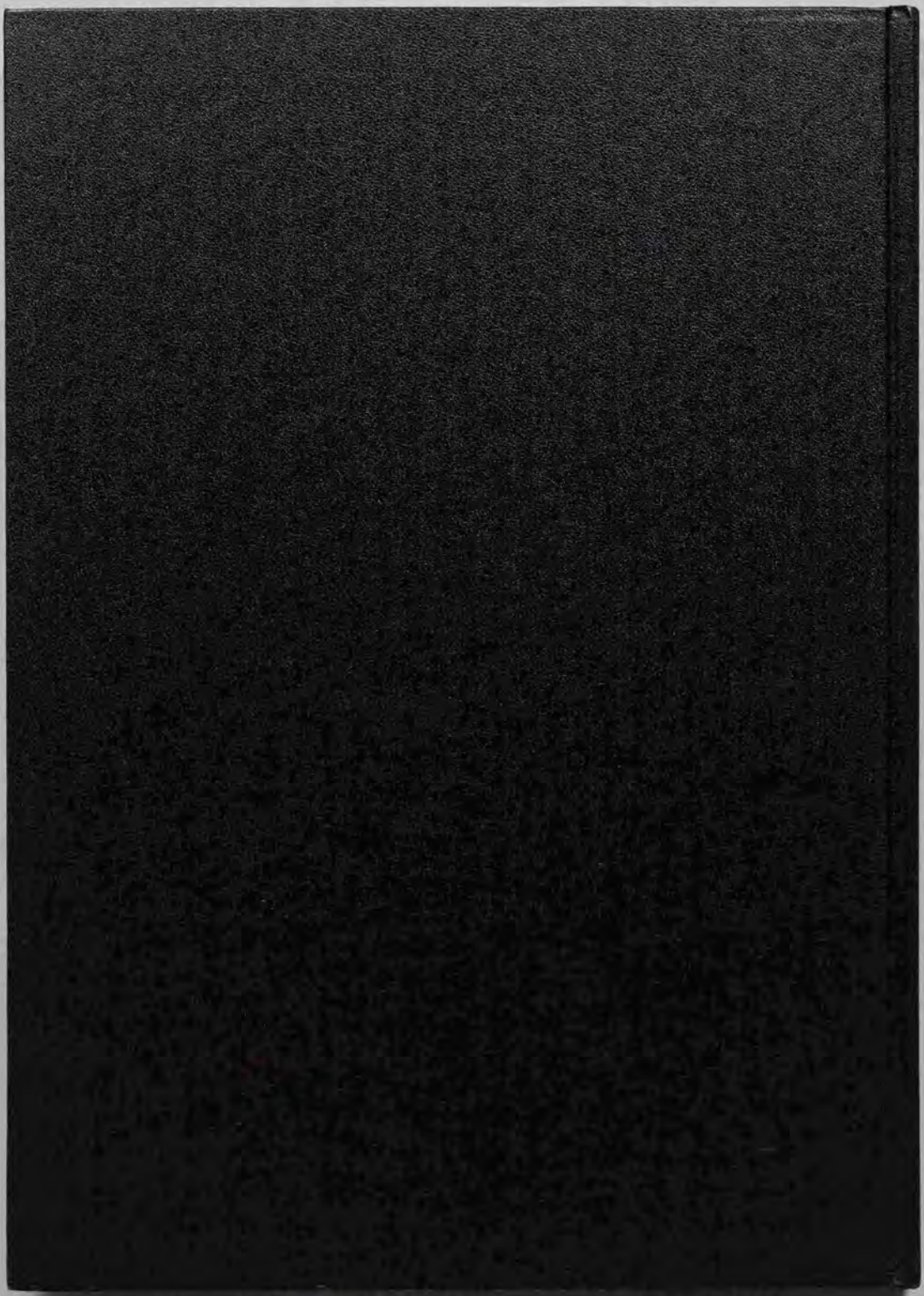

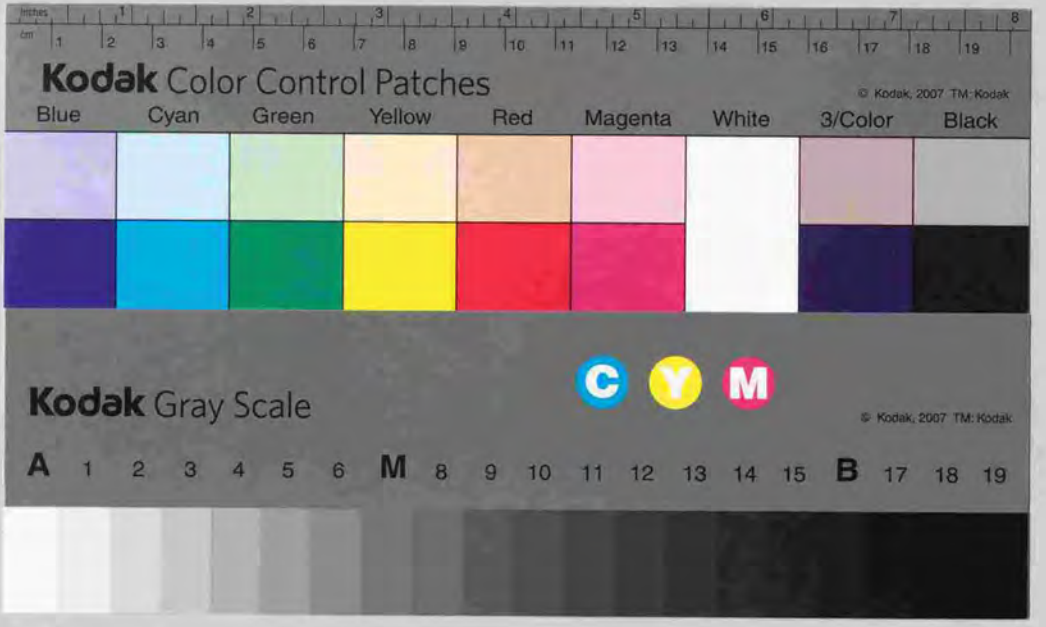
Kodak Color Control Patches
© Kodak, 2007 TM: Kodak
Blue
Cyan
Green
Yellow
Red
Magenta
White
3/Color
Black
Kodak Gray Scale
C
Y
M
© Kodak, 2007 TM: Kodak
A 1 2 3 4 5 6 M 8 9 10 11 12 13 14 15 B 17 18 19